AN EXPERIMENTAL INVESTIGATION OF COMPRESSOR PERFORMANCE IN ROTATING STALL

by

ANTHONY HENRY JAMES EASTLAND

B.A., Oxford University
(1980)

SUBMITTED IN PARTIAL FULFILLMENT

OF THE REQUIREMENTS FOR THE

DEGREE OF MASTER OF SCIENCE

at the

MASSACHUSETTS INSTITUTE OF TECHNOLOGY

June, 1982

Signature of Author _____
Department of Aeronautics and Astronautics
May 19, 1982

Certified by _____
Edward M. Greitzer

Accepted by _____
Harold Y. Wachman
Chairman, Departmental Graduate Committee

AN EXPERIMENTAL INVESTIGATION OF COMPRESSOR PERFORMANCE IN ROTATING STALL

by

Anthony Henry James Eastland

Submitted to the Department of
Aeronautics and Astronautics on May 19, 1982
in partial fulfillment of the requirements for
the degree of Master of Science.

ABSTRACT

This thesis describes the design and construction of a test facility for low speed multistage compressors, and the steady state results obtained from a three stage compressor operating in rotating stall. The results include compressor pressure rise and torque characteristics as well as some initial high response data, taken to determine the size and propagation speed of the stall cell.

It was found that the pressure rise characteristics displayed a "secondary characteristic" on the double valued part of the speedlines. In this regime the slope of the pressure rise characteristic was strongly negative. The torque characteristics were discontinuous and, for the same pressure rise, less torque was absorbed in the stalled flow regime than in the unstalled flow regime.

Thesis Supervisor: Edward M. Greitzer
Title: Associate Professor of
Aeronautics and Astronautics

ACKNOWLEDGEMENTS

The author is indebted to many members of the Gas Turbine Laboratory staff. In particular I would like to thank Professor E. M. Greitzer for his continual support and guidance throughout the project, and Dr. C. S. Tan for his help in the design of the data acquisition systems. In addition, the experience and helpful comments of Professor E. E. Covert were much appreciated in the design phase of the project. Special thanks go to J. Marksteiner, G. Paluccio and R. Andrew for their craftsmanship and tireless work in constructing and helping to run the rig. Many thanks go to Miss Nancy Ivey for typing this thesis.

Support for this project was provided by Pratt and Whitney Aircraft, Government Products Division, and this is gratefully acknowledged. Acknowledgement is also made to Pratt and Whitney Aircraft, Commercial Products Division for the loan of the compressor.

TABLE OF CONTENTS

TABLE OF CONTENTS Continued

NOMENCLATURE

A	area
C	orifice plate calibration constant
C_p	specific heat capacity at constant pressure
C_x	compressor axial velocity
K	a constant
P	static pressure
P_T	total pressure
R_m	blade mean radius
T_T	total temperature
$\bar{u}$	mean blade speed
v	velocity
ρ	density
ϕ	flow coefficient $C_x/\bar{u}$
τ	torque

SUBSCRIPTS

a	ambient
c	compressor
ex	compressor exit
in	compressor inlet
op	orifice plate
sta	stage
th	throttle

COMPRESSOR CHARACTERISTICS

PRESS — static pressure referenced to inlet static pressure

$$P - P_{in} \,/\, 1/2\ \rho_a\ \bar{u}^2$$

PSTA — stage static pressure coefficient

$$\Delta P_{sta} \,/\, 1/2\ \rho_a\ \bar{u}^2$$

SS — static to static pressure rise coefficient

$$P_{ex} - P_{in} \,/\, 1/2\ \rho_a\ \bar{u}^2$$

TEMP — total temperature referenced to inlet total temperature

$$(T_T - T_{Tin})\ C_p \,/\, 1/2\ \bar{u}^2$$

TS — total to static pressure rise coefficient

$$P_{ex} - P_{Tin} \,/\, 1/2\ \rho_a\ \bar{u}^2$$

TT — total to total pressure rise coefficient

$$P_{Tex} - P_{Tin} \,/\, 1/2\ \rho_a\ \bar{u}^2$$

TORQ — torque coefficient

$$\tau \,/\, 1/2\ \rho_a\ \bar{u}^2\ \ A_c\ R_m$$

LIST OF FIGURES

LIST OF FIGURES Continued

LIST OF TABLES

CHAPTER I

INTRODUCTION

Rotating stall is a mode of compressor operation in which zones or cells of severely stalled flow propagate around the compressor annulus. In multistage compressors the rotational speed of these cells is commonly between 20 and 50 per cent of the rotor speed. In this operating regime the flow consists of a stall cell (or cells) with low or even negative axial velocities and high tangential velocities, and a region (or regions) of unstalled flow. The latter have been found to roughly correspond to local operating points on the unstalled part of the characteristic. A compressor operating in stall can thus be approximately regarded as two compressors working in parallel [1].

Two types of rotating stall have been observed: "part span" stall in which the stall cell does not cover the complete annulus height (and in which up to 12 stall cells have been found [2]), and "full span" stall in which the stall cell does cover the complete annulus height (and which occurs as a single cell). An important aspect of compressor performance in rotating stall is the hysteresis between stall inception and cessation. This can be quite severe in full span stall and its occurrence can seriously affect the ability of a compressor to recover from stall.

Although rotating stall has been known for over thirty years, it is only recently that the stalled performance of a compressor and its ability

to recover from stall have become of interest. Most of the early interest in the subject was focused on stall inception and the theoretical work done was based on linear small perturbation analyses (e.g. [3], [4]). These analyses, however, are unsuitable for predicting a compressor's performance in the presence of the large amplitude non-uniformities which characterize fully developed rotating stall. An advance on these was made by Takata and Nagano [5] who used a nonlinear (time marching) technique. However they did not include several aspects of the problem [6], for example the coupling between the compressor and the rest of the compression system, which has been shown to be important in [1], [7], and [8].

Investigation of rotating stall has been complicated by the difficulty of obtaining detailed information about the flow field in stall. This was overcome by Day using a phase locked sampling technique and ensemble averaging. Using these methods Day and Cumpsty [6] have been able to present a general description of the flow in a stalled compressor and Greitzer and Cumpsty [9] have developed a successful model to predict stall cell speed in multistage compressors. Of more practical importance to the designer, Day, Greitzer and Cumpsty [1] have developed an approximate scheme for predicting the stalled part of a compressor characteristic.

Despite these advances, however, there is still much that is not understood about the basic fluid mechanics of rotating stall. In particular, it is still not possible to predict a complete characteristic from "first principles" using just the design parameters. Reviews of rotating

stall and our knowledge of pumping system instabilities in general can be found in [10] and [11] respectively.

Rotating stall is initiated by the separation of either the boundary layer on the suction surface of the blade and/or one of the endwall regions. As first described by Emmons [4] this creates a blockage in one blade passage that tends to stall the blade ahead and unstall the blade behind. Taking this concept further, we can note that when fully developed the stall cell can be thought of as presenting a blockage to the flow, and the most important idea in the Day et al. prediction scheme is that of a critical stall cell blockage. Above this value of blockage part span stall does not occur and below it full span stall does not occur.

The important features of the detailed structure of stalled flow in multistage compressors [6] are that the stall cell extends axially through the compressor with the flow patterns repeating stage by stage, that the flow patterns in the multistage compressors tested so far show many of the same general characteristics and that the stall cell is characterized by high velocities ahead of the rotor and low velocities behind. The last two observations lead to the idea that in the stall cell the rotors act somewhat as paddle wheels with fluid leaving from the leading edge.

The high velocity fluid ahead of the rotor impinges at large incidences on the trailing edge of the stators, dissipating its kinetic energy. This has been used to explain the observation that a compressor absorbs almost as much torque when it is stalled as at its design point, resulting

in a continuous torque characteristic [2]. This is surprising considering the large drop in pressure rise which is usually associated with the onset of rotating stall in a multistage compressor.

The paddle wheel action of the rotors imparts large centrifugal accelerations to the fluid in the stall cell and the flow is thus strongly three dimensional. It is clear then that in order to understand the flow in stall a knowledge of the radial velocities in the stall cell is required. The main thrust of the second phase of this project will be toward this. It is also to be expected that design parameters such as aspect ratio and hub to tip ratio will have an effect on the details of the stalled flow, and perhaps also on overall compressor performance, although it is not possible to perform these parametric studies in the present framework of this project.

The work reported herein is the initial phase of a long-term investigation of compressor performance in rotating stall. It involved the design and construction of a new low speed compressor test facility, including data acquisition systems for both steady state and high response data. This thesis will be concerned with the design and construction of the system and the overall performance characteristics of the compressor. In particular, many of the details of the design of the system are presented so as to provide adequate documentation for future workers on this facility.

Preliminary investigations of the effect of the throttle line on compressor performance [1] and the effect of Reynolds number on the stall point are also reported. Subsequently it is hoped to obtain detailed information about the flow field in stall, in particular the radial velocities in the stall cell, using the phase locked averaging techniques of Day.

CHAPTER II

THE DESIGN OF THE NEW LOW SPEED TEST FACILITY

In order to allow two test programs to run concurrently the GTL low speed test facility was substantially modified. Specifically, a frame and drive system were built for the three stage compressor to be used in this work (described in [12]) and an exhaust duct system was constructed for use with both the existing single stage compressor (described in [13]) and the new compressor. This exhaust system utilized a fan situated outside the test cell; the fan being required to investigate the effects of the throttle line on the compressor characteristic [1], and to avoid recirculating the air in the test cell which had previously caused problems with clogging of probes.

It was decided that, despite the longer initial set up time, a much faster turnaround time would result if the new compressor were mounted on a new frame with a separate drive transmission run from the back of the existing DC motor. It was also decided that the best arrangement as far as efficient use of available space and simplicity of the ducting system were concerned was to align the rig parallel to the outside wall. One concern with this configuration was that the inlet of the single stage compressor might be too close to the side wall of the test cell and that a vortex might form. Flow visualization, however, showed that this was not the case. Thus, the first part of this work involved the design and

construction of the frame and drive system for the new compressor, and the assembly of the ducting for both compressors within the following constraints.

The frame had to support the compressor and vibration isolate it. The drive system had to provide enough power to run the compressor at a maximum of 3000 RPM and have a critical speed above this. The ducting had to be arranged so that turnaround time was a minimum. In addition parametric tests may be undertaken in the future by testing different compressors on the new frame. These compressors are expected to differ dimensionally from the present one in length and hub to tip ratio and thus both frame and drive system had to be designed to accommodate the longest and most powerful compressor projected for these tests.

It has been shown in [14] that a diffuser or nozzle downstream of a compressor can have a significant effect on its stability. To accommodate the possibility of a study of this phenomenon the ducting immediately downstream of the compressor had to be designed to match the different hub to tip ratios that might be encountered and to be able to contain diffusing and accelerating annuli.

It was also necessary to design a soundproofing device to help reduce the noise levels in both the test cell and surrounding areas.

Sketches of the new floor plan and a general plan of the new test stand are shown in Figs. 1 and 2.

2.2 The Compressor Drive System

2.2.1 The Drive Transmission

The transmission was to drive the compressor at a maximum of 3000 RPM, at which speed it was expected to require 110 HP [12], from a DC motor whose maximum shaft speed was 1500 RPM. It was decided to design the system so that a compressor of similar loading to the one used in this work but with a hub to tip ratio of 0.7 (as opposed to 0.88) could be tested. This latter compressor was regarded as absorbing as much torque as any that might be tested and was calculated to require 185 HP at 3000 RPM. A belt drive system using 8 Browning 5VX Gripnotch belts on sheaves of pitch diameter 14.9" and 7" was chosen for the drive; this gives a maximum speed of 3200 RPM at which speed the belts are rated to 228 HP. The maximum belt tension should be 126 lbf.

2.2.2 Shafts and Bearings

The large sheave is cantilevered on the motor shaft which has a diameter of 3". The smaller sheave is mounted between two pillow blocks (SKF type SAF 22511) on a 1 15/16" diameter shaft. The bearings are split taper roller bearings; it was assumed that all thrust is taken by the thrust bearing in the compressor. Estimating a maximum equivalent load of 250 lb. on each of these bearings from a static analysis of the shaft loading and using a safety factor of 5, their life is expected to be 7500 million revolutions or about forty thousand hours at 3000 RPM.

An important consideration was the convenience of aligning the shaft. This was achieved by providing rotation and horizontal translation perpendicular to the shaft at the compressor mountings, and vertical translation at the pillow block mountings. The pillow blocks are mounted on a plate held by 3/4" bolts above two welded steel supports. These supports and the shaft arrangements are shown in Fig. 3.

The compressor is driven from the inlet flange and the drive shaft is in three sections. The first is a 26" length of 1 15/16" diameter steel shaft (the diameter being determined by the bushing in the sheave), and is supported by two pillow blocks. The second is a torque meter rigidly mounted in the spool piece, and the third is an 18" length of 1 1/2" diameter steel shaft connecting the torque meter and the compressor shaft.

The couplings on either side of the torque meter are Browning CHFGC 15X gear type flexible couplings, and the coupling joining the drive shaft to the compressor shaft is a Browning CSP rigid coupling. A rigid coupling was used here in preference to a flexible coupling as any shaft misalignment should be taken up by the flexible couplings at the other joints, and the extra weight of a flexible coupling at this point was calculated to reduce the critical speed considerably.

The shaft has a total length of 56 3/4" and, assuming the compressor can be regarded as a fixed end and the torque meter as a solid 1 1/2" steel shaft, was calculated to have a critical speed of

approximately 3900 RPM. When the single stage compressor on the other end of the DC motor is run the shaft is broken at the first flexible coupling and the resulting arrangement has a critical speed of approximately 16,000 RPM.

2.3 The Frame and Support Mountings

2.3.1 Main Frame

The main frame was built from two 6" steel I-beams welded to the motor frame at one end and to a 10" steel channel acting as a cross-brace at the compressor exit flange. The other end was left free. The channel was supported by six Toro-pads.* These are small air filled plastic cushions designed as shock load protection for pallets carrying fragile cargoes and were recommended for use as vibration isolators. It was decided to vibration isolate the new frame in this manner rather than trying to create an underdamped system mounted on springs (as was the case with the old frame) due to the uncertainty in calculating the natural frequencies and modes of vibration of the complete system.

2.3.2 Pillow Block Mountings

The pillow blocks were mounted on a single 1/2" steel plate, which was supported above two portal frame type structures by twelve 3/4" bolts. Mounting the pillow blocks on a single plate greatly increased the stability of the drive system by coupling the motor frame

*Trademark of Hardigg Industries

and the new frame more closely. This was considered important as it was undesirable to allow the possibility of the new frame and the old frame being able to vibrate in two virtually independent modes - especially as there is a large starting transient. Sketches of the pillow block mountings are shown in Figs. 4 and 5.

2.3.3 Compressor Mountings

The compressor was supported at the inlet and exit flanges. There were two 7/8" studs attached to the inlet flange and these were mounted in two small pillow blocks having brass contact bearings. These pillow blocks were mounted on a frame made from welded 1/2" steel plate and which was bolted to the main frame. This mounting is shown in Fig. 6.

The exit flange was supported by two turnbuckles attached to small pads bolted to the main frame. This arrangement gave the required flexibility in the length of compressor that could be tested. By lengthing or shortening the turnbuckles the compressor could be rotated around the inlet flange and this was used to align the shaft.

2.3.4 Other Mountings

The other sections that had to be supported from the main frame were the extension piece and throttle assembly, and the plenum volume (refer to Fig. 2). These were also supported by turnbuckles to allow easy alignment.

The torque meter was mounted on a frame made from 1/8" steel plate bolted to the inside of the spool piece. This frame was designed to give the maximum flexibility in aligning the torque meter with the rest of the shaft system and was positioned so that the torque meter was easily accessible. A sketch of this frame is shown in Fig. 7.

2.4 The Exhaust Duct System

2.4.1 Sizing Considerations

2.4.1.1 Main Duct

The ducting was to withstand internal pressures from +5 psig to -1 psig and mate with the fan inlet whose inside diameter was 37 5/8". The main body of the ducting was designed with an inside diameter of 36" and was constructed from 1/8" rolled aluminum sheet. The flanges were made from rolled 1 1/2" x 1 1/2" x 1/8" aluminum angle welded to the ends of each section. Sealing was achieved using 1/4" thick 40 Durometer Neoprene gaskets.

2.4.1.2 Plenum Volumes & Connections to Main Duct System

The plenums were built in two pieces for ease of construction using 1/8" aluminum sheet and 1 1/2" x 1 1/2" x 1/8" aluminum angle for the flanges. In order to provide as uniform a stress distribution as possible they were made with a circular cross section. The

plenum diameters were limited by the width of the main frames because of space considerations, and were set at 48". The depth of the plenum for the single stage compressor was limited by the distance between the compressor exit flange and the pillow block mounting, and the depth of the plenum for the three stage compressor was limited by the necessity of there being sufficient space between it and the back wall.

Due to these limitations in depth it was not possible to connect the plenums to the main duct using 36" diameter sections and so 24" diameter sections were used.

A 24" diameter hole was cut into the back of the plenum for the single stage compressor to allow easy access to the shaft; this was so that the shaft could easily be broken at the flexible couplings when the three stage compressor was run. Figure 8 shows a plenum assembly and Fig. 9 details of the main duct sections.

2.4.2 Duct Assembly

The main frame was positioned so that the centre line of the plenum for the single stage compressor was aligned with the fan centre line. The ducting from the plenum of the three stage compressor ran parallel to the compressor and was offset slightly to allow room for a traversing rig to be mounted on the compressor. This arrangement is shown in Fig. 10. An angled duct connects the exhaust from the plenum of the single stage compressor into the system through a hole cut in the

elbow. A cross sectional view of this set up is shown in Fig. 11. When the single stage compressor is run, a plate is bolted to the upstream flange of the elbow, and when the three stage compressor is run the angled section is removed and a plate is bolted over the hole in the elbow.

The ducting rests on rails supported by portal frames built from Unistrut. This layout is shown in Fig. 12.

2.5 Extension Piece and Throttle Arrangement

The extension piece had to connect the exit flange of the three stage compressor to the plenum, be easily adapted for different hub to tip ratio compressors and for diffusing and accelerating passages, and contain a mechanism to throttle the flow from the compressor. It was made from concentric cylinders of rolled aluminum. The outer shell was made 1/4" thick and the cylinders forming the inside diameter of the flow path were 1/8" thick. The flange at the compressor exit end was a machined aluminum ring as it was roughly one compressor radius downstream of the last blade row and it was important there be no discontinuities or ovalization in the flow path there. The other flange was made of rolled aluminum angle.

The cylinder forming the outside wall of the flowpath had an inside diameter of 24". The inside wall of the flowpath was formed from two cylinders, one with a 21.12" outside diameter (this being the inside diameter of the compressor) and 12" in length and one with a 12" outside diameter and 25" in length. The latter was supported at the plenum end

by two sets of struts welded to the outer shell. The former was press fitted over two support rings. One of these was bolted to the compressor exit while the other was bolted to another ring which was press fitted into the smaller cylinder. With this arrangement the hub to tip ratio can be changed and diffusing or accelerating passages installed by fabricating a new cylinder or cone and new support rings.

The throttle is conical and slides on a hollow 4 7/8" outside diameter aluminum shaft. This shaft was supported by the same struts that support the smaller cylinder. A bearing surface was produced by shrink fitting a steel sleeve onto the shaft and press fitting a brass ring into the throttle. The throttle is driven by two power screws attached to two DC generators.

Throttle position was monitored using a linear potentiometer and two microswitches activating two relays in the motor circuits prevented the throttle being driven too far in either direction. A ring of closed cell Neoprene was glued to the inside wall of the plenum so that a more effective seal could be obtained when the throttle was in the fully closed position, and a cylinder that slid over the inside diameter of the extension piece was attached to the throttle to form the flowpath as the throttle was opened.

An assembly drawing of the extension piece is shown in Fig. 13 and the drive system for the throttle is shown in Fig. 14.

The fan has adjustable inlet guide vanes and these could also be used to throttle the compressor.

2.6 Acoustic Box

It was expected that the worst of the noise produced by the compressor would propagate from the inlet, and thus the noise reduction device was constructed as an octagonal box, open on one face, which was placed around the inlet. The depth of the box was determined by the distance between the inlet bellmouth and the pillow block mountings and its height by the height of the duct supports. It was built from plywood with 2" fiberglass acoustic treatment glued to the inside. The octagon has a height of 5'10" and a depth of 3'2". Eight inch outside diameter PVC pipe was used to give rounded edges and prevent flow separation.

2.7 Flow Measurement Device

It is necessary to measure the mass flow through the three stage compressor when it operates in stall. It is not possible to do this using an inlet calibration as the flow field there is severely non-uniform in stall and the methods used for axisymmetric flow are not valid [2]. It was thus decided to use an "orifice plate" placed in the ducting downstream of the plenum volume. This "orifice plate" was to produce as large a pressure drop as possible (so as to give an easily measureable pressure difference at low flow coefficients) consistent with the compressor being able to produce a large enough pressure rise to drive the flow at high flow coefficients. It was sized to operate at a flow coefficient of 0.8 and from an estimate of the losses in the ducting it was calculated that the pressure drop acorss it should be half an inlet dynamic head.

To give consistent results the streamlines upstream of an orifice plate should be straight and parallel. In rotating stall a high degree of swirl is introduced to the flow which, although being reduced, would not be totally eliminated in the plenum. To overcome this, three porous plates were placed in the main ducting upstream of the "orifice plate". The plate was made of 1/4" aluminum plate with 300 1" diameter holes placed in a square grid, this giving the most uniform distribution of "capture area" for each hole. The plate was placed 4' upstream of the elbow, as shown in Fig. 10.

CHAPTER III

EXPERIMENTAL PROCEDURES AND FACILITY CALIBRATION

The experimental part of this project can be divided into two parts: mapping of the overall compressor performance and detailed measurements of the flow field in rotating stall. It was not possible to perform the latter set of experiments within the time constraint of this thesis but some work has been done on instrumentation and data acquisition systems for these tests. This work and the experimental procedures used to obtain the compressor characteristics are described in this chapter.

3.1 Test Compressor

The test compressor was loaned to the GTL by Pratt and Whitney Aircraft. It has three stages, a hub to tip ratio of 0.88, is of rather low aspect ratio (averaging 0.8 for the rotors and 1.17 for the stators), and has a design flow coefficient of 0.67. A full description of the compressor design parameters can be found in Table 1.

3.2 Instrumentation for Steady State Data Acquisition

In addition to measuring pressure rise characteristics it was felt desirable to measure the torque characteristic and the temperature distribution through the compressor when in stall. To do this a strain gage type torque meter was installed as part of the drive shaft. In addition, thermocouples were placed at approximately midspan between each of the blade rows. These thermocouples were left unshielded as it was desired to measure the

TABLE 1

COMPRESSOR DESIGN PARAMETERS

Number of Stages	3
Design Speed, rpm	5926
Design Mass Flow, lb/sec	19.2
Design Pressure Ratio	1.489
Tip Diameter, in.	24.0
Hub-Tip Ratio	0.88

Blade Row	No. of Blades	Chord in.	Aspect Ratio	Midspan Stagger Deg. from Axial*
Inlet Guide Vane	124	0.826	1.746	-8.1
First Rotor	54	1.779	0.811	37.8
Second Rotor	55	1.764	0.817	38.5
Third Rotor	49	1.996	0.722	39.6
First Stator	85	1.235	1.168	21.0
Second Stator	88	1.232	1.170	23.0
Third Stator	90	1.235	1.168	15.0

*Stagger angles are measured from an axial line through the leading edge, and are positive for the rotors and negative for the stationary blade rows in the direction of rotation.

average total temperature in stall, where the flow directions vary over a wide range. Corrections for the recovery temperature and radiation were not included in the data reduction. An estimate of the radiation correction showed it to be much less than one degree Kelvin in all cases, and the difference between recovery and stagnation temperature is on the order of one degree or less at the Mach numbers encountered here. It should also be noted that differences in temperature rather than absolute values were the quantities of interest, and the corrections to the thermocouple readings should not be greatly different either for the different thermocouple locations or for the different conditions studied.

At the inlet there are eight static pressure taps and two total pressure rakes of three probes each. The static taps are spaced evenly around the annulus alternately at hub and tip. The total pressure rakes had probes at 30%, 50%, and 70% of the annulus height and were placed 120° apart. Four kiel probes were located at the axial midpoint of the bellmouth, and outside diameter static pressure taps were placed between each of the blade rows. At the exit there are eight static pressure taps. These are positioned 2 1/2" downstream of the last stator and are arranged in the same way as the inlet. Downstream 5 1/4" of the last stator, there are six kiel probes distributed as evenly as was possible around the annulus and located at its midspan. Two total pressure rakes and four outside diameter static taps were placed at a location one diameter compressor downstream of the last stator. A schematic of the compressor instrumentation is shown in Fig. 15.

In addition to the instrumentation in the compressor, two thermocouples were placed in the exit ducting 18" upstream of the orifice plate so that the density there could be calculated. Another two thermocouples monitored the compressor bearing temperatures. Four static pressure taps 2" upstream and four 18" downstream of the orifice plate were averaged to measure the pressure difference across the orifice plate.

Some concern was expressed that the scanivalve transducer would not see steady pressures when the compressor was in rotating stall and that each channel may have to be sampled for a considerable length of time to obtain a true average pressure. The transducer cavity in the scanivalve has negligible volume and thus any attenuation of a fluctuating pressure signal is solely due to viscous damping in the pressure tubing. An analysis was carried out regarding this viscous dampimg as capacitance and it was calculated that the expected stall cell frequencies would be attenuated. This, in fact, proved to be the case.

Information was also required about the size and rotational speed of the stall cell. A hot wire was traversed in front of the second rotor and also behind the last stator and the output from this monitored on a storage oscilloscope.

The rotational speed of the compressor was measured using a magnetic pick up mounted above a sixty tooth gear in the torque meter. This was connected to a frequency counter which thus directly read RPM.

3.3 Data Acquisition Systems

All pressures were measured using a scanivalve multiplexing system. This allowed 47 pressure to be measured simultaneously (reserving one port for a reference) by a single transducer. The one exception to this was at the low flow rates in stall when the pressure drop across the orifice plate was measured with a micromanometer. This was necessary as in this flow range the pressure drops could become of the same order as the transducer error. All 12 temperatures were measured using an Analog Devices μMAC 4000 temperature multiplexer.

Data acquisition was controlled by a MINC RT-11 minicomputer, with data being stored in dimensional form on floppy disks. Schematics of the computer data acquisition system and the interface circuit required to control the scanivalve are shown in Figs. 16 and 17. The software used and an explanation of the interface circuit are presented in Appendix A.

3.4 Orifice Plate Calibration

As stated, to obtain the speedlines it was necessary to calibrate the orifice plate. This was done by relating the pressure drop across the orifice plate (see Appendix B) to the axial velocity through the compressor as measured at the inlet in unstalled flow.

The first stage of the calibration was to calibrate the inlet. Radial traverses were performed in front of the inlet guide vanes at four different speeds giving a range of Reynolds number based on the compressor

axial velocity and the length of the bellmouth inlet of 4.2×10^5 to 8.7×10^5. From these, the blockage associated with the inlet boundary layers was found. For axisymmetric flow the mass flow calculated only from measurements of free stream total and inlet static pressure could now be corrected to give the actual mass flow.

The change in blockage was found to affect the average velocity by 0.05% over this range of Reynolds number. For the experiments reported herein, therefore, no Reynolds number dependence was included in the inlet calibration, and the average value of blockage of 3.6% was used throughout. If the blockage-Reynolds number dependence is assumed to obey a half power law, then it can be shown that the resulting error is 0.008 in flow coefficient at a rotational speed of 1000 RPM and a compressor axial velocity of 4 m/s. This was considered to be acceptable.

The orifice plate calibration was carried out by running the compressor at speeds from 1200 RPM to 2500 RPM and throttling it to its stall point at each speed. Low flow rates were achieved using the exit fan and allowing the compressor to windmill. In this way a range of compressor inlet axial velocities from 4 m/s to 66 m/s was achieved, corresponding to flow coefficients of 0.11 at 1200 RPM to 0.73 at 3000 RPM.

A plot of calibration constant (compressor axial velocity divided by corrected orifice plate pressure difference) against a Reynolds number based on velocity through the small orifices and orifice diameter is presented in Fig. 18. Above a Reynolds number of 9350 the data collapses

satisfactorily to a value of 2.76. Below this value the calibration constant increases as the Reynolds number decreases. This is consistent with other published data for orifice plates [15]. It was decided to approximate this curve by two straight lines as shown in Fig. 18. The orifice plate calibration is:

$$\begin{aligned} \text{Re} > 9350 \qquad & C = 2.76 \\ 9350 > \text{Re} > 4350 \qquad & C = 2.76 + 0.24 \times (\text{Re} - 4350)/5000 \\ \text{Re} < 4350 \qquad & C = 4.1 - 1.34\ \text{Re}/5100 \end{aligned}$$

It was estimated that the greatest error that would result from this approximation was 10% in the calibration constant. At a Reynolds number of 5000 this corresponds to an error in axial velcotiy of 0.8 m/s. In the worst case, with the compressor running at 1000 RPM, this would produce an error in flow coefficient of 0.027. This was considered to be acceptable.

Throughout the experiments, whenever the compressor was operating in the unstalled flow regime, the flow coefficient obtained from the orifice plate measurements was compared to that obtained from measurements of the inlet total and static pressure. These were found for the most part to differ by less than 1%, and in all cases to differ by no more than 4%.

The final check of the orifice calibration was to ensure that the porous plates upstream of the orifice plate removed all the swirl from the flow when the compressor was stalled. If the streamlines upstream of the

orifice plate are straight and parallel for all compressor flow regimes, then the ratio of the pressure drop across the orifice plate to the pressure drop in the ducting downstream of it should be a constant irrespective of the flow regime. In other words the orifice plate and the ducting downstream of it are passive elements, as long as the fan rotor is locked, and can be regarded as resistances, and the pressure drops are analogous to voltage differences. The results of this test are presented in Fig. 19.

Below a Reynolds number of 7500 there was considerable scatter as the pressure downstream of the orifice plate became of the same magnitude as the transducer error. Above this value, however, the data collapses satisfactorily to a constant value of 2.45. It should be noted that the abscissa is the Reynolds number based on velocity through the small orifices and orifice diameter, and that the data presented was taken at four different rotational speeds. There are, therefore, several regions of the graph which represent stalled flow at one speed and unstalled flow at a lower speed. Points taken in the unstalled flow regime are plotted as 'x's and those taken in the stalled flow regime are plotted as 'o's.

The system was also checked for leaks by comparing the calibration constants when 1) only the fan was running, 2) the compressor was throttled by the throttle valve, and 3) the compressor was throttled by the fan inlet guide vanes. This gave a range of pressure at the upstream orifice plate station of 6000 Pa below to 5400 Pa above ambient pressure. The calibration constant was found to vary by 2% in this range, which was considered satisfactory.

A check of the circumferential distributions of inlet total and static pressure was also carried out. The total pressure was found to vary by less than 1% of the inlet dynamic head at all throttle positions in unstalled flow. However, there was found to be a two lobed static pressure distortion of at most 5% of the inlet dynamic head. This was most severe when the throttle was in the fully open position and thus was not considered to affect the performance of the compressor near stall.

3.5 Acquisition of Overall Performance Data

In this phase of the project, speedline data was taken at five different rotational speeds - 1170, 1700, 2000, 2500 and 3000 RPM. This gave a range of Reynolds number based on inlet relative velocity at the stall point and on first stage rotor chord of 45.2 mm of 0.81×10^5 to 2.08×10^5. Data was also taken at 1800 RPM with the fan running to change the downstream throttle characteristic. At each speed the throttle was moved in from the fully open position to fully closed and back out again until the compressor unstalled. In this way complete speedlines including the stall-unstall hysteresis were obtained.

The data is presented in non-dimensional form; mass flow is presented as $C_x / \bar{u}$ (where $\bar{u}$ is the mean blade speed), pressure differences are non-dimensionalized by $1/2\ \rho\ \bar{u}^2$ and temperature differences are non-dimensionalized by $1/2\ \bar{u}^2/C_p$. The torques are corrected for tare torque from data in [12] and non-dimensionalized by $1/2\ \rho \bar{u}^2 A_c R_m$. The outputs of

the data reduction program are flow coefficient, total to static pressure rise coefficient, total to total pressure rise coefficient (measured both immediately after the last stator and at the downstream station), static to static pressure rise coefficient (measured from both before and after the inlet guide vanes), stage and blade row pressure and temperature rise coefficients and the torque coefficient. These results are presented in Chapter IV. Some general notes on running the system are presented in Appendix C.

3.6 High Response Instrumentation and Data Acquisition Systems

Although little high response data has been taken as yet, some thought has been given to the problem. It is proposed to take the high response data using the phase locked averaging technique of Day [2]. Measurements of velocity, flow direction, total pressure and tip static pressure are required. Day's technique involved rotating on axial hot wire and a pitot tube through 10° increments and finding the maxima at each data point to give velocity and flow direction.

It appears, however, that a quantity of interest may be the rapid changes that occur over several blade passages as one enters and leaves the stall cell, and it is proposed to sample at a high enough rate to provide good resolution in these regions. This would produce a large amount of data using Day's technique and it is thus proposed to use a hot wire inclined at 54.7° to its axis and a Kiel probe. Rotating the hot wire twice

through 120° gives three mutually perpendicular directions [16] and thus velocity and flow direction (to values in four quadrants) can be determined. The latter can be uniquely determined using the Kiel probe which, due to its insensitivity to flow direction can be rotated in increments of 30° to 35°. This will greatly reduce the amount of data handled and will also allow the radial component of the velocity to be measured.

One problem with this method is that the range of flow directions that can be measured is limited by probe holder effects and uncertainty in the accuracy of the calibration used for flows that are not perpendicular to the hot wire. A program has been developed to determine what range of flow directions can be measured using the technique (see Appendix A). When the hot wire has been calibrated, this program and the data presented by Day [2] can be used to determine whether the technique is acceptable.

Figure 20 shows the high response pressure probes that have been built for this work. Both probes use Gaeltec $\pm$1 psid transducers. The total pressure probe is an adapted Kiel probe with the transducer mounted just above the sensing head in the probe stem. The larger sensing head was inserted to increase frequency response. The Helmholtz frequency of this probe was calculated to be 6.1 kHz. The samping frequency will be limited by this and if greater resolution is required a probe with higher frequency response will have to be made.

A programmable real time clock has been installed in the computer. This will be used to control data acquisition. Using the A/D converter in

external mode the clock will set the sampling frequency and data acquisition will be started by using whichever of the hot wire or pressure signals gives the most consistent waveform to set the clock's Schmitt trigger.

CHAPTER IV

PRESENTATION AND DISCUSSION OF RESULTS

In this chapter the compressor overall performance data is presented and discussed.

4.1 Pressure Rise Characteristics

The compressor pressure rise characteristics are presented in Figs. 21 to 26. The pressure rise coefficients (pressure rise divided by $1/2\ \rho\bar{u}^2$) are plotted on the vertical axes and flow coefficient ($C_x/\bar{u}$) on the horizontal axes. The characteristics have the same general form at all speeds, as would be expected since Mach number and Reynolds number effects are small. One interesting feature is a "secondary characteristic" on the double valued part of the speedline. Such characteristics have been observed before by Freeman [17] and are discussed below.

The total to static pressure rise characteristics measured at 2500, 2000 and 1170 RPM are shown in Figs. 21 to 23. On these graphs the data points obtained as the throttle valve was closed are plotted as 'x's, and those obtained as the throttle was reopened are plotted as 'o's. It can be noted that the minimum pressure rise coefficient in stall tends to decrease as the speed increases (from 0.75 to 1170 RPM to 0.66 at 3000 RPM).

The total to total pressure rise characteristics as given by 1) probes 5 1/4" downstream of the last stator and 2) probes one compressor diameter downstream of the last stator, are both displayed in Fig. 24. The data measured after the last stator is plotted as 'x's and that measured one diameter downstream is plotted as 'o's. The two characteristics match well in the unstalled flow regime and also on the double valued part of the characteristic. For most of the deep stall regime, however, the total to total pressure rise characteristic measured at the downstream station is about 15% greater than that measured after the last stator. This difference decreases as the shut off point is approached and the two characteristics seem to converge at very low flow coefficients. A possible explanation of this may be that the static pressure distribution at the compressor exit tends to decrease the size of the stall cell as one moves downstream. The total pressure probes measure an area average of the total pressure in the unstalled part of the flow, which thus increases as the size of the stall cell decreases. However, it could also be due to changes in the stator exit discharge profile. This can be examined in future tests. When the stall cell covers either very little of the annulus or most of the annulus, the change in this area averaged total pressure and appears to be negligible.

Figure 25 shows the static to static pressure rise characteristics measured using taps placed 1) in front of and 2) behind the inlet guide vanes. Pressure rise coefficients measured from in front of the inlet guide vanes are plotted as 'x's and those measured from behind them

are plotted as 'o's. As expected the static to static pressure rise coefficient measured from in front of the inlet guide vanes is less than that measured from behind them in the unstalled flow regime. As the flow coefficient is decreased, however, the two characteristics cross and near the shut off point the static to static pressure rise coefficient measured from in front of the inlet guide vanes is substantially larger than that measured from behind them.

In stall it is thought that the time averaged static pressure rise across a blade row is the weighted average of the pressure rise in the stall cell and the pressure rise in the unstalled part of the flow. This crossing of the static to static pressure rise characteristics in deep stall shows that the static pressure rise across the inlet guide vanes increases as the stall cell size increases. This, therefore, supports the idea that the pressure rise in the stall cell occurs ahead of the rotors [2].

Further support for this is shown in Fig. 26, in which the static to static pressure rise coefficients for each stage are plotted on the same axes. It can be seen that the third stage (having no rotor behind it) produces a far lower pressure rise in stall than the first and second stages.

Figure 27 shows the distribution of static pressure through the compressor at a flow coefficient of 0.044, at which point the stall cell covers approximately 90% of the annulus. In this graph the horizontal

axis represents axial location (the numbers representing stations after successive blade rows), and the vertical axis the static pressure referenced to the inlet static pressure and nondimensionalized by $1/2\ \rho\ \bar{u}^{2}$. This graph shows clearly the large pressure rises across the inlet guide vanes and the first two stators, the relatively small pressure rises across the rotors, and the poor performance of the last stage.

4.2 The Effect of Reynolds Number on Stall Point

Table 2 presents a summary of the flow coefficients at the stall and unstall points and at the first points after stall and unstall.

The scatter in the data (especially for the unstall points) is due to the difficulty in accurately controlling the throttle position around these points with the present system. In the region of the stall and unstall points the compressor operating point is very sensitive to the position of the throttle valve and thus it was often difficult to obtain these points with as much accuracy as was desired.

It appears that in the range tested the Reynolds number has no effect on the stall or unstall points. However, there is a significant increase in the flow coefficient of the first point after stall as the Reynolds number decreases. This is believed to be due to a combination of the change in density and a change in effective throttle area when the compressor stalls. The effective throttle area is defined in Appendix D, and is basically the inverse of the constant of proportionality relating the pressure drop across the

throttle to the local dynamic head multiplied by the throttle to compressor area ratio.

Assuming this effective throttle area changes very little between the stall point and the first point after stall, one can calculate the flow coefficient of the first point after stall using the other data taken at this point and data taken at the stall points (see Appendix D). In this way the effect of changes of density on the flow coefficient of the first point after stall was investigated.

Figure 28 shows a plot of the predicted flow coefficients ('x's) and those actually measured ('o's) against rotational speed. It should be noted that the slightly anomalous values of stall point flow coefficient measured at 3000 and 1700 RPM were corrected to agree with the other values obtained for the purposes of these calculations. It can be seen that the changes in density do cause a slight increase in flow coefficient as the speed decreases, but it is not sufficient to account for the results observed.

Figure 29 shows the nondimensional effective throttle area measured at the stall points ('x's) and at the first points after stall ('o's) plotted against rotational speed. It is not thought that changes in the actual throttle area cause the marked differences in the effective throttle area observed. Changes in actual throttle area could be brought about by the differences in the absolute values of the pressure drops when the compressor stalls, and some hysteresis in the valve drive

system. However, this could only be caused by the threads of the power screw and nut (refer to Fig. 14), as the gear in the gearmotor was a worm gear. This was not considered sufficient to account for the observed variations.

The change in effective throttle area is thought, instead, to be due to slight changes in flow regime, for example in the absolute magnitude of the swirl associated with rotating stall at different rotational speeds. The flow through the throttle is no longer axisymmetric when the compressor operates in stall and it is thought its performance is thus modified, altering the constant K_T in Eq. 1 of Appendix D. It should be noted that this effect should not depend on the ratio of axial velocity to swirl velocity, as this should scale with the rotational speed.

This hypothesis is supported in part by the fact that the flow coefficients of the first points after unstall show no consistent variation and are fairly uniform. This is to be expected if the change in effective throttle area is indeed due to a swirl effect, as the magnitude of the swirl at the unstall point is far less than that at the first point after stall. The changes in swirl, therefore, are far less significant in the unstalling process than in the stalling process.

4.3 The Effect of the Throttle Characteristic on the Shape of the Compressor Characteristic

Figure 30 shows the total to static pressure rise characteristics measured at 1700 RPM (plotted as 'x's) and measured at 1800 RPM with the exit fan running so that the throttle line is altered (plotted as 'o's). For clarity the first points after stall and unstall have been plotted as 'z's.

As can be seen little change in performance was observed. Table 2 shows that the flow coefficients of the first point after stall and the first point after unstall are substantially increased and reduced respectively, and this is consistent with the increase in the slope of the throttle characteristic produced by the exit fan.

It has been conjectured that by steepening the slope of the throttle characteristic the blockage at the stall point might be reduced enough to change the stalled flow regime. However, estimating blockages from the speedlines it appears that for this to occur the throttle characteristics would have to be nearly vertical, and this could not readily be achieved with the system in its present configuration.

4.4 Torque Characteristic

The torque characteristics obtained in these tests were all discontinuous and showed that the compressor absorbed considerably less torque

in stall than at the design point. The torque characteristics measured at 2500 and 1700 RPM, and also at 1800 RPM with the exit fan running are shown in Figs. 31 to 33. In these graphs the vertical axes are the absolute value of torque nondimensionalized by $1/2\ \rho\ \bar{u}^{-2}\ A_c R_m$ and the horizontal axes are the flow coefficient. Points taken as the throttle was closed are plotted as 'x's and those taken as the throttle was reopened are plotted as 'o's.

Note that there are virtually no differences in the three characteristics and that at most points in stall the compressor absorbs less torque than for the same pressure rise when operating on the unstalled part of the characteristic. The latter can only occur if the momentum transfer in the stall cell is less than that in the unstalled part of the flow, i.e., if the mass flow rate in the stall cell is very small or if the change in tangential velocity across the rotors in the stall cell is small. What combination of these mechanisms is responsible for this effect cannot be determined until the high response data is taken, and information about the detailed structure of the stalled flow is obtained. It is possible, however, that this effect is associated with the low aspect ratio of the blading.

It was shown in [2] that there are strong radial pressure gradients in the stall cell, suggesting that fluid in the stall cell is centrifuged outwards by the rotors. From an examination of the stall cell size and the temperature distributions near the shut off point obtained in these

tests (see ection 4.5) it has been concluded that for this compressor there is a net backflow in the stall cell, though its magnitude has not yet been determined. It is possible that due to the relatively longer length of a low aspect ratio blade the centrifuging effect is enhanced. It is suggested that due to the stagger of a rotor blade the magnitude of the backflow is decreased at the tip by this centrifuging effect, and that this results in a substantially reduced average mass flow across the rotors in the stall cell. This, as stated, would reduce the momentum transfer across the rotors and thus the torque absorbed by the compressor.

4.5 Overall Stall Cell Properties

Figures 34 and 35 show measurements of stall cell size and speed plotted as functions of flow coefficient. Stall cell size is presented as the percentage of the annulus area occupied by the stall cell and stall cell speed is presented as the percentage of the compressor rotational speed at which the stall cell is rotating. Again the 'x's represent points taken as the throttle was closed, and the 'o's point taken as the throttle was reopened. There are several points of interest in these plots.

Firstly, there seems to be a limit to the size of the stall cell of 88% of the compressor annulus, suggesting that there is a net backflow in the stall cell. This is supported by the temperature distribution through the compressor near the shut off point. A typical temperature distribution near shut off is shown in Fig. 36. This was taken at a flow

coefficient of 0.075 when the stall cell covered 88% of the annulus. The horizontal axis represents axial position (the numbers representing stations after successive blade rows), and the vertical axis represents the absolute value of total temperature referenced to the inlet total temperature and nondimensionalized by $1/2\ \overline{u}^{\,2}/C_p$. Since the total temperature of the fluid can only be raised through work done on it by the rotors there must be a net backflow in the stall cell to produce the overall decrease in temperature observed between the first rotor and the compressor exit. This is consistent with Day's data [2,6], the present compressor having a design coefficient of 0.67 which lies between the intermediate (0.55) and high (1.00) design flow coefficient builds tested in that work.

Secondly, the stall cell speed decreases towards the shut off point. Other data [2,18] has shown the stall cell speed either remaining constant or increasing as shut off is approached.

Thirdly, on the double valued part of the characteristic between flow coefficients of approximately 0.5 and 0.6 the stall cell size appears to be relatively constant as a function of flow coefficient, while the stall cell speed increases. On the "secondary characteristic" (above a flow coefficient of about 0.61) the stall cell size rapidly decreases while the stall cell speed remains constant.

The fourth and most interesting observation is that the peak of the "secondary characteristic" occurs when the stall cell occupies about 30% of the compressor annulus, the so called critical value of blockage.

For flow coefficients above this, where the blockage is less than 30%, extensive investigation with the hot wire showed that the stall cell still covered the complete annulus height, and thus appeared to be a full span stall cell.

It was initially thought that the "secondary characteristic" and this "full span" stall cell with less than 30% blockage could be due to the stages being mismatched. The compressor was being run below its design speed of 5900 RPM, and it was thought that the first stage could be more severaly stalled than the last stage. The stage characteristics (Fig. 26) show that there is a degree of mismatching, however by placing the hot wire behind the last stator, at a flow coefficient of 0.64 the stall cell was found to extend through the whole length of the compressor and also to be the same size at inlet and exit. High response total pressure and velocity data will be taken here in the second phase of the project in an attempt to confirm this.

4.6 Temperature Distribution in Stall

The temperature distribution near the shut off point has already been presented (Fig. 36) to support the conclusion that in this compressor there is a net backflow in the stall cell. Figure 37 shows another temperature distribution in stall taken at a higher flow coefficient of 0.262.

There are two points to note here. The first is that there are temperature rises across some of the stators. The second is that these temperature rises occur only across the first stator at a flow coefficient of 0.075 but occur across both the first and second stators at the higher flow coefficient of 0.262.

No ready explanation can be found for this but the fact that in both cases there is no temperature rise across the third stator suggests that it is in some way due to the high temperature fluid that leaves the leading edges of the rotors.

4.7 The "Secondary Characteristic"

As stated previously, secondary characteristics have been observed before [17], but no attempts have been made to explain them. In this regard it is pertinent to make some general observations about the compressor's operation in this regime. The two features that distinguish this flow regime from other stalled flow regimes are that 1) the pressure rise coefficients decrease markedly with increasing flow coefficient and 2) the stall cell appears to be a full span stall cell that presents less than 30% blockage. The former is sometimes observed when an axisymmetric stall exists at shut off . As the throttle is reopened and the axisymmetric stall becomes a rotating stall, a decrease in the pressure rise coefficients has been observed [2]. The latter has not been observed before and contradicts the established idea that below about 30% blockage a full span stall cell cannot exit [1,2]. It is therefore interesting to note that the peak of

the secondary characteristic, or the point at which the pressure rise coefficients start to decrease, occurs approximately at the 30% blockage point (see Fig. 34).

These observations suggest that the mode of operation in this flow regime is in some way basically different from that in other stalled flow regimes. A possible explanation of this is that the mechanism of stall cell propagation is different.

As no high response data is available as yet, it is possible only to speculate upon how the mechanism of stall cell propagation may differ in this flow regime. It is suggested that due to the low aspect ratio of the rotors, separated flow from the endwall region may be centrifuged from hub to tip to cause blockage in the blade passages. The propagation speed would be determined primarily by the rate at which this stalled fluid was centrifuged outwards and, assuming zero axial velocity in the stall cell, would depend solely on the rotor blade speed and, as observed, be independent of the average flow coefficient.

CHAPTER V

SUMMARY AND CONCLUSIONS

5.1 Summary

A new facility was designed and constructed for the testing of low speed multistage compressors. The system can drive compressors up to roughly 3000 RPM and with a maximum of 175 HP. The system was designed so that the mass flow rate through the compressor could be measured when was operating in rotating stall using a downstream orifice plate.

In this investigation compressor speedlines were measured at five different rotational speeds. Limited high response data was also taken to determine the size and rotational speed of the stall cell.

5.2 Conclusions

The shape of the compressor characteristics have been found to differ from those previously published in that a "secondary characteristic" has been observed on the double valued part of the speedlines. This has been shown to correspond to a mode of compressor operation seemingly different from those of other stalled flow regimes. In this regime a full span stall cell presenting a blockage of less than 30% propagates around the annulus, and the pressure rise across the compressor decreases sharply with increasing flow coefficient.

It has been found that the torque characteristic is discontinuous and that the compressor absorbs less torque when stalled than when operating on the unstalled part of the characteristic. It was concluded that this is due to lower momentum transfer across the rotor in the stall cell. This may be due to the rather low aspect ratio of the compressor. If this is so, it appears aspect ratio can be an important design parameter as far as the detailed structure of the flow in the stall cell is concerned.

In the range 0.81×10^5 to 2.08×10^5 no Reynolds number effect was observed on either the stall or unstall points. However, the flow coefficient of the first point in stall was observed to increase as the rotational speed of the compressor decreased.

Changing the slope of the throttle line decreased the blockage at stall, but did not change the stalled flow regime.

From the measurements of stall cell size and the temperature distribution through the compressor near shut off, it was concluded that this compressor operates with a net backflow in the stall cell.

The observation that the pressure rise in the stall cell occurs ahead of the rotors, made in [6], was supported by the static to static pressure rise characteristics and the pressure distribution measured near shut off.

TABLE 2

SUMMARY OF THE FLOW COEFFICIENTS AT THE STALL POINT, THE FIRST POINT AFTER STALL, THE UNSTALL POINT AND THE FIRST POINT AFTER UNSTALL

Reynolds Number[1]	Flow Coefficient			
	Stall Point	First Point After Stall	Unstall Point	First Point After Unstall
2.08×10^5	0.502	0.269	-[2]	-
1.73×10^5	0.487	0.274	0.656	0.717
1.39×10^5	0.482	0.295	0.653	0.725
1.18×10^5	0.495	0.326	0.659	0.694
0.81×10^5	0.487	0.354	0.633	0.679
1.25×10^5 (with exit fan)	0.485	0.421	0.645	0.660

[1] Based on first stage rotor velocity triangles at the stall point.

[2] Due to bearing overheating during this run, these points were not measured.

CHAPTER VI

SUGGESTIONS FOR FUTURE WORK

The following recommendations are made for work on this facility:

1) A study of the static pressure distribution downstream of the compressor be carried out to investigate the increase in the total pressure measured as one moves downstream. Also in this study it would be useful to investigate the changes in effective throttle area with rotational speed to ensure that this is not a system error.
2) A more extensive investigation of the effect of the throttle characteristic on the shape of the compressor speedlines be carried out. In particular an attempt shhould be made to reduce the blockage at the stall point to below 30%.
3) When high response data is taken the first priority should be to confirm that a full span stall cell exists on the secondary characteristic, and to determine its structure. In addition the radial velocities and radial static pressure gradients in the stall cell should be investigated to determine the relative importance of centrifugal effects in the stall cell. Also the leading and trailing edges of the stall cell should be investigated to determine the nature of the transitions between stalled flow and unstalled flow.

In general it is recommended that parametric studies of the effect of aspect ratio and hub to tip ratio on overall compressor performance would be useful. However, it is also thought that the fluid mechanics of

rotating stall will only be understood by gaining a knowledge of the flow in the rotor passages in the stall cell.

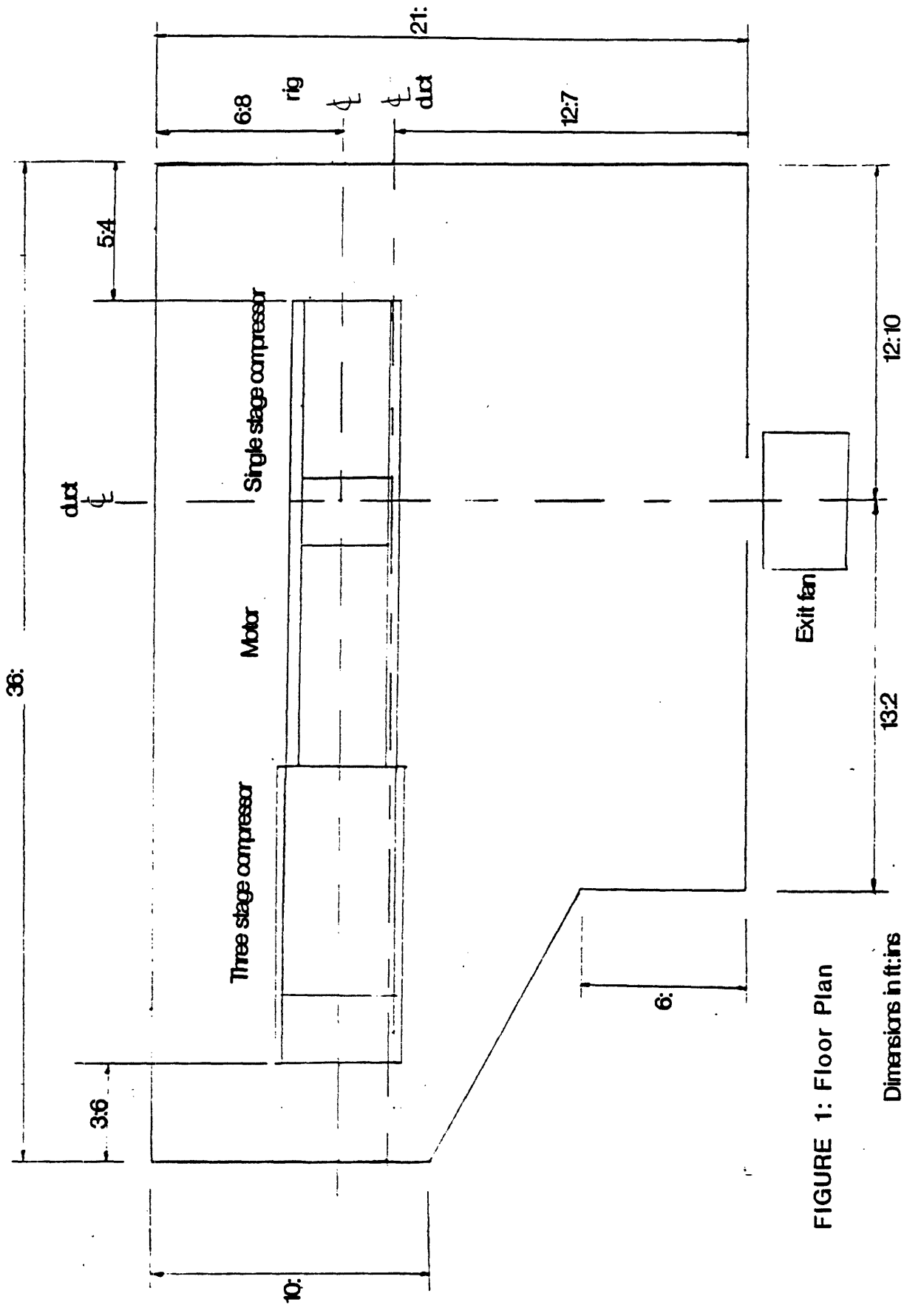

FIGURE 1: Floor Plan

Dimensions in ft:ins

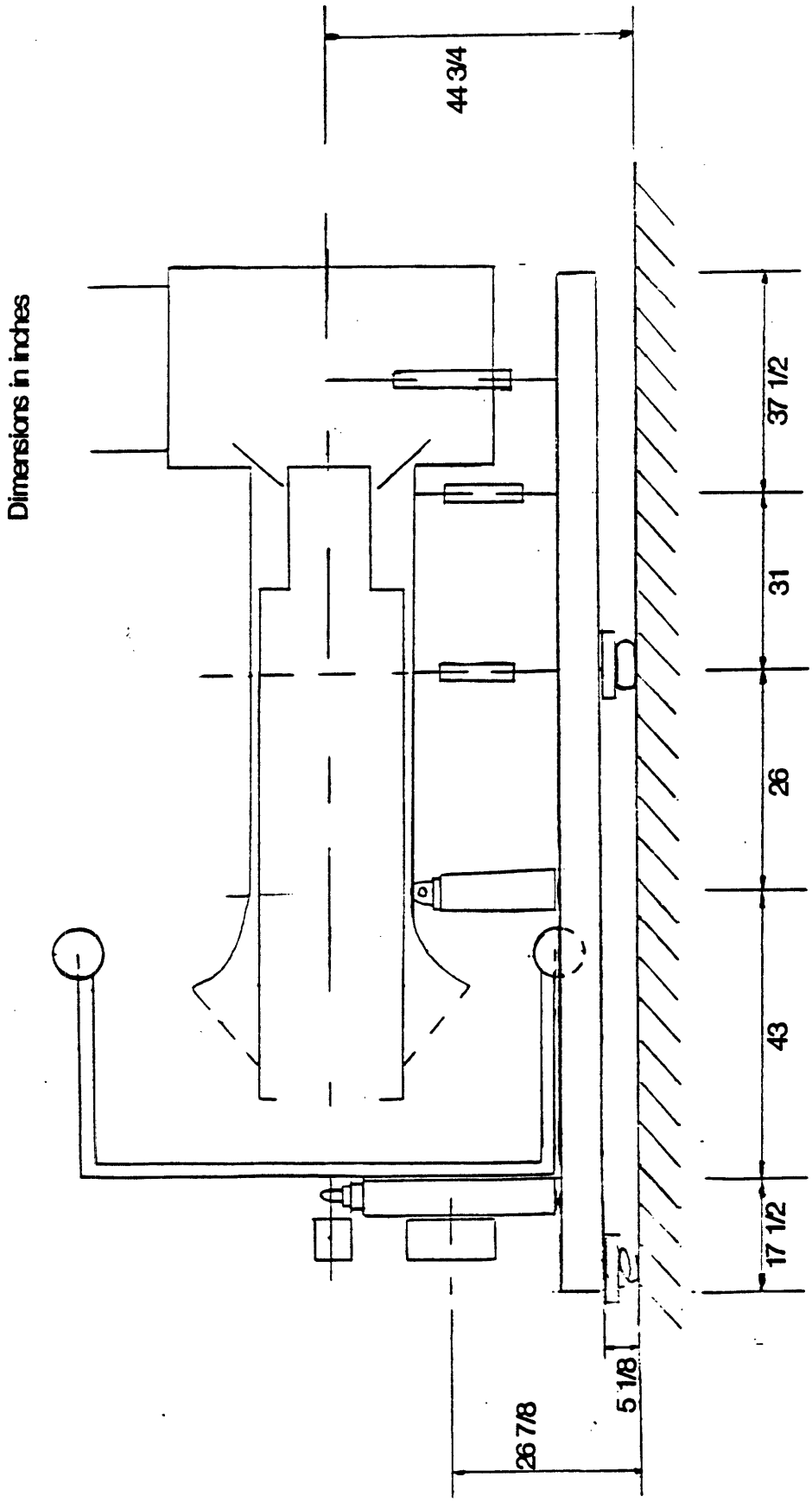

FIGURE 2: Side View of Rig

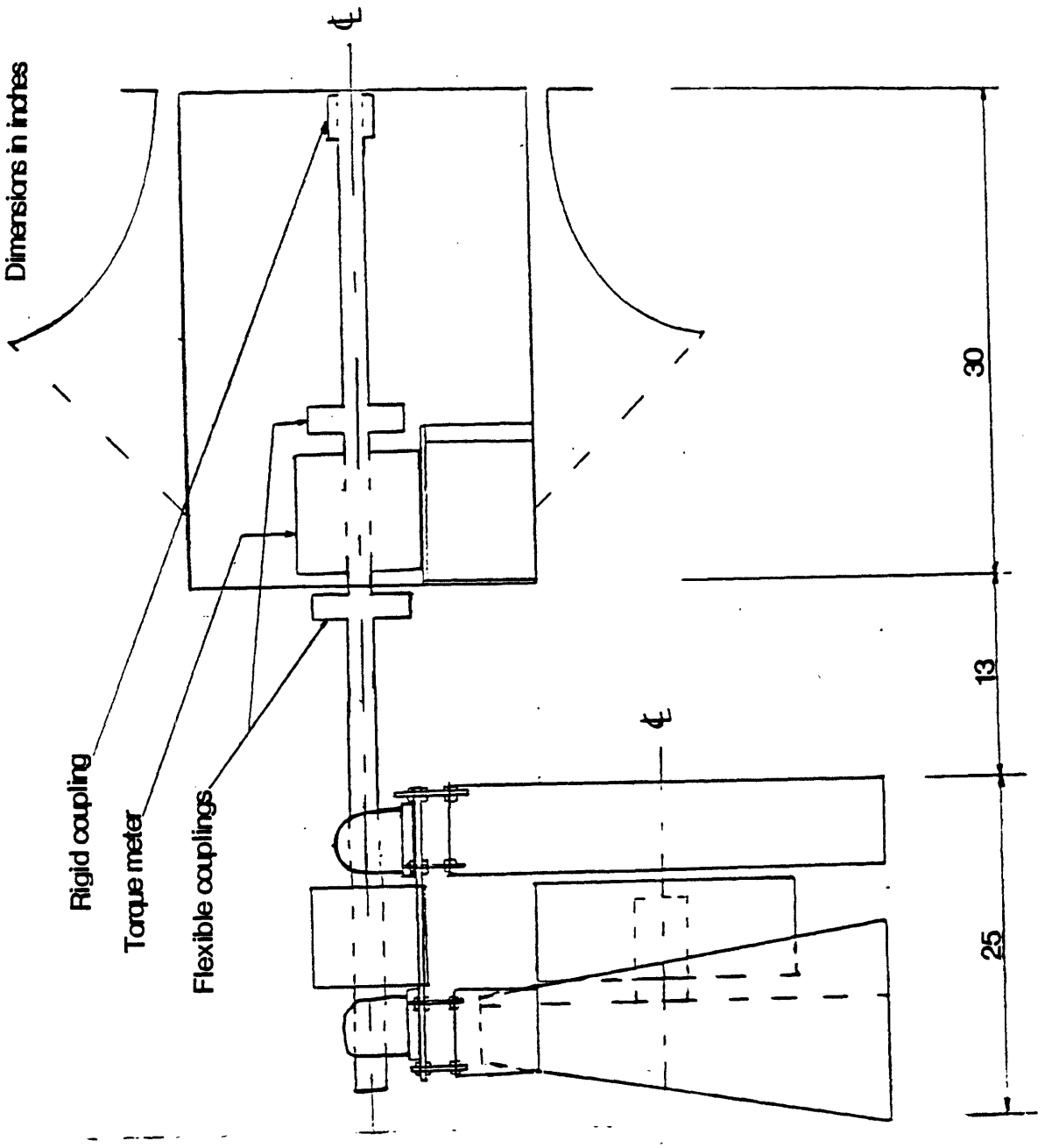

FIGURE 3: Drive System

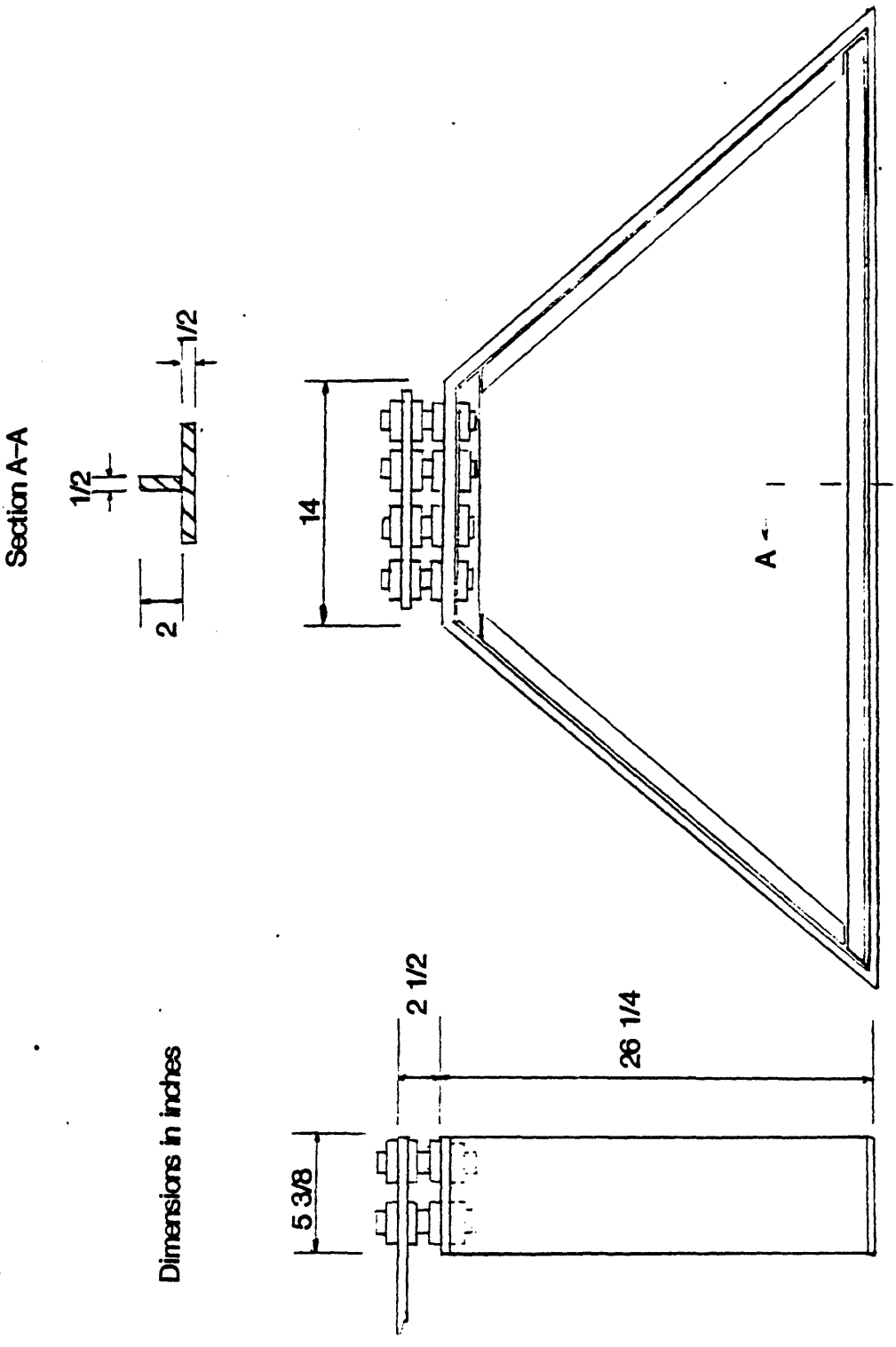

FIGURE 4: Front Pillow Block Mounting

Dimensions in inches

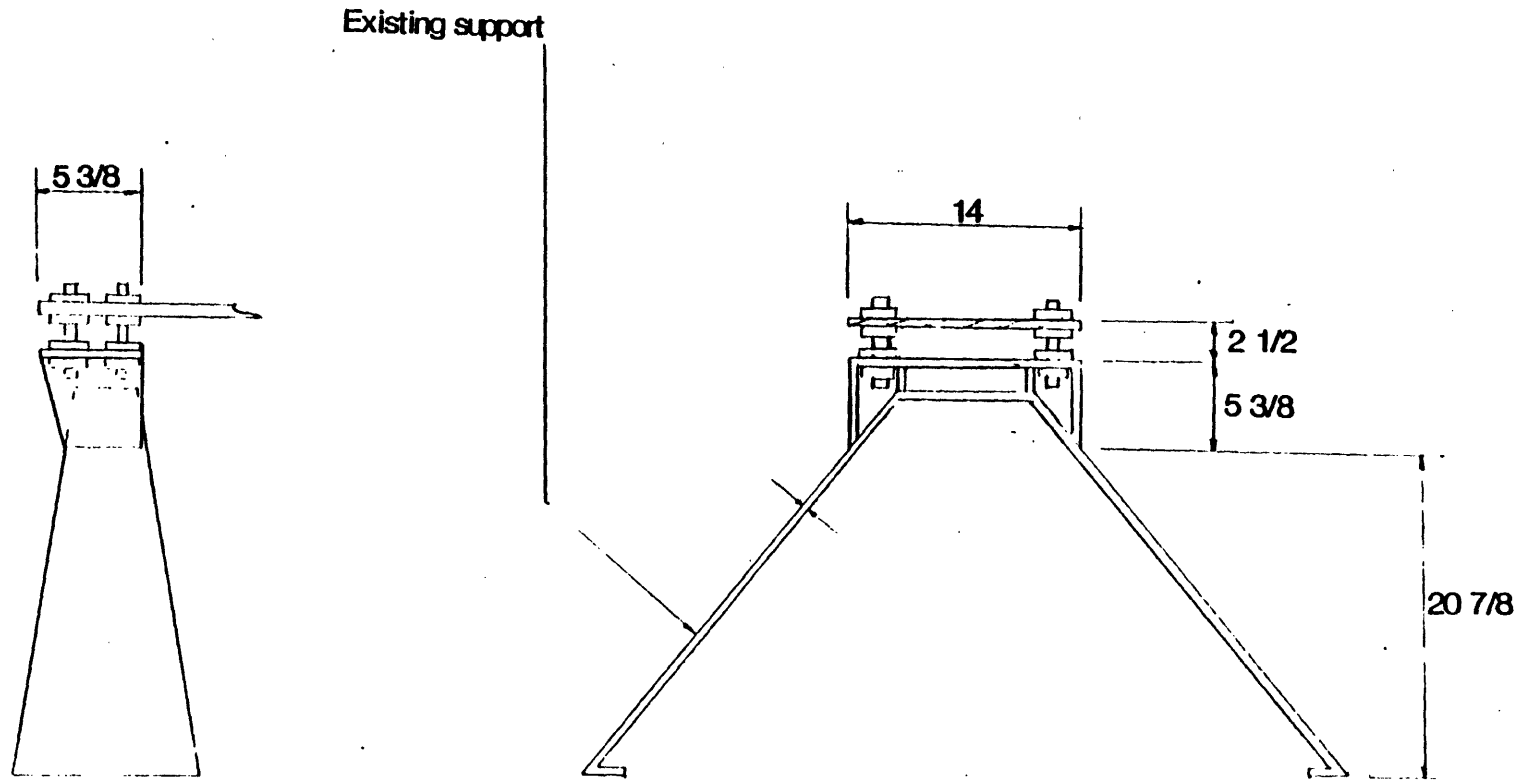

FIGURE 5: Rear Pillow Block Mounting

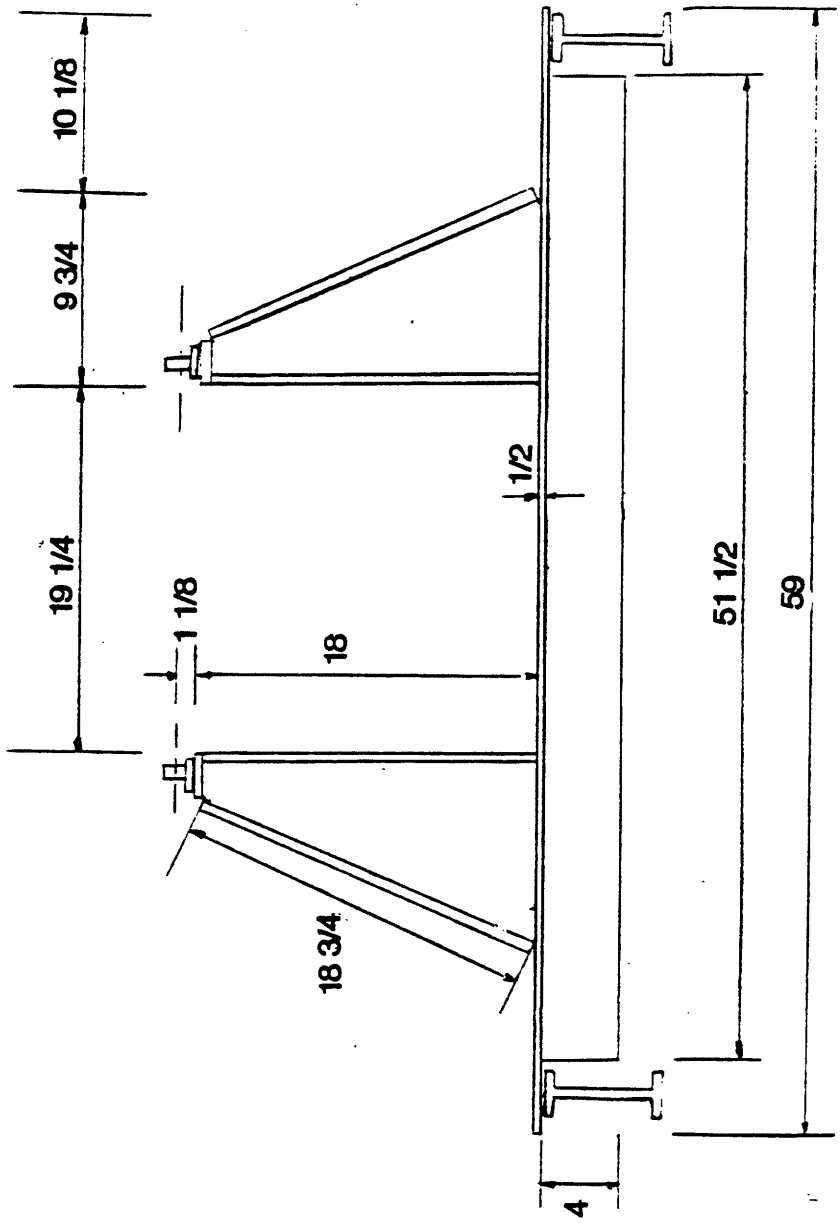

FIGURE 6: Inlet Flange Mounting

Dimensions in inches

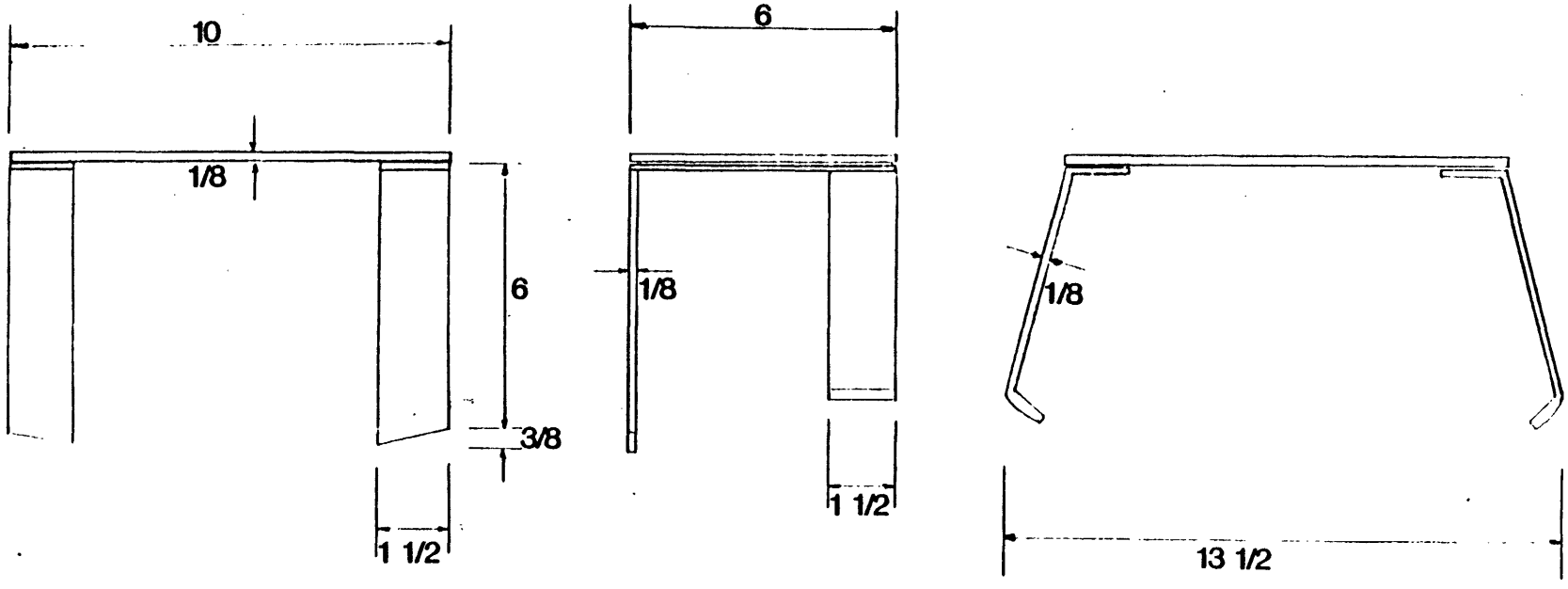

FIGURE 7: Torque Meter Mounting

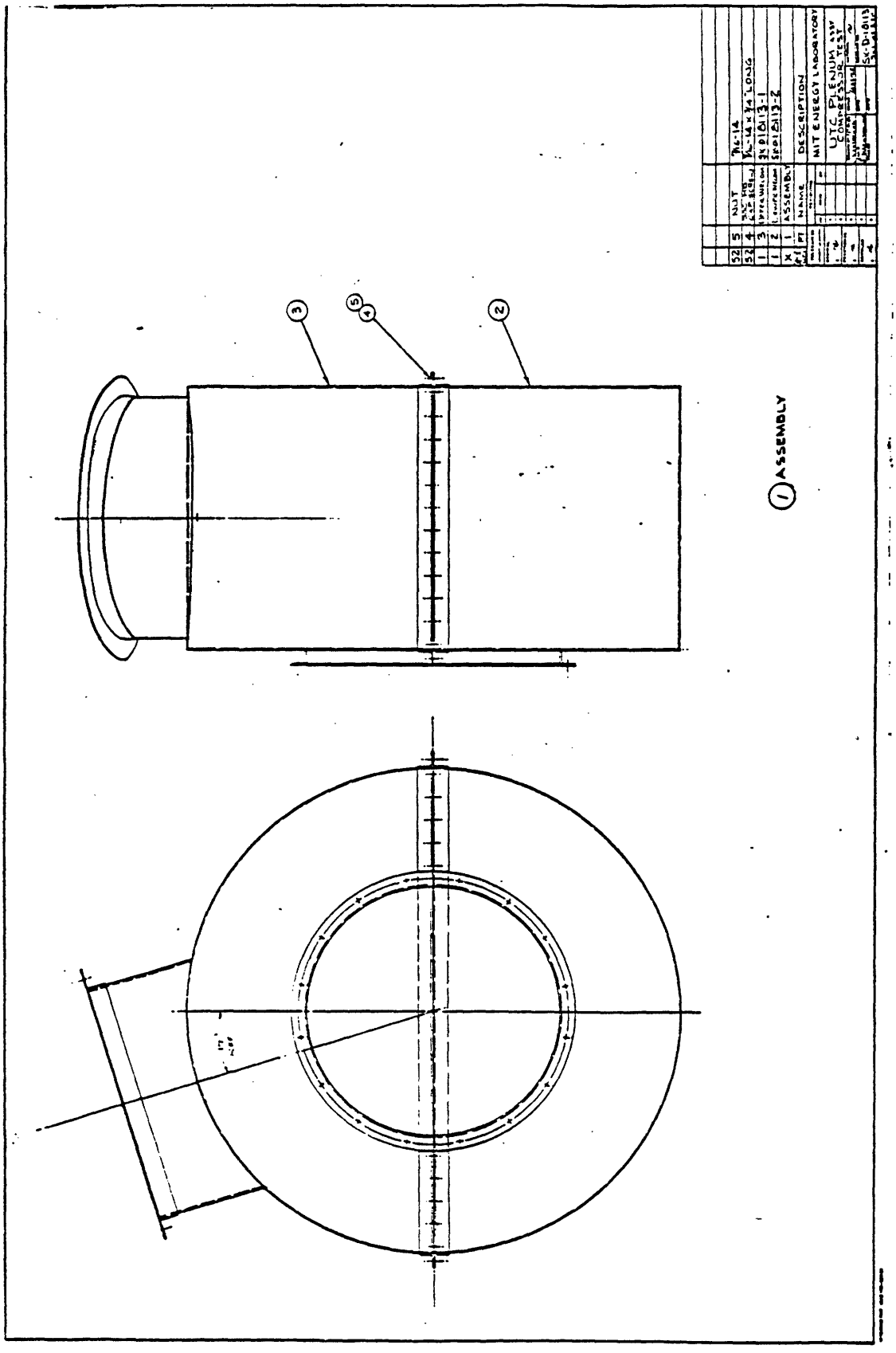

FIGURE 8: Assembly Drawing of Plenum for Three Stage Compressor

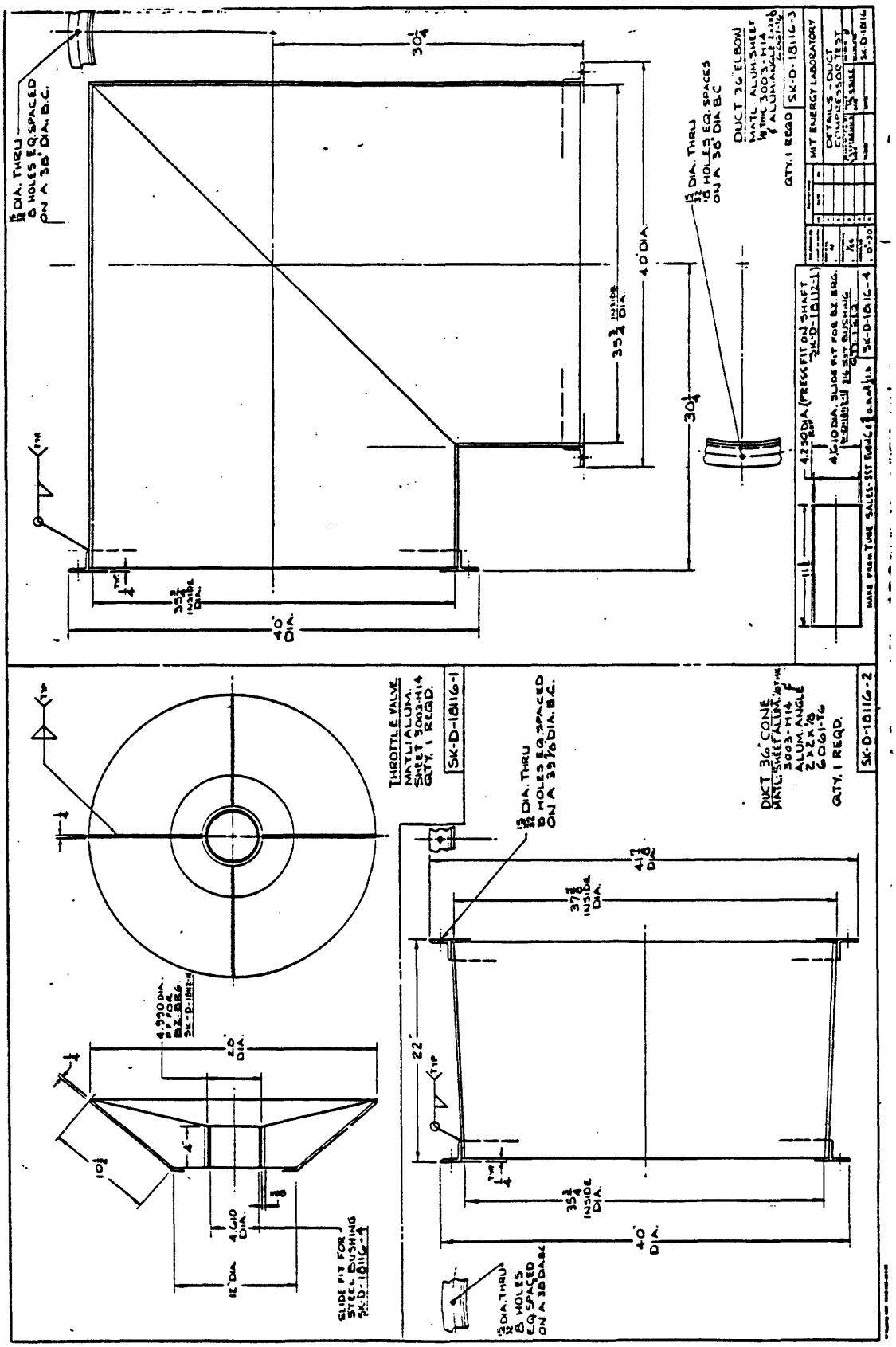

FIGURE 9: Drawing of Duct Details

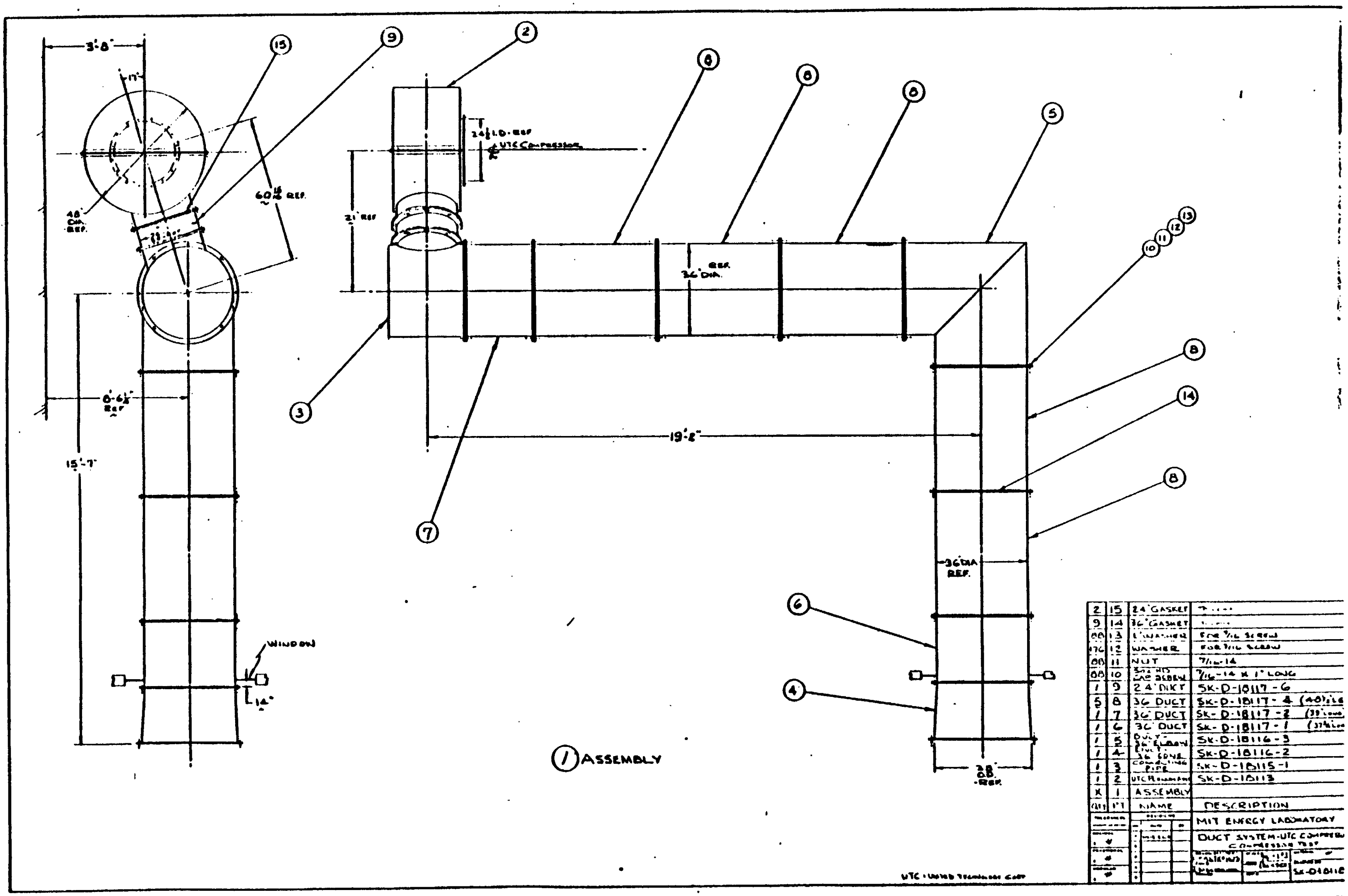

FIGURE 10: Assembly Drawing of Duct Arrangement for Three Stage Compressor

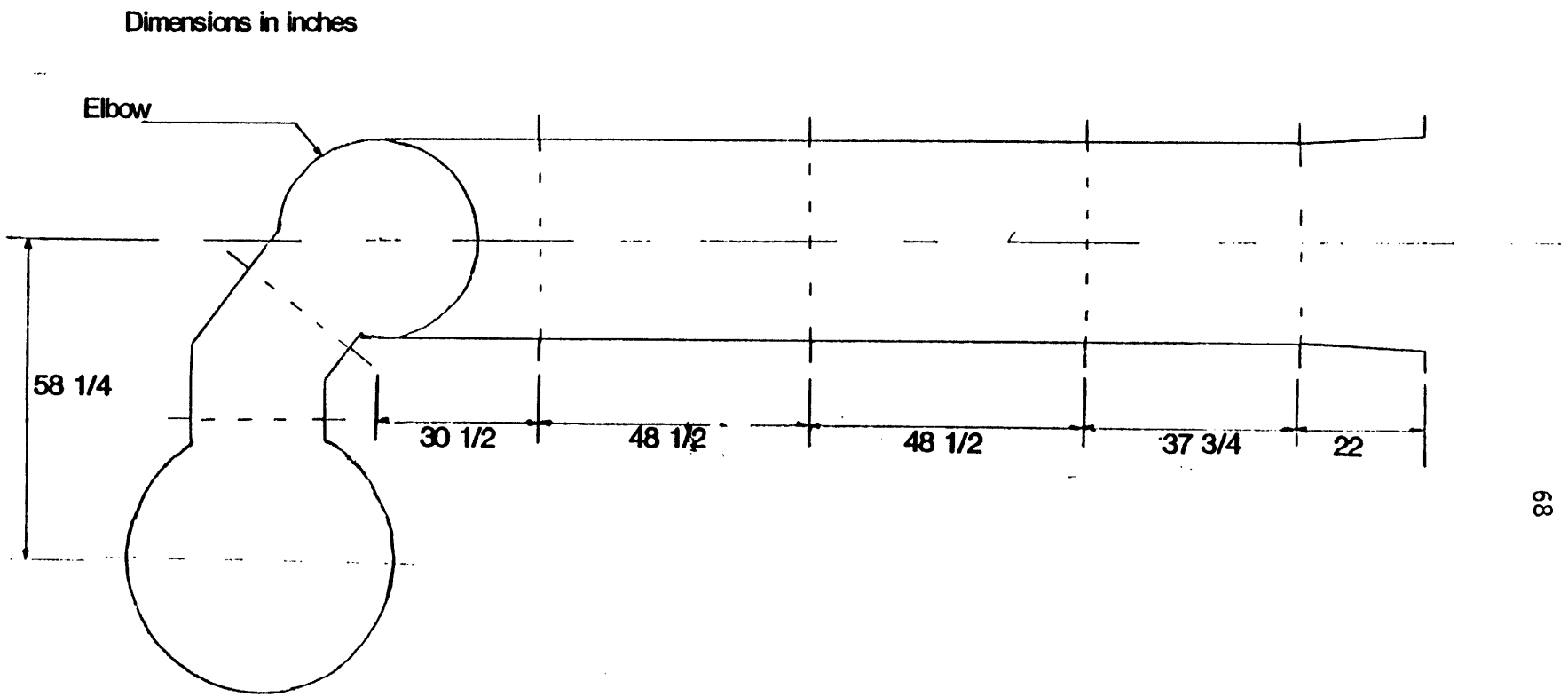

FIGURE 11: Duct Arrangement for Single Stage Compressor

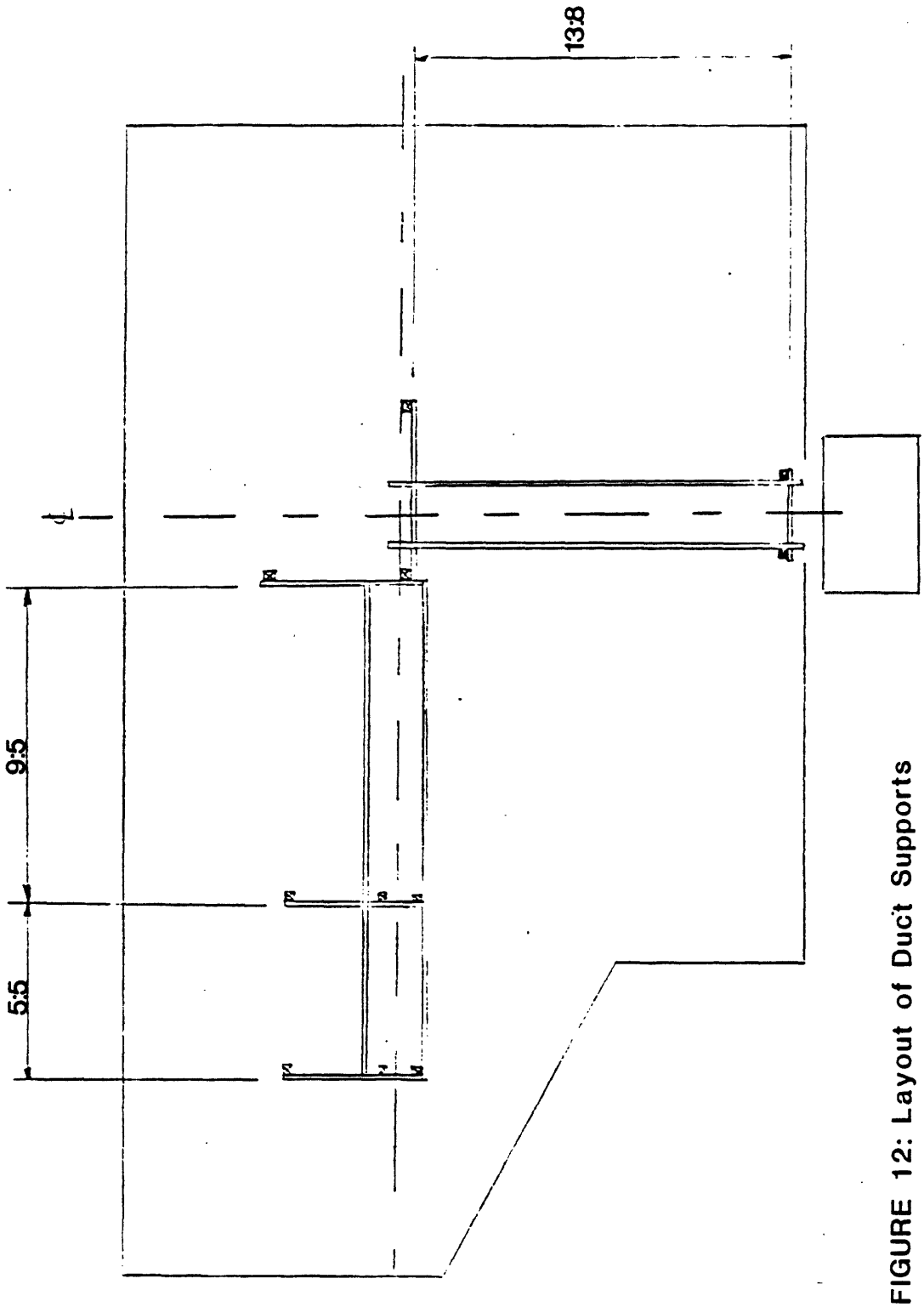

FIGURE 12: Layout of Duct Supports

Dimensions in ft:ins

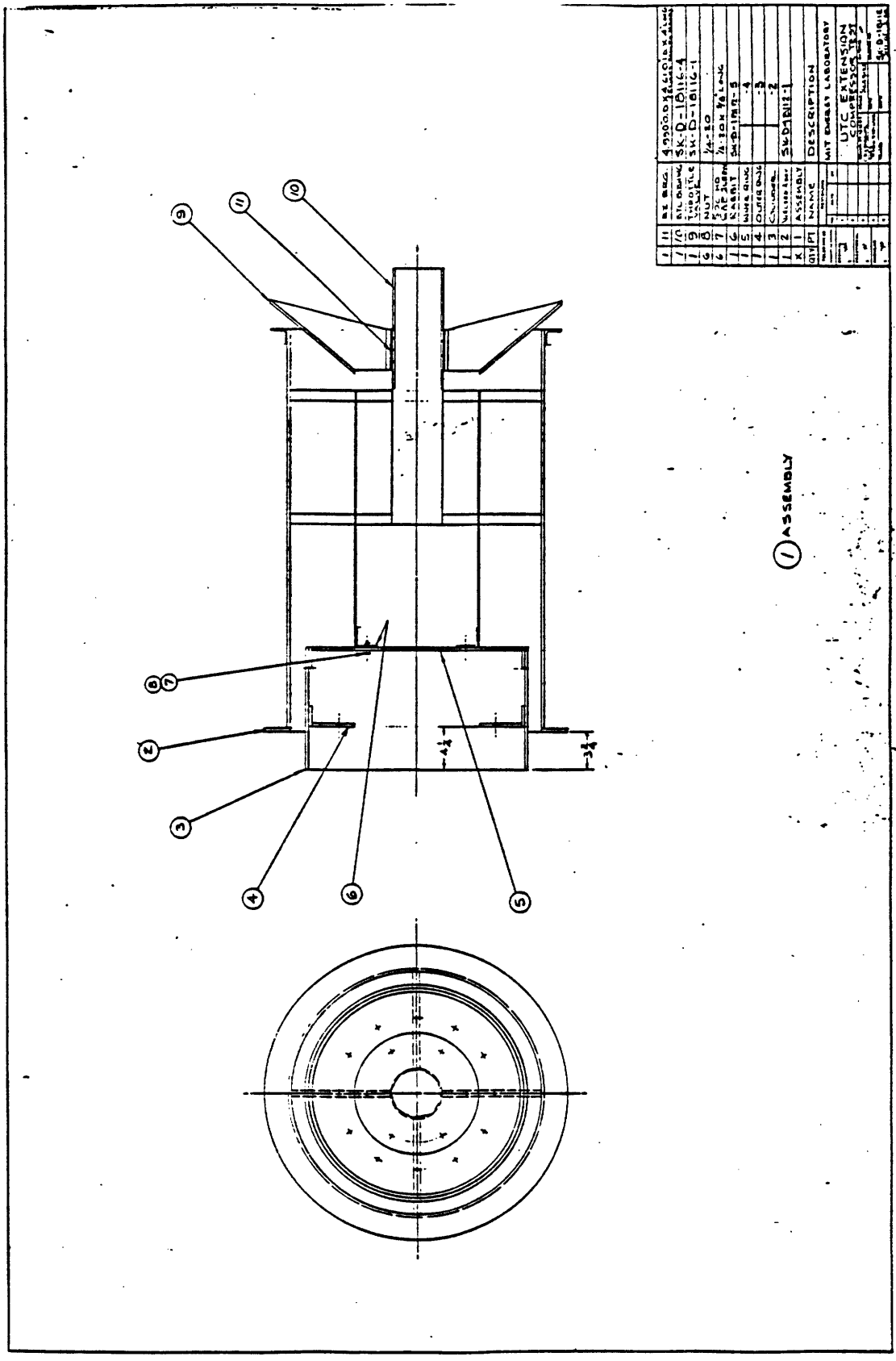

FIGURE 13: Assembly Drawing of Extension Piece and Throttle

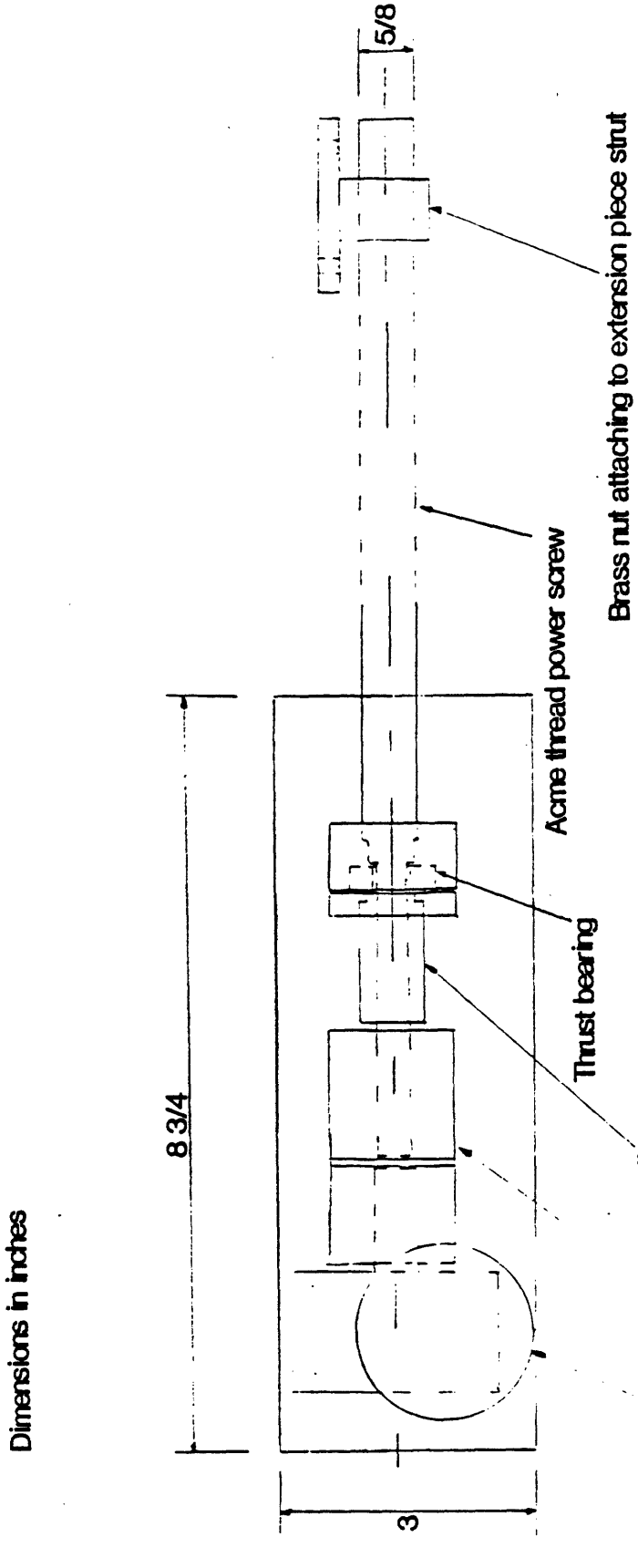

FIGURE 14: Throttle Drive System

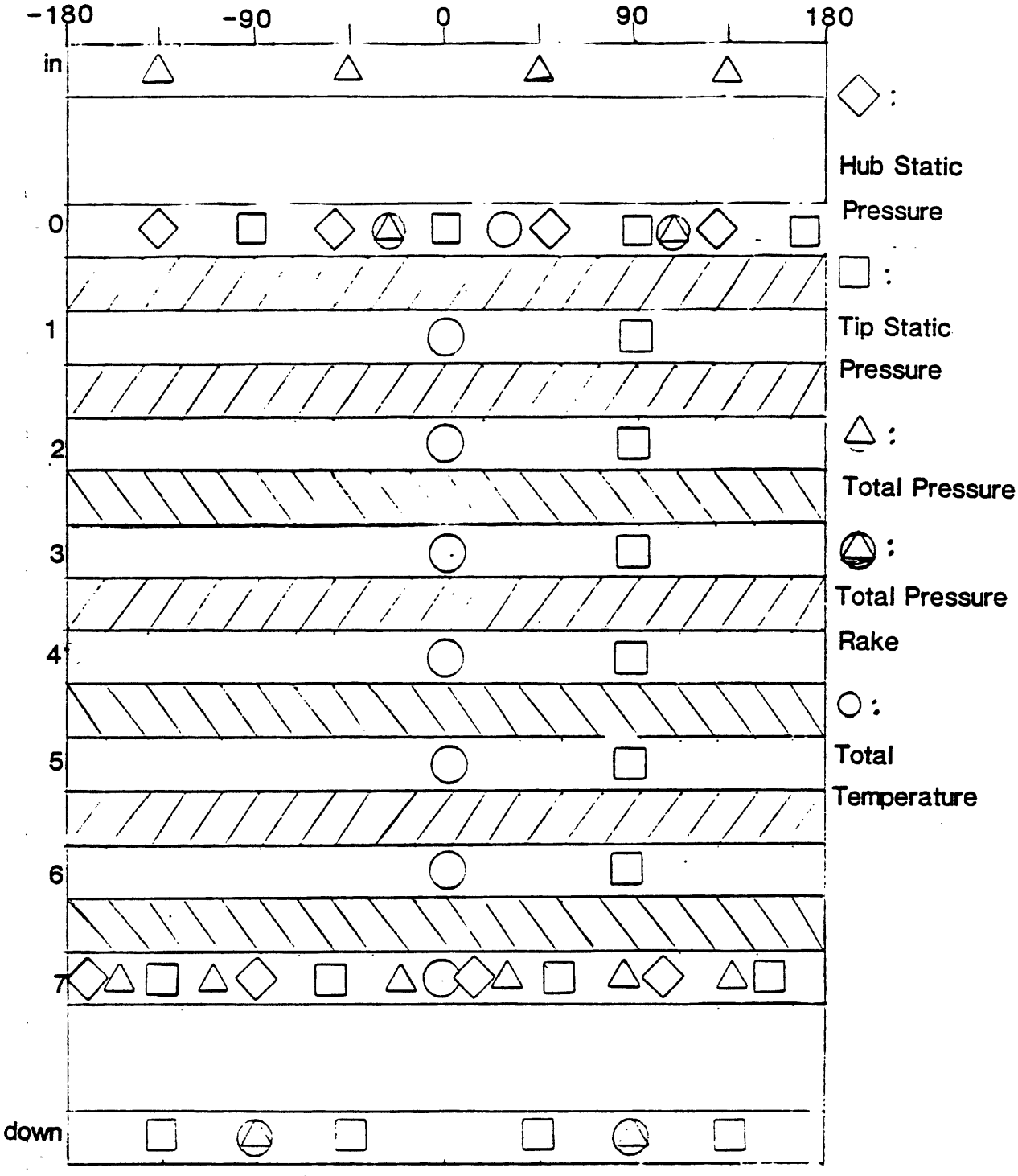

FIGURE 15: Compressor Instrumetation

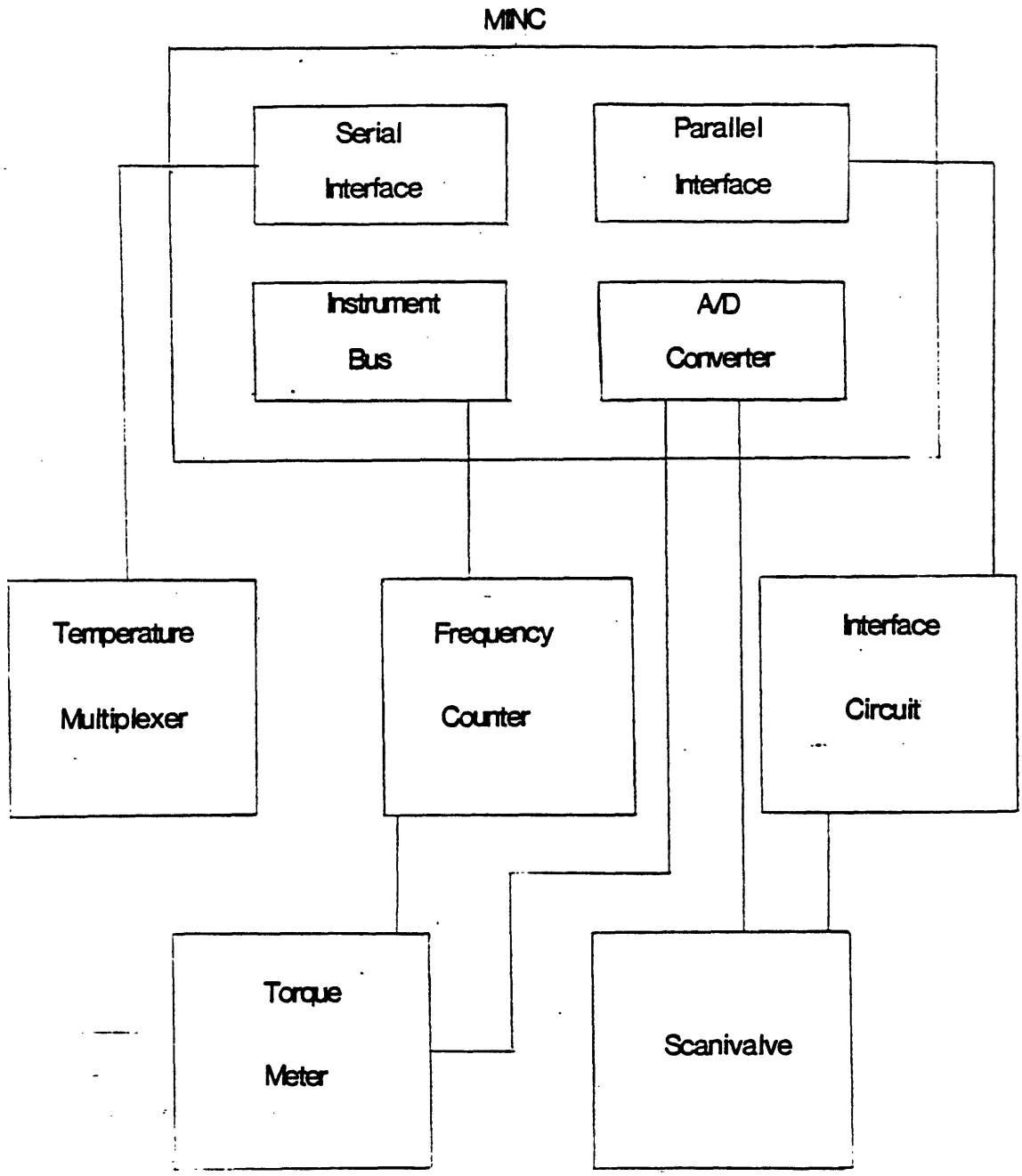

FIGURE 16: Data Acquisition System

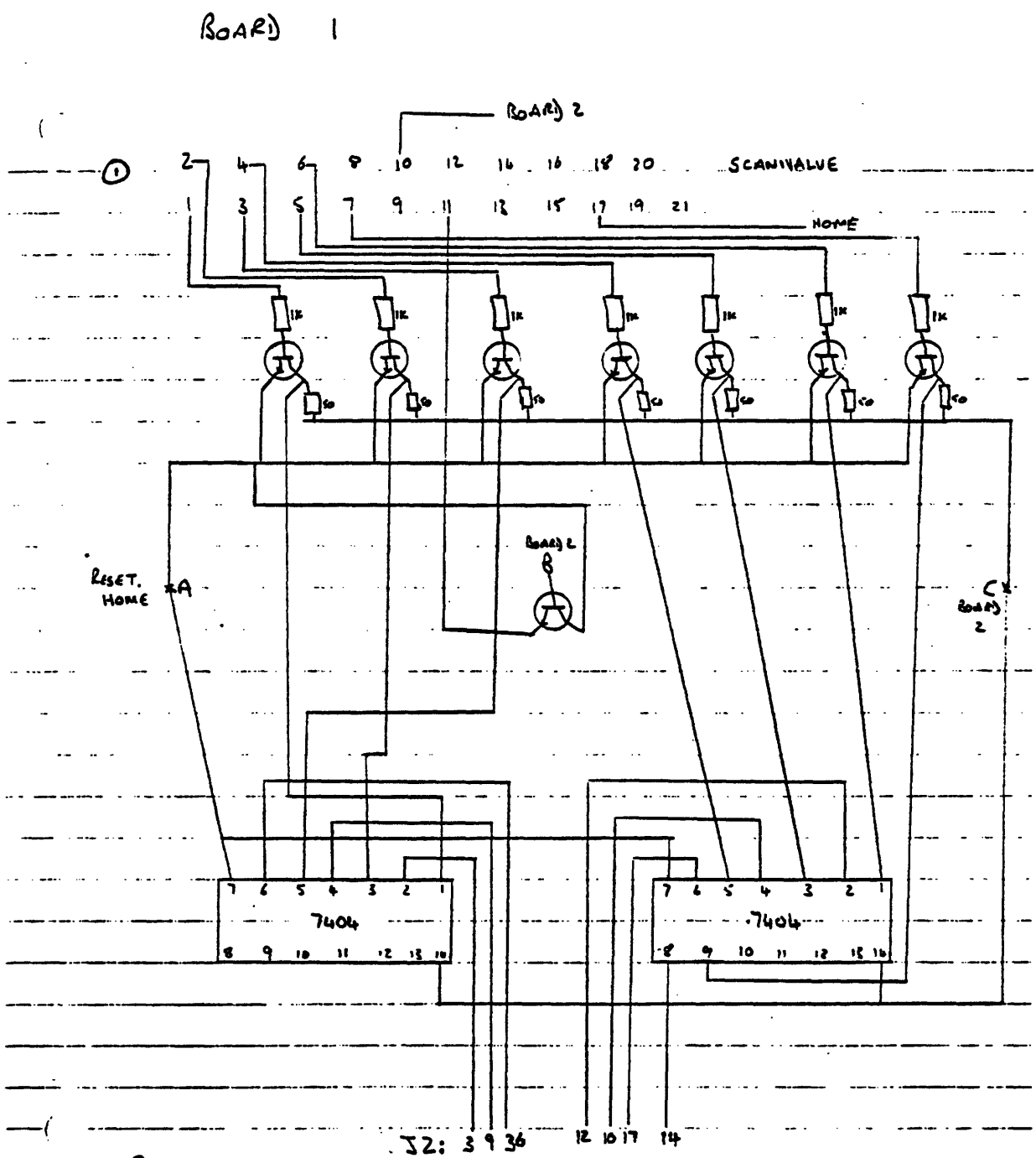

FIGURE 17a: Scanivalve Interface Circuit-Board 1

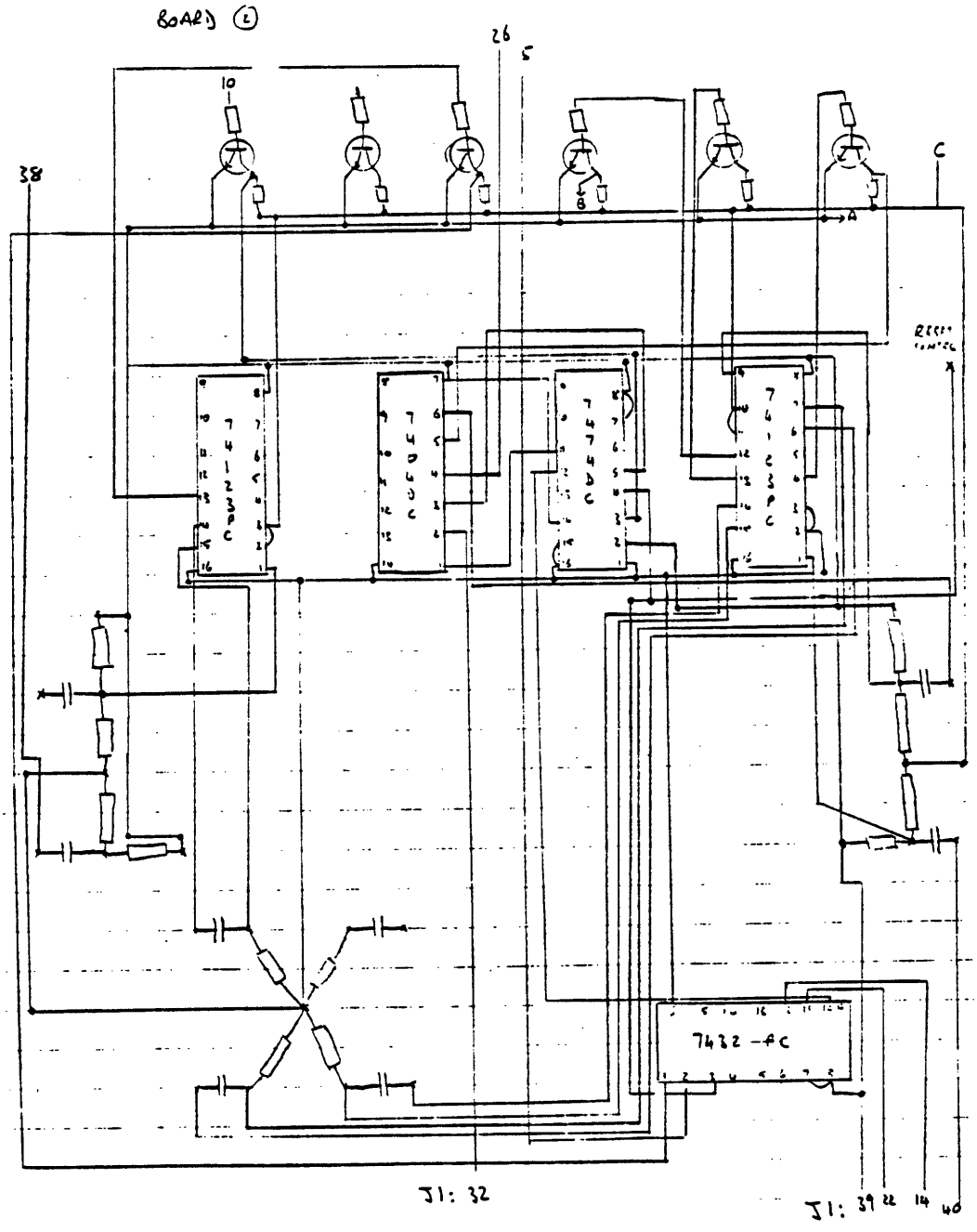

FIGURE 17b: Scanivalve Interface Circuit-Board 2

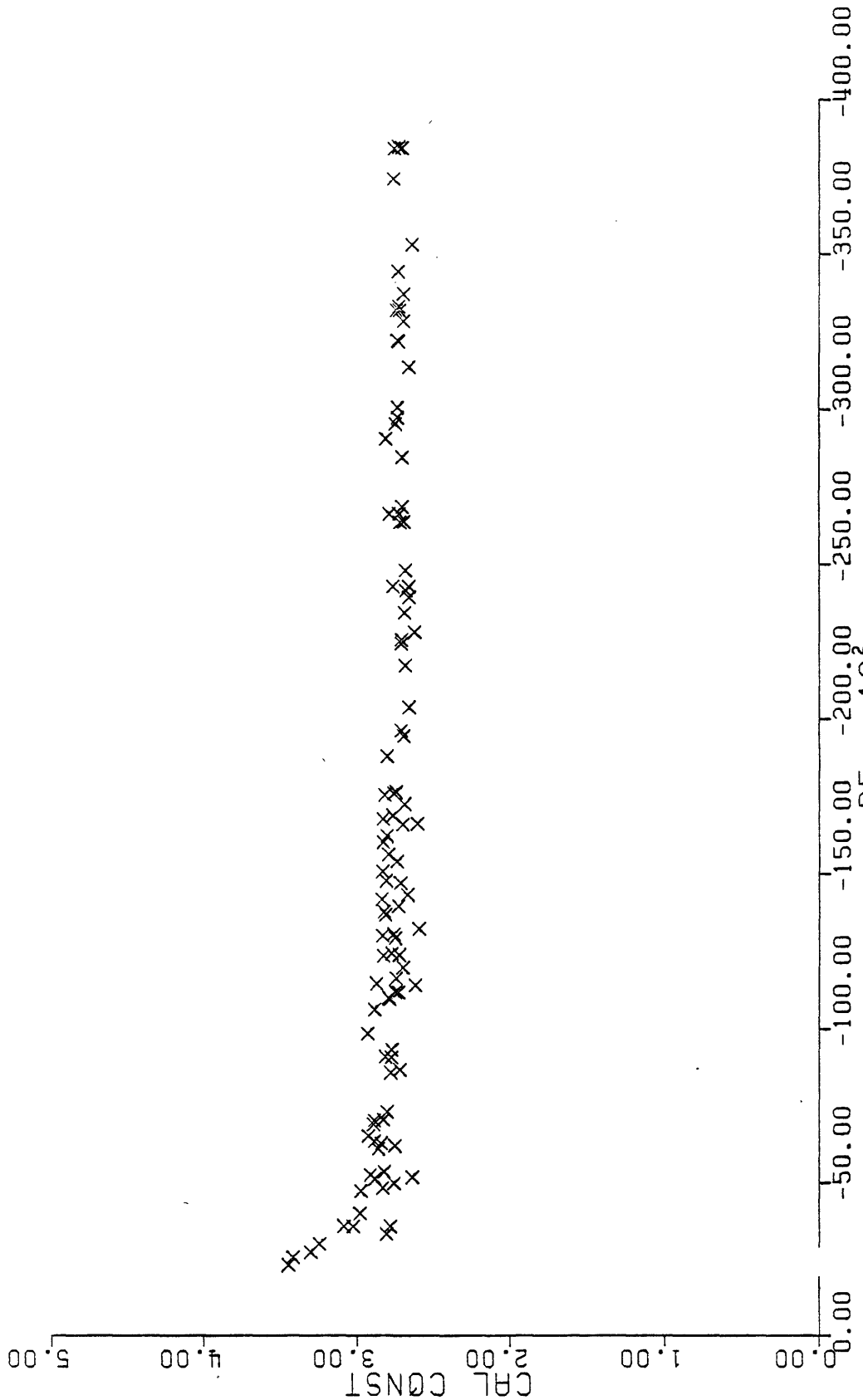

FIGURE 18: Orifice Plate Calibration

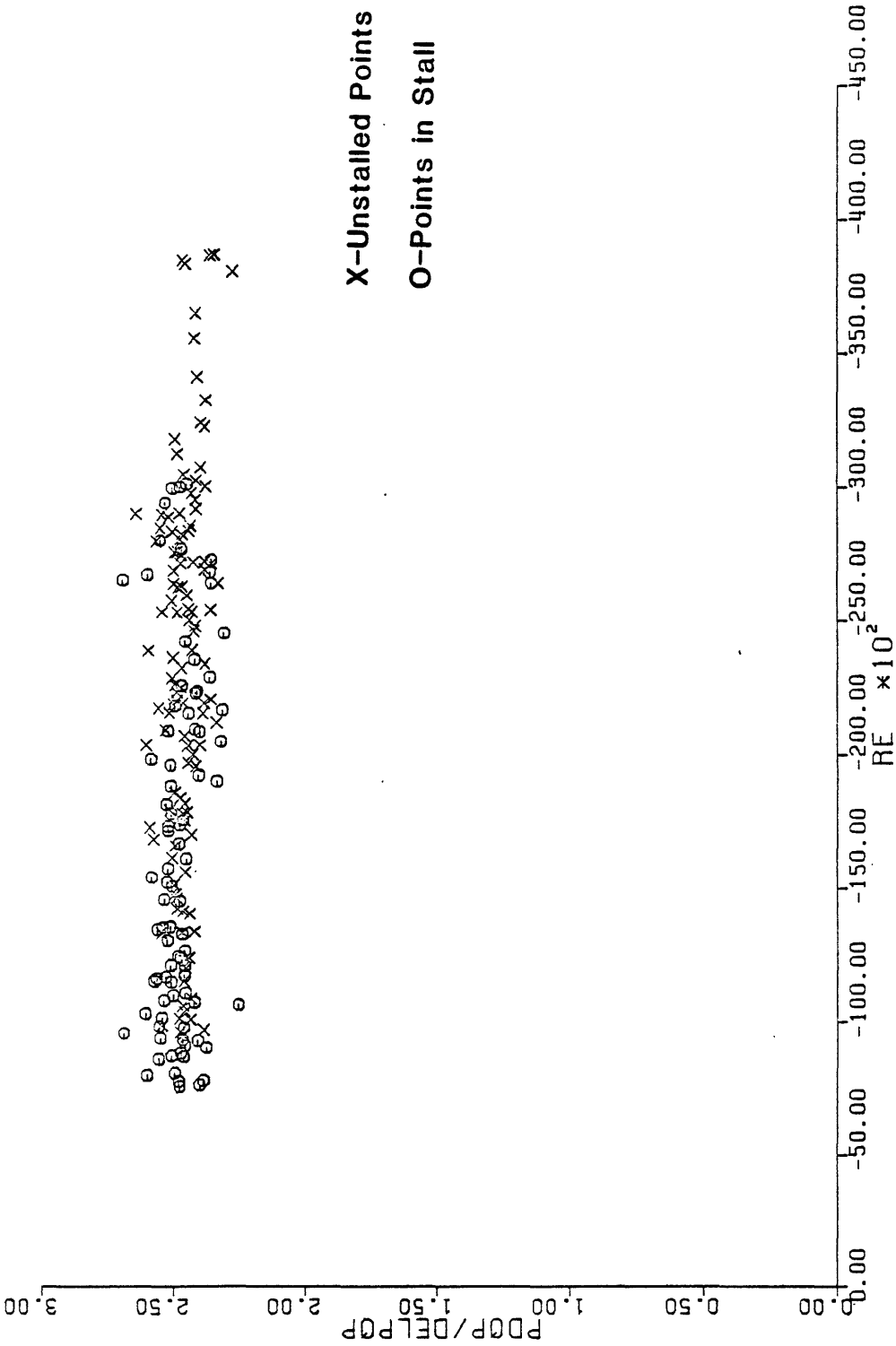

FIGURE 19: Ratio of Downstream Orifice Plate Pressure to Orifice Plate Pressure Difference

Static Pressure Probe

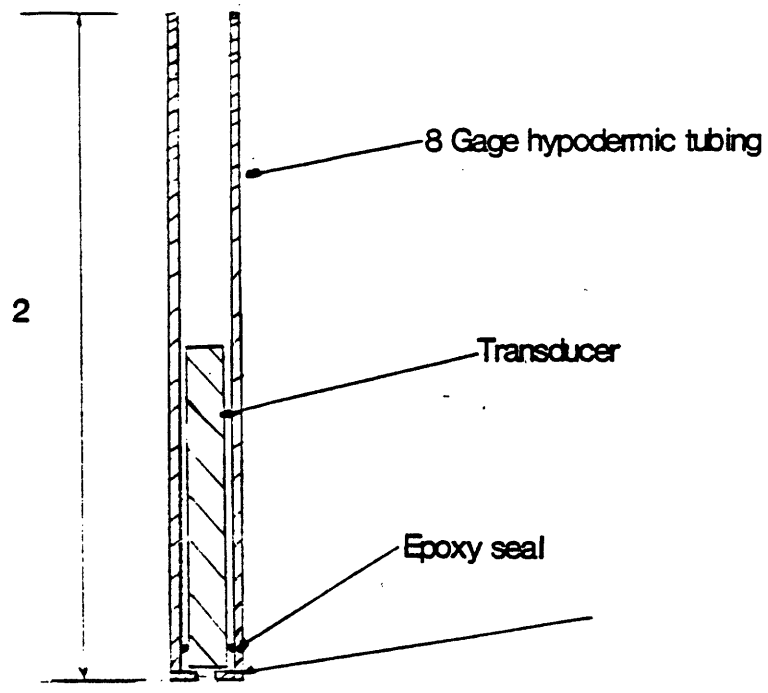

Dimensions in inches

Total Pressure Probe

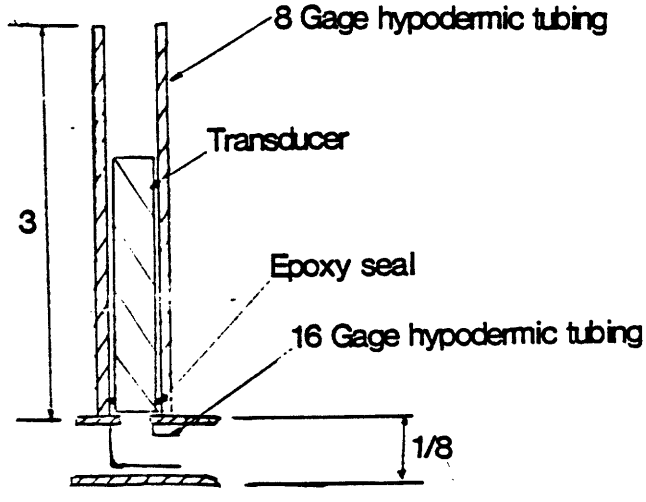

FIGURE 20: High Response Pressure Probes

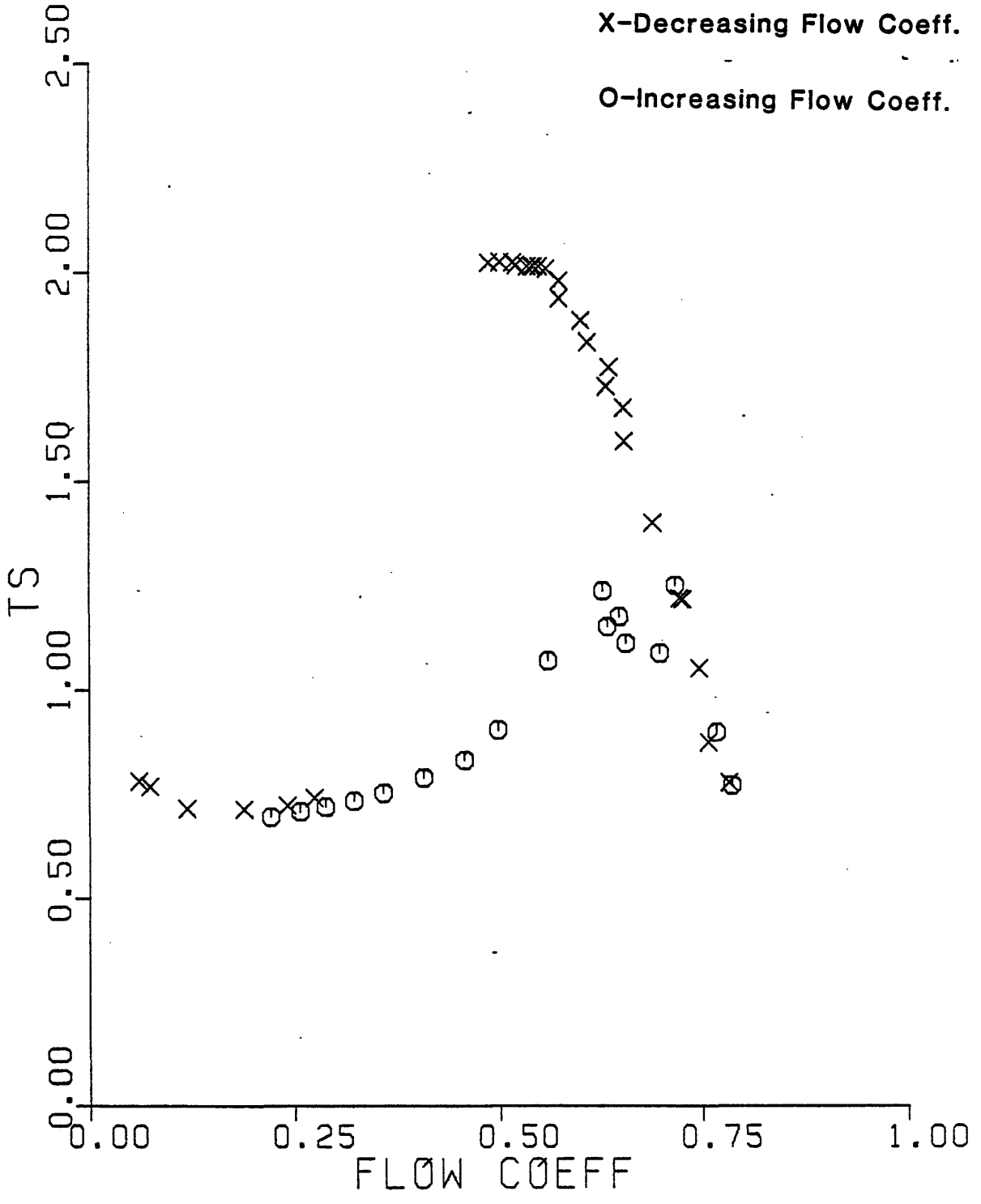

FIGURE 21: Total to Static Pressure Rise Characteristic 2500RPM

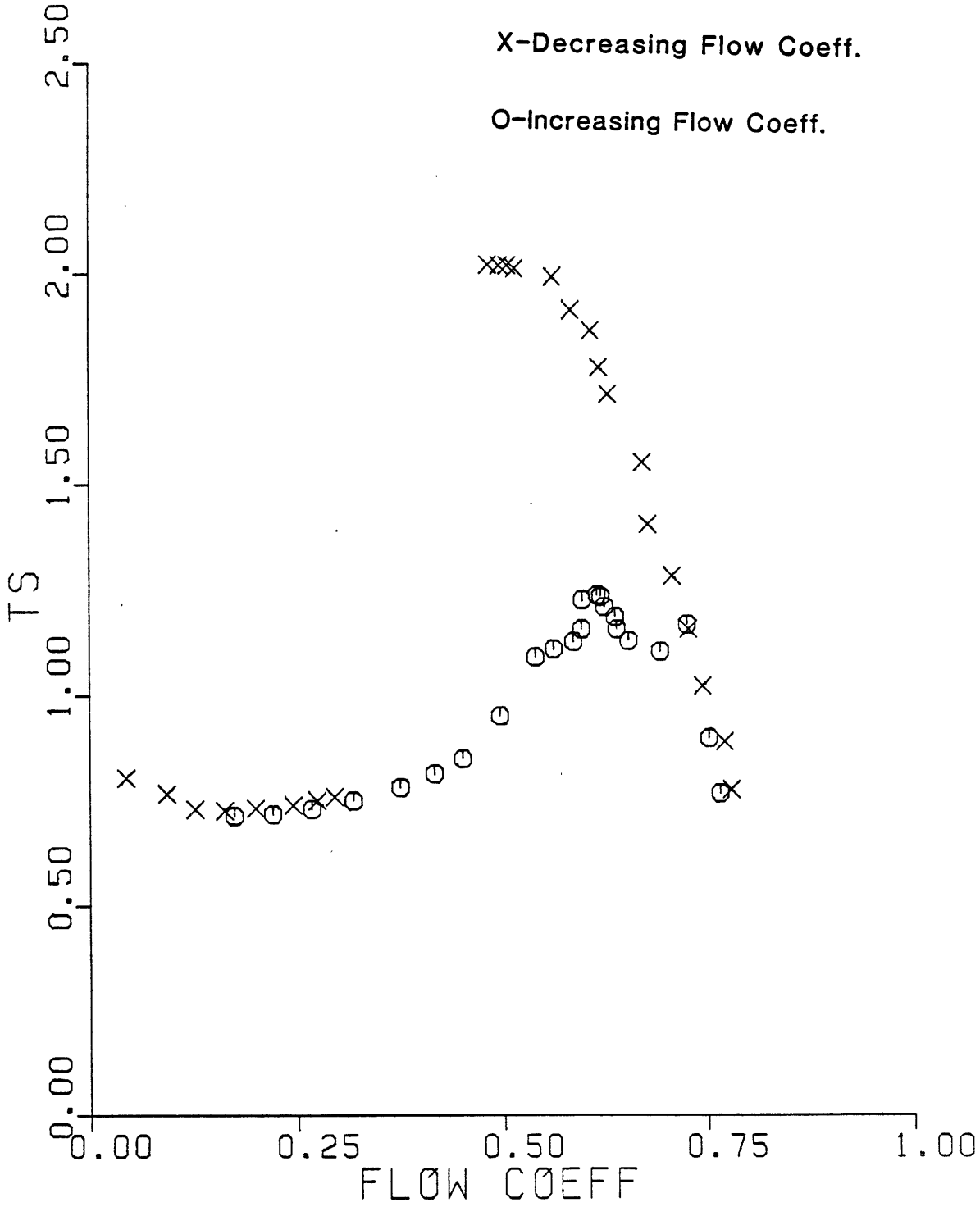

FIGURE 22: Total to Static Pressure Rise Characteristic 2000 RPM

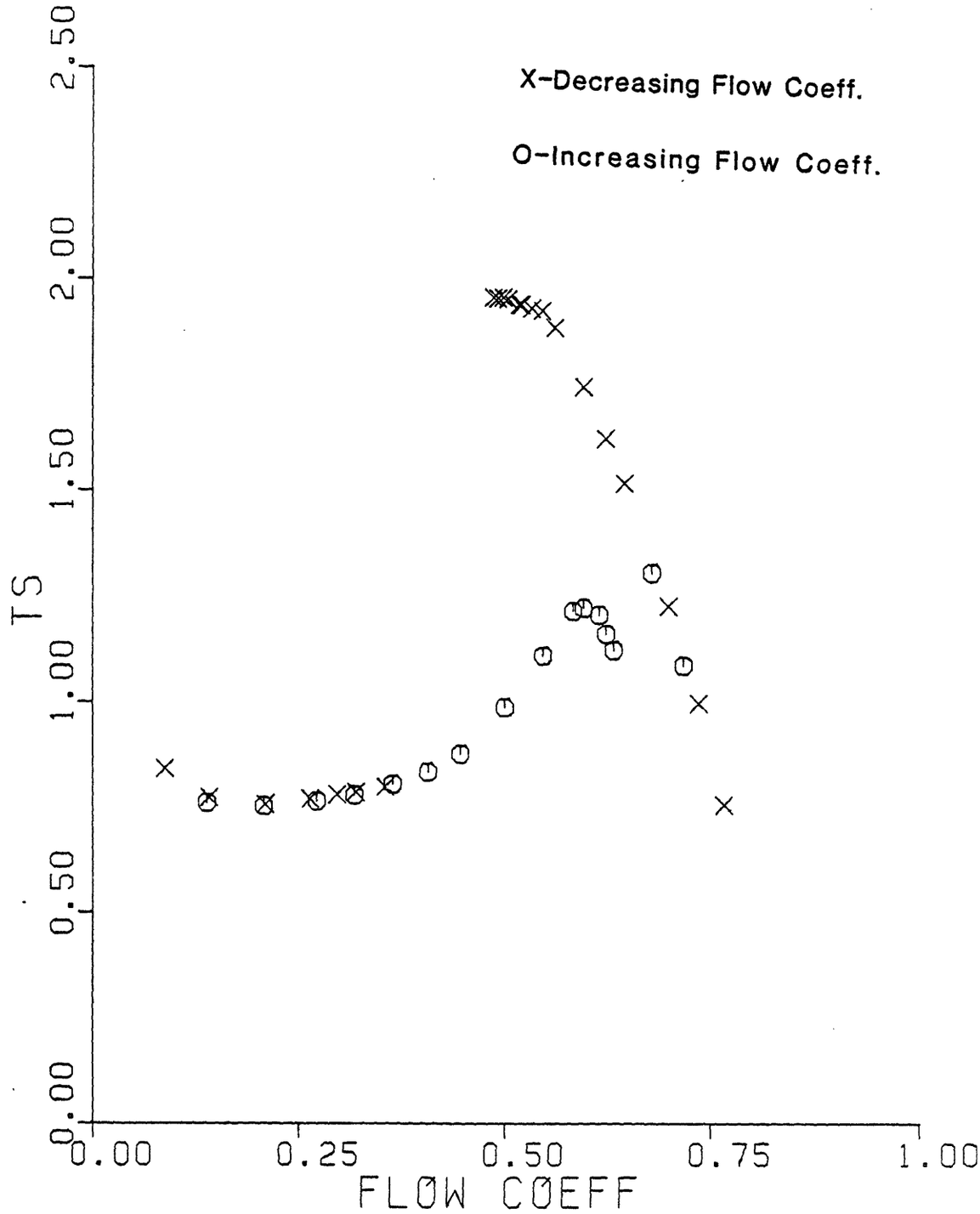

FIGURE 23: Total to Static Pressure Rise Characteristic 1170 RPM

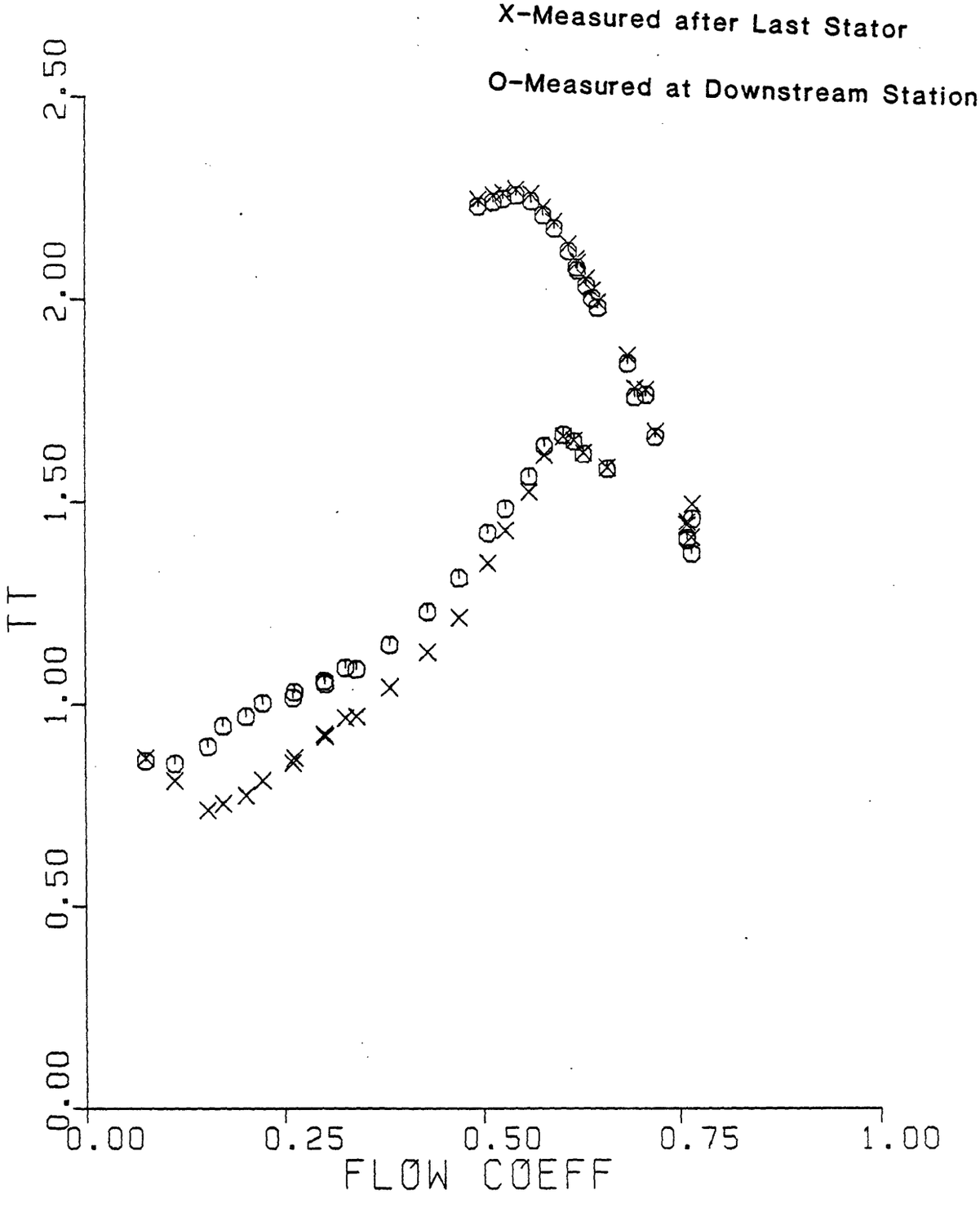

FIGURE 24: Total to Total Pressure Rise Characteristics

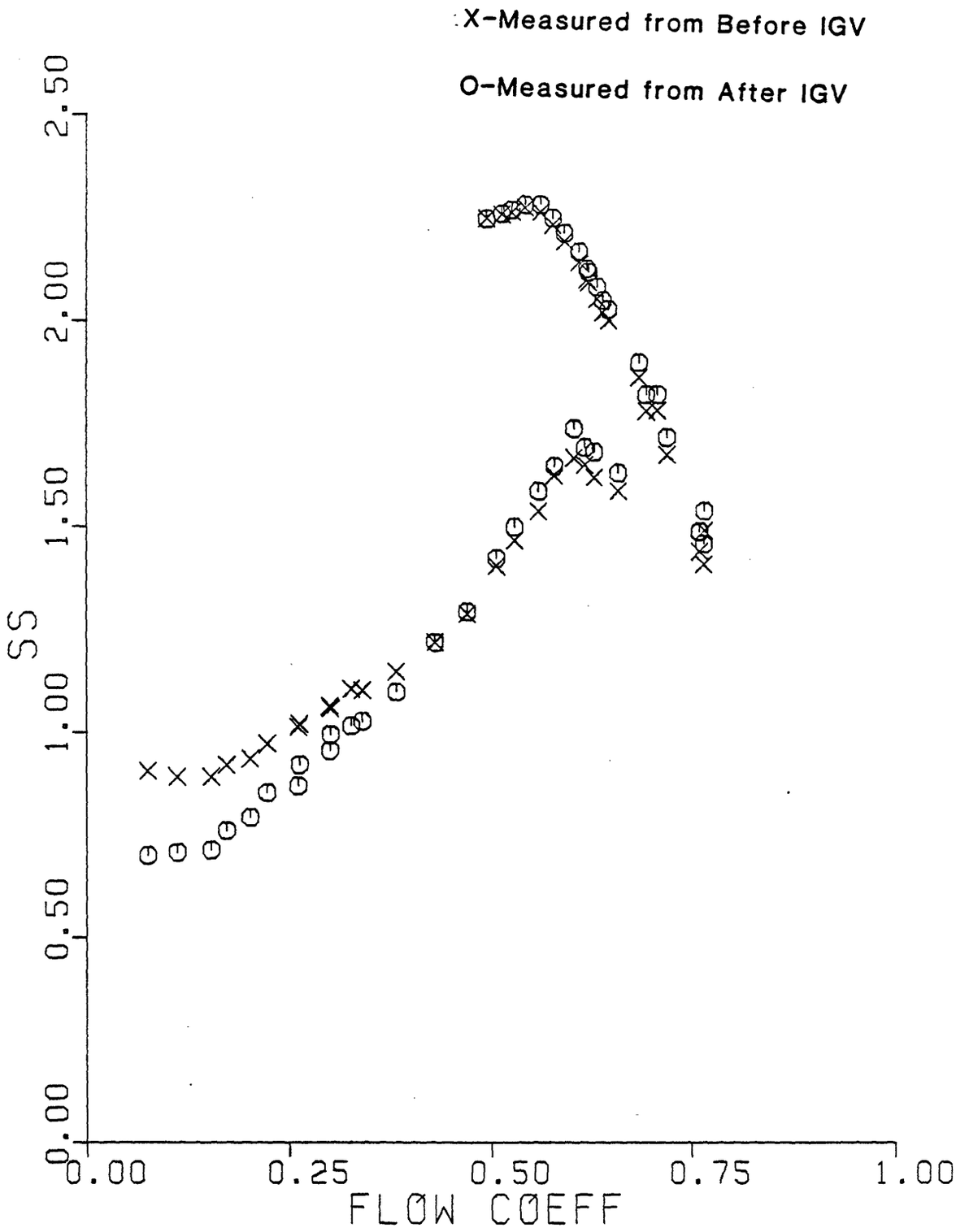

FIGURE 25: Static to Static Pressure Rise Characteristics

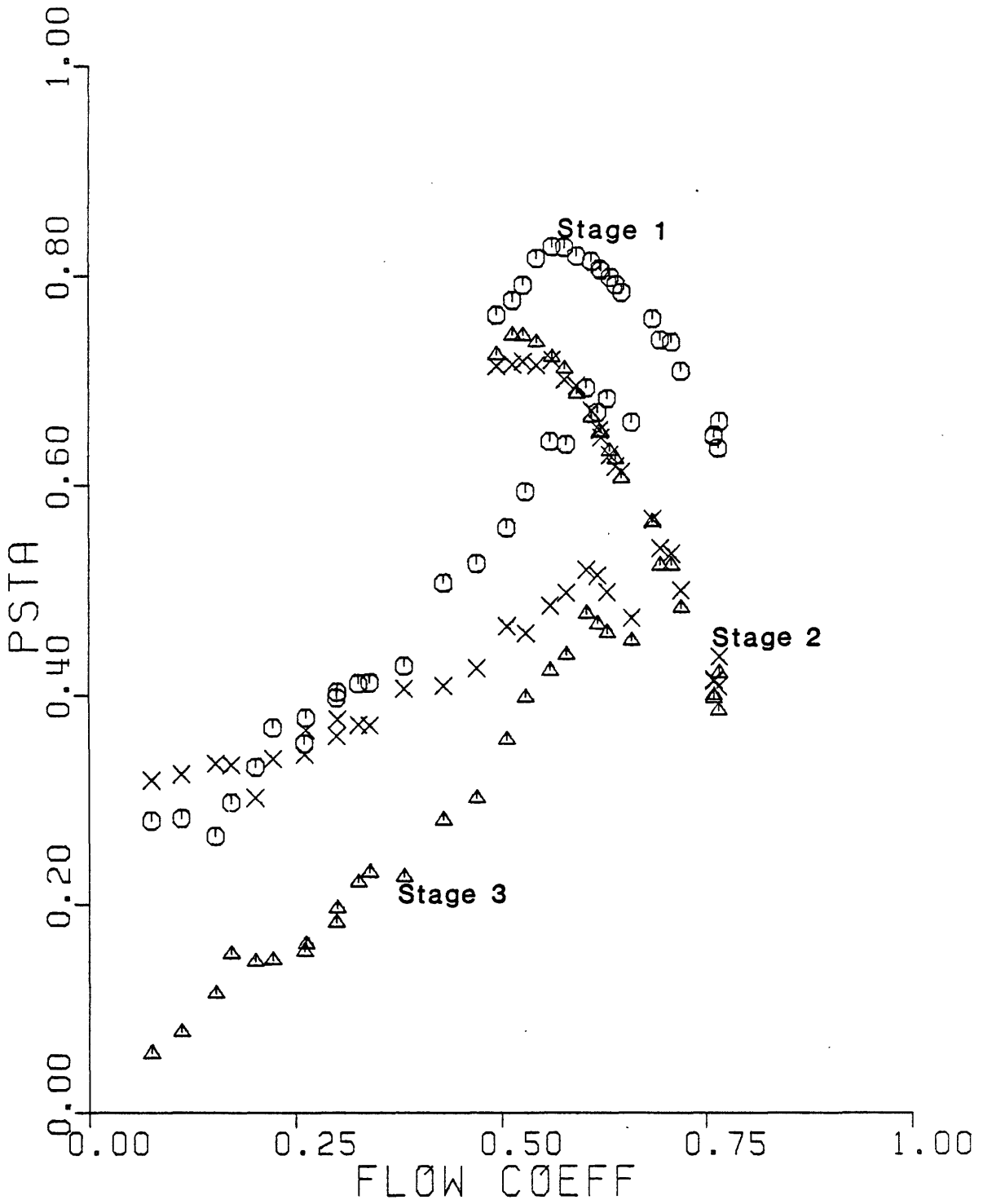

FIGURE 26: Stage Pressure Rise Characteristics

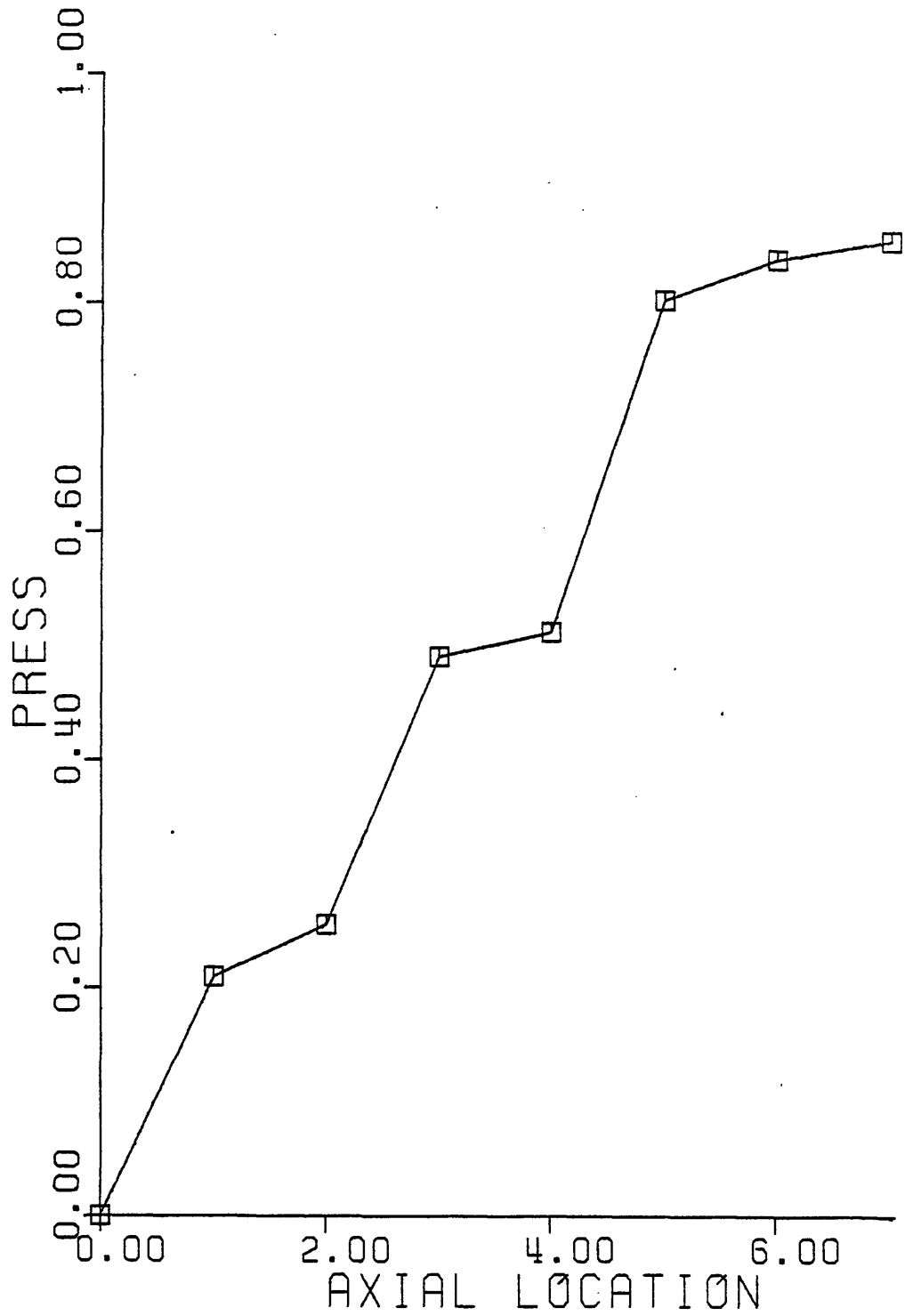

FIGURE 27: Pressure Distribution at Flow Coeff. 0.044

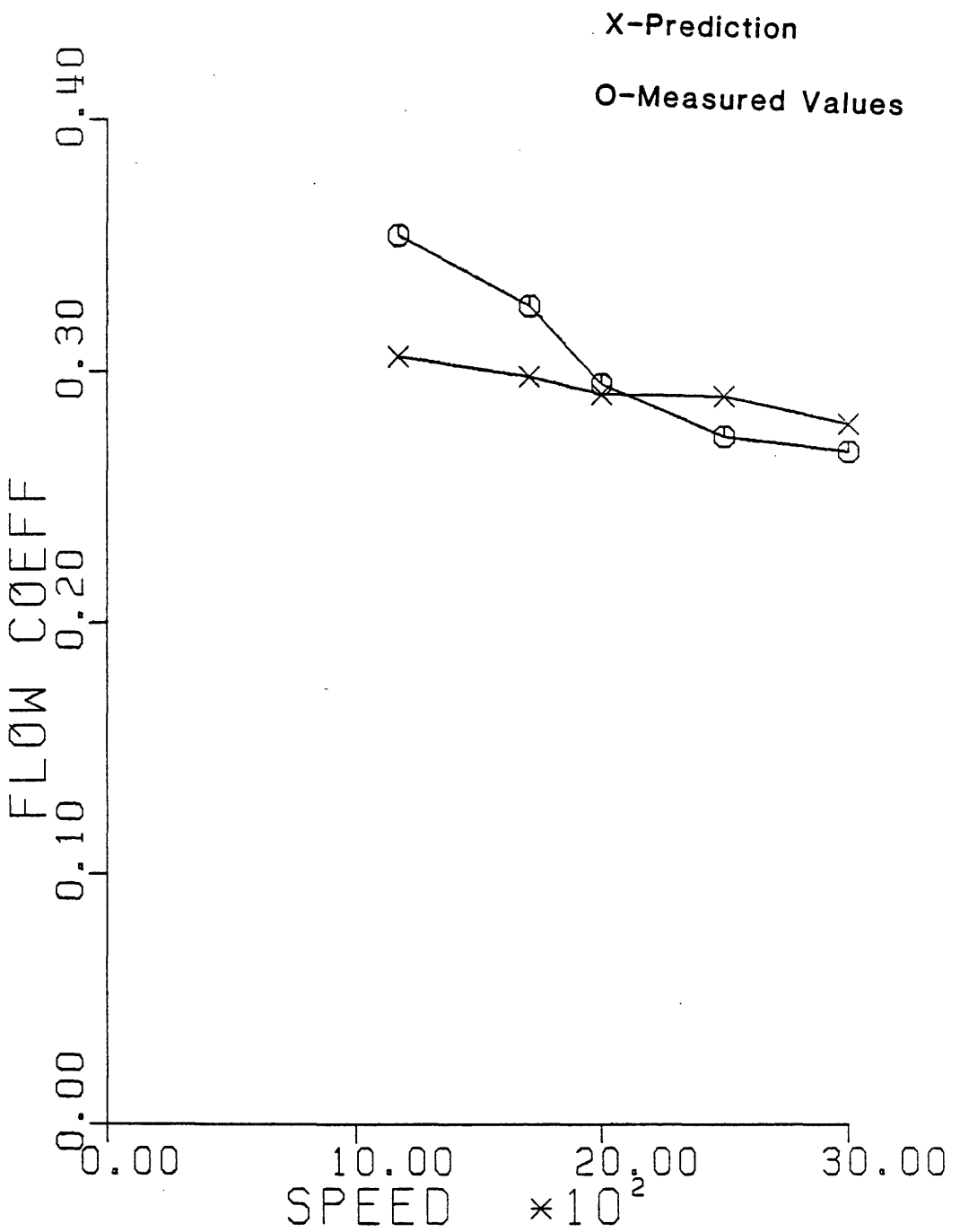

FIGURE 28: Predicted and Measured Flow Coeffs.

at the First Point after Stall

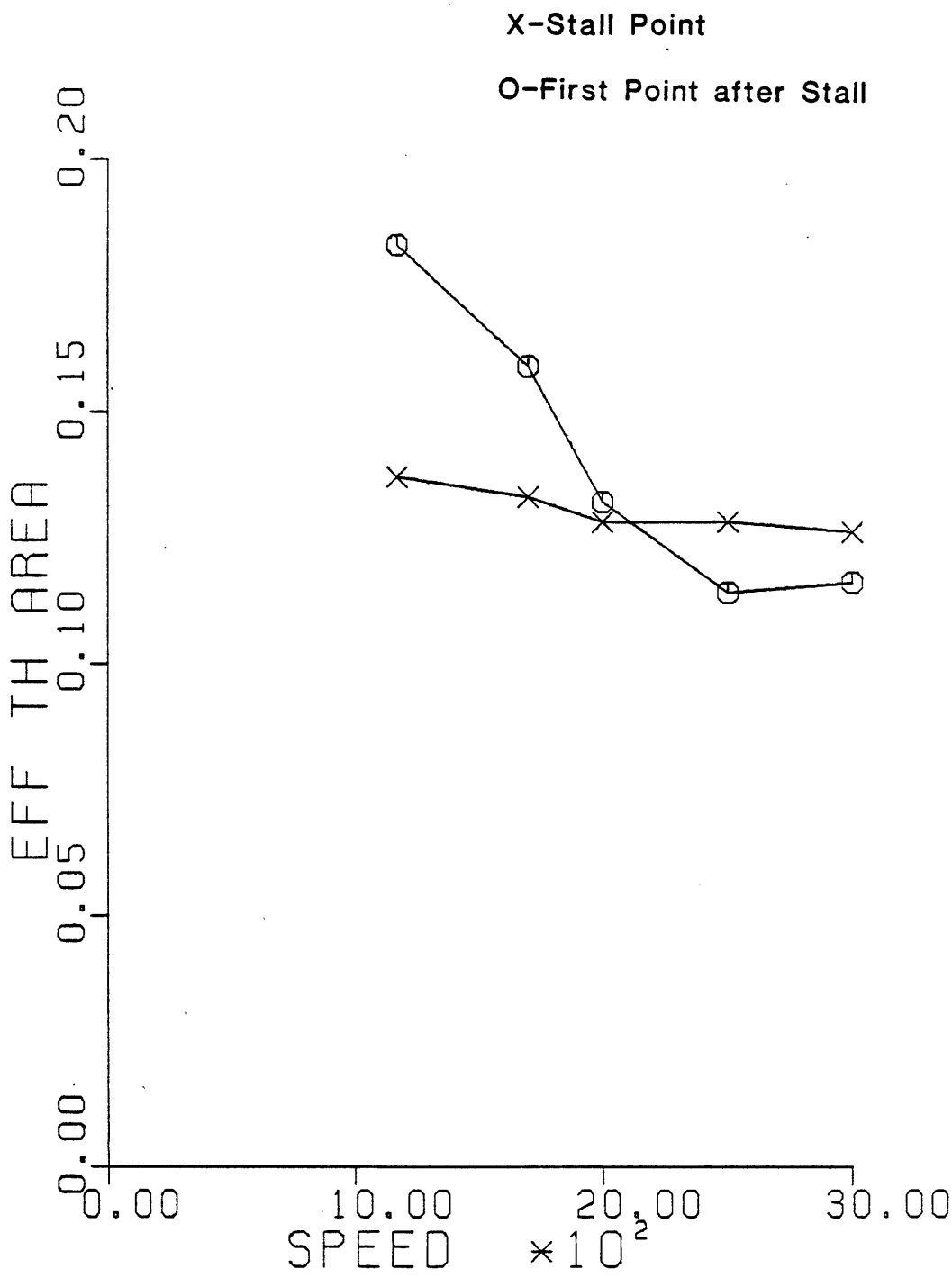

FIGURE 29: Effective Throttle Area at Stall and the First Point after Stall

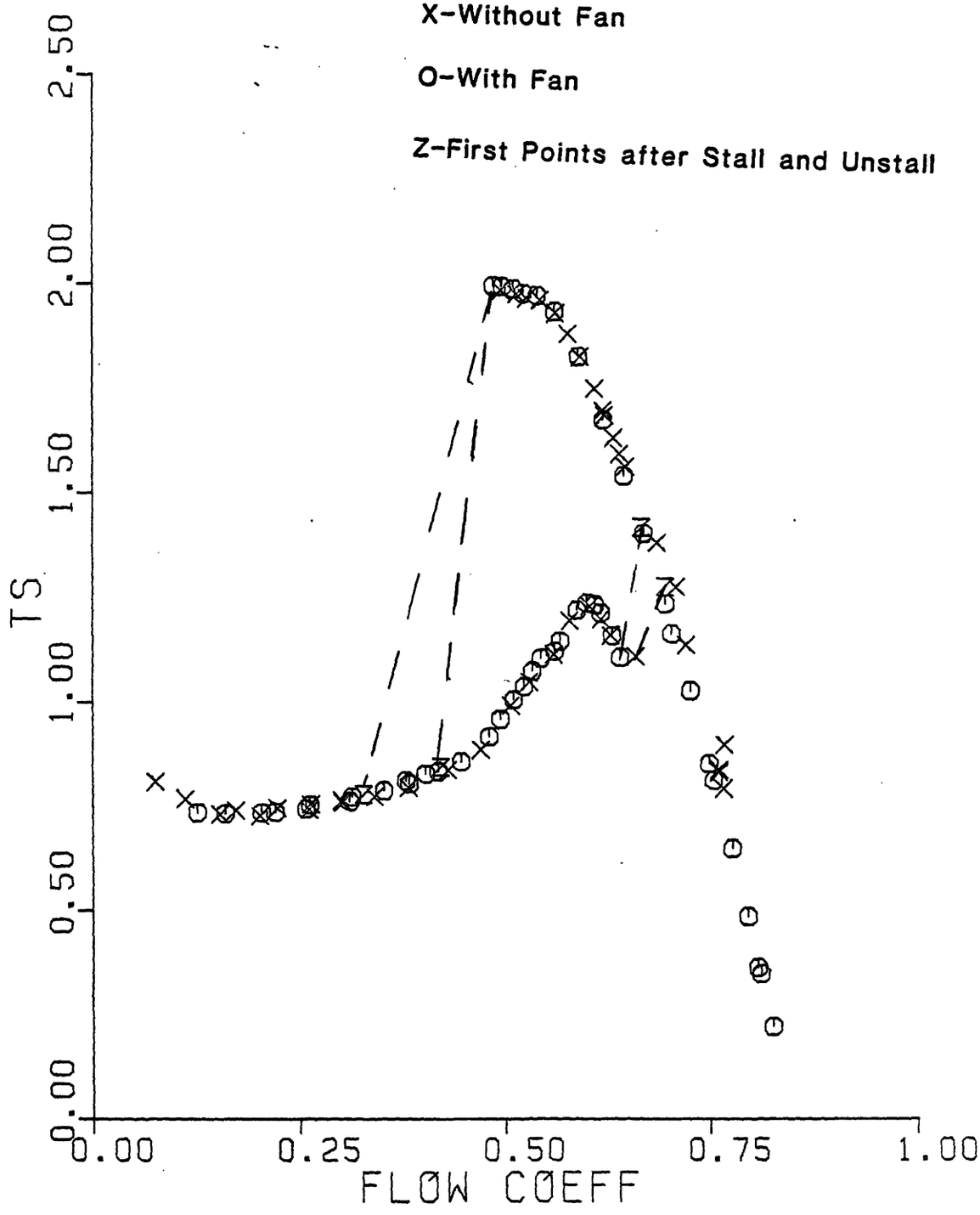

FIGURE 30: Total to Static Pressure Rise Characteristic 1700 RPM, 1800 RPM with the Exit Fan Running

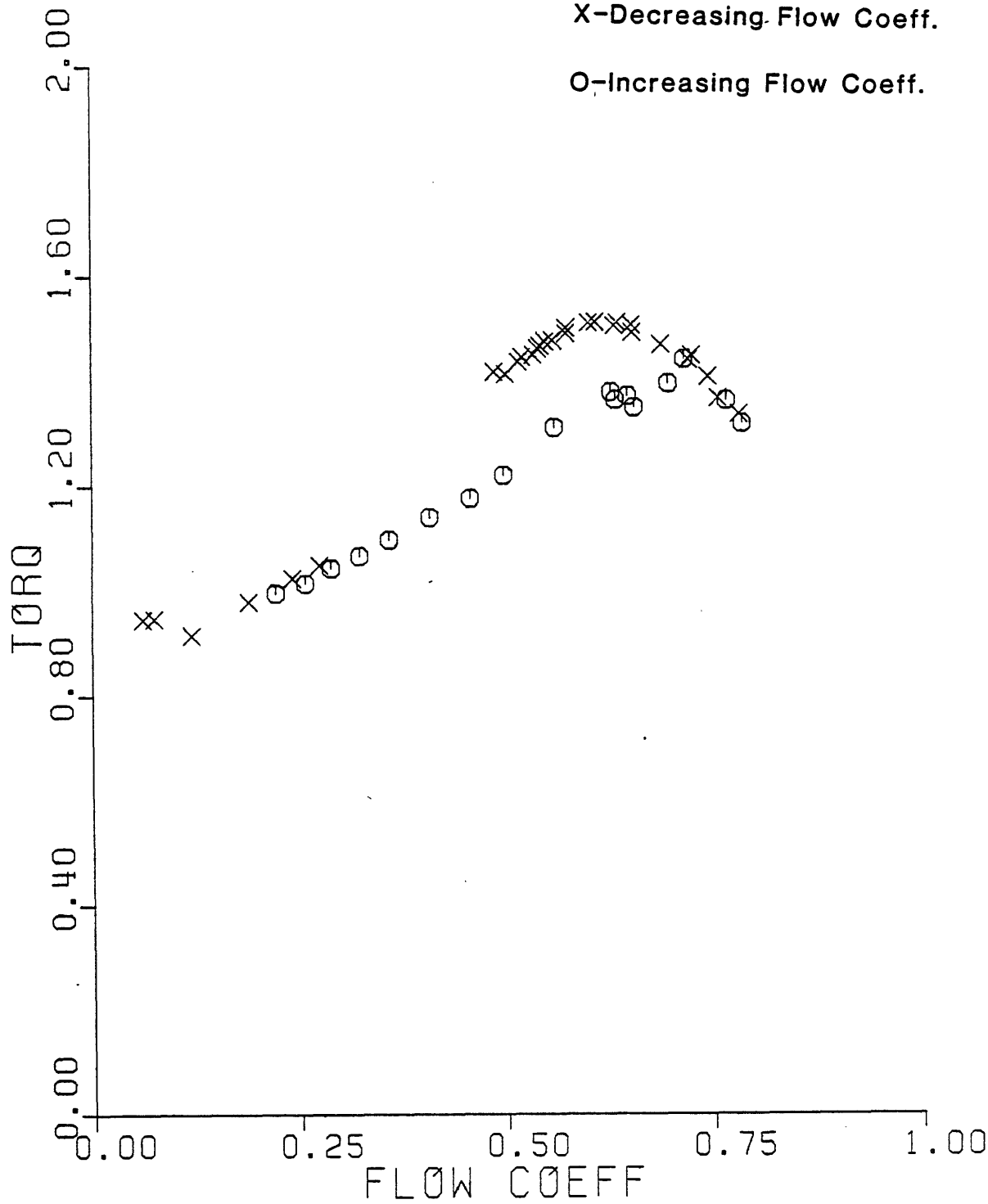

FIGURE 31: Torque Characteristic 2500 RPM

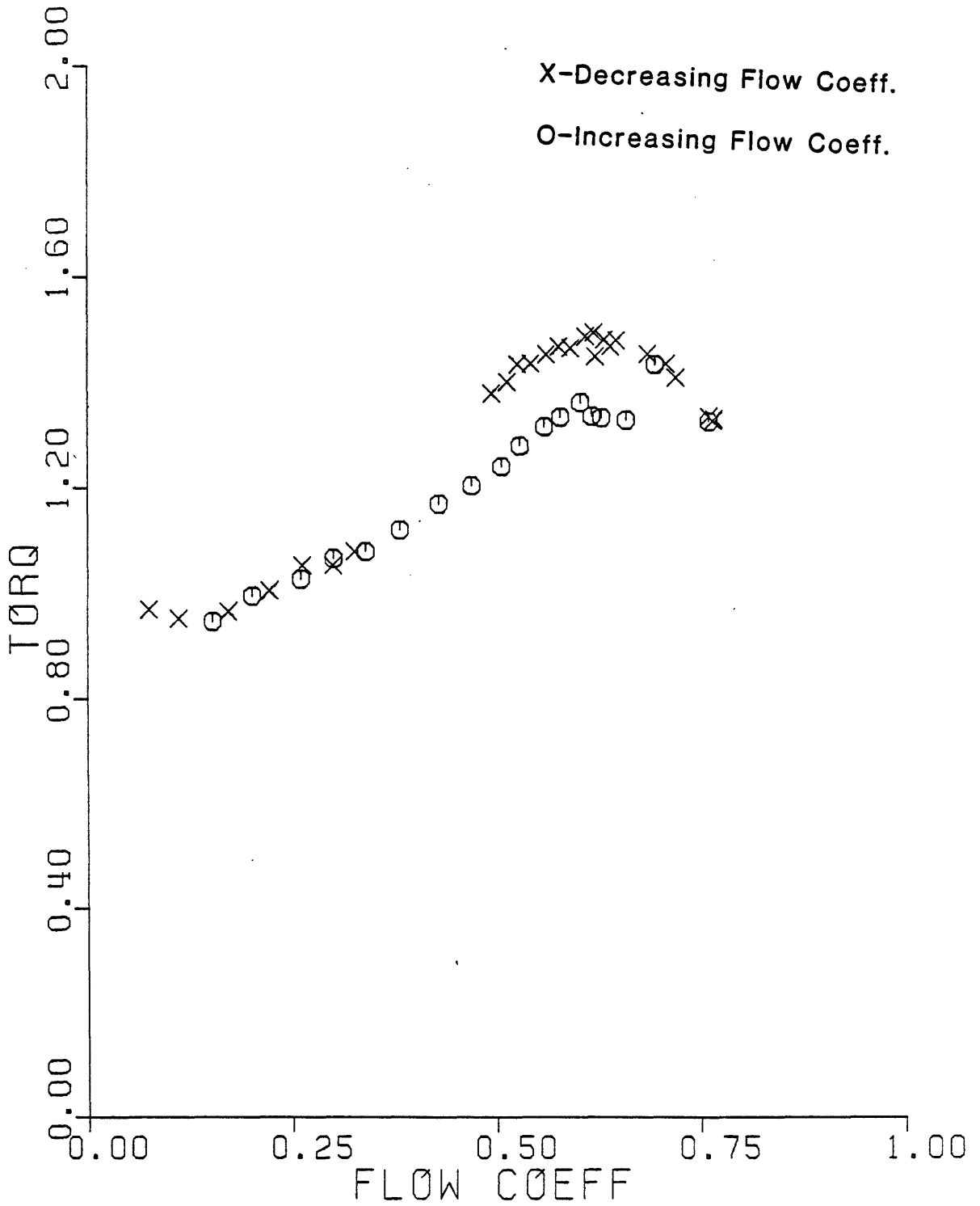

FIGURE 32: Torque Characteristic 1700 RPM

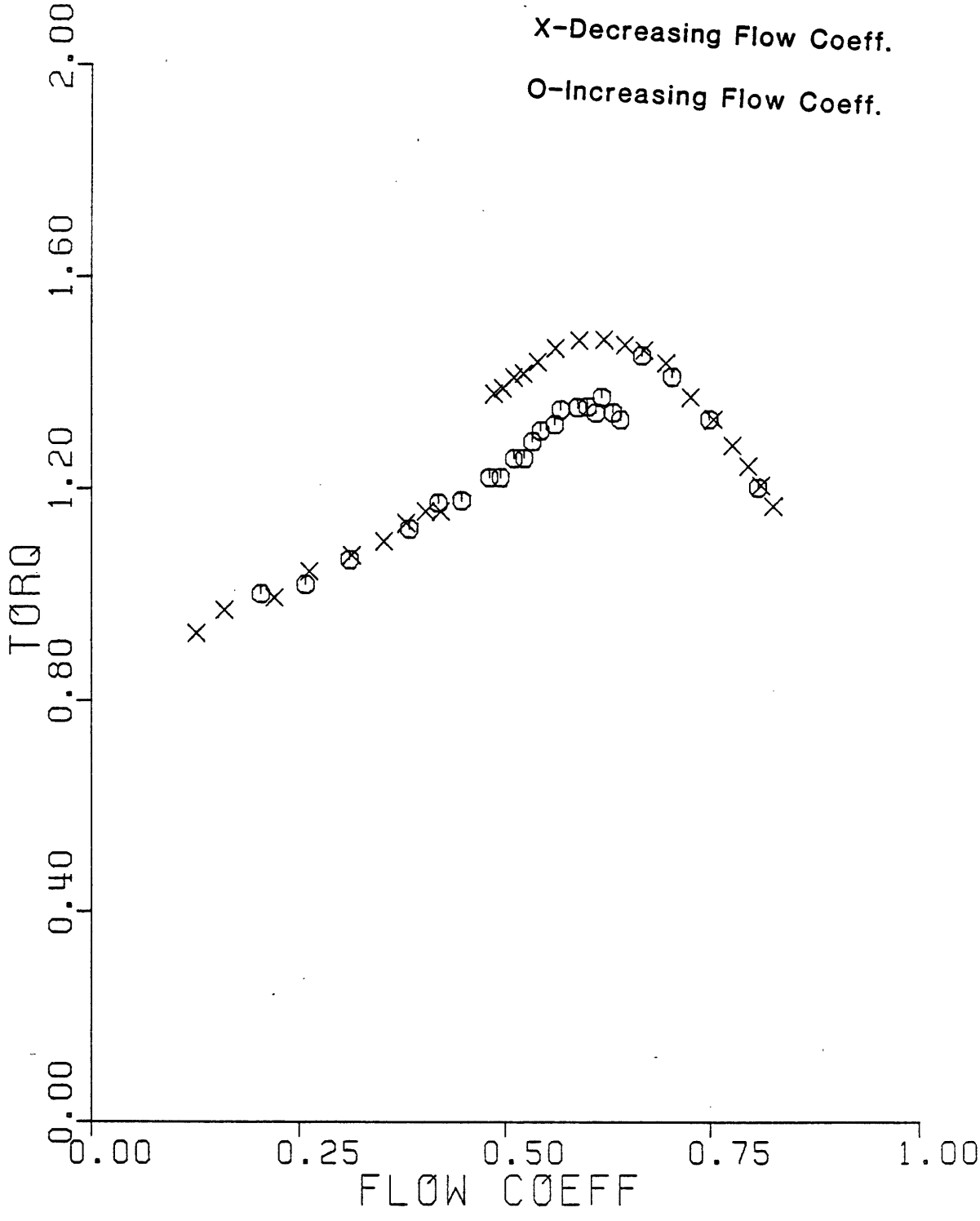

FIGURE 33: Torque Characteristic 1800 RPM with Fan

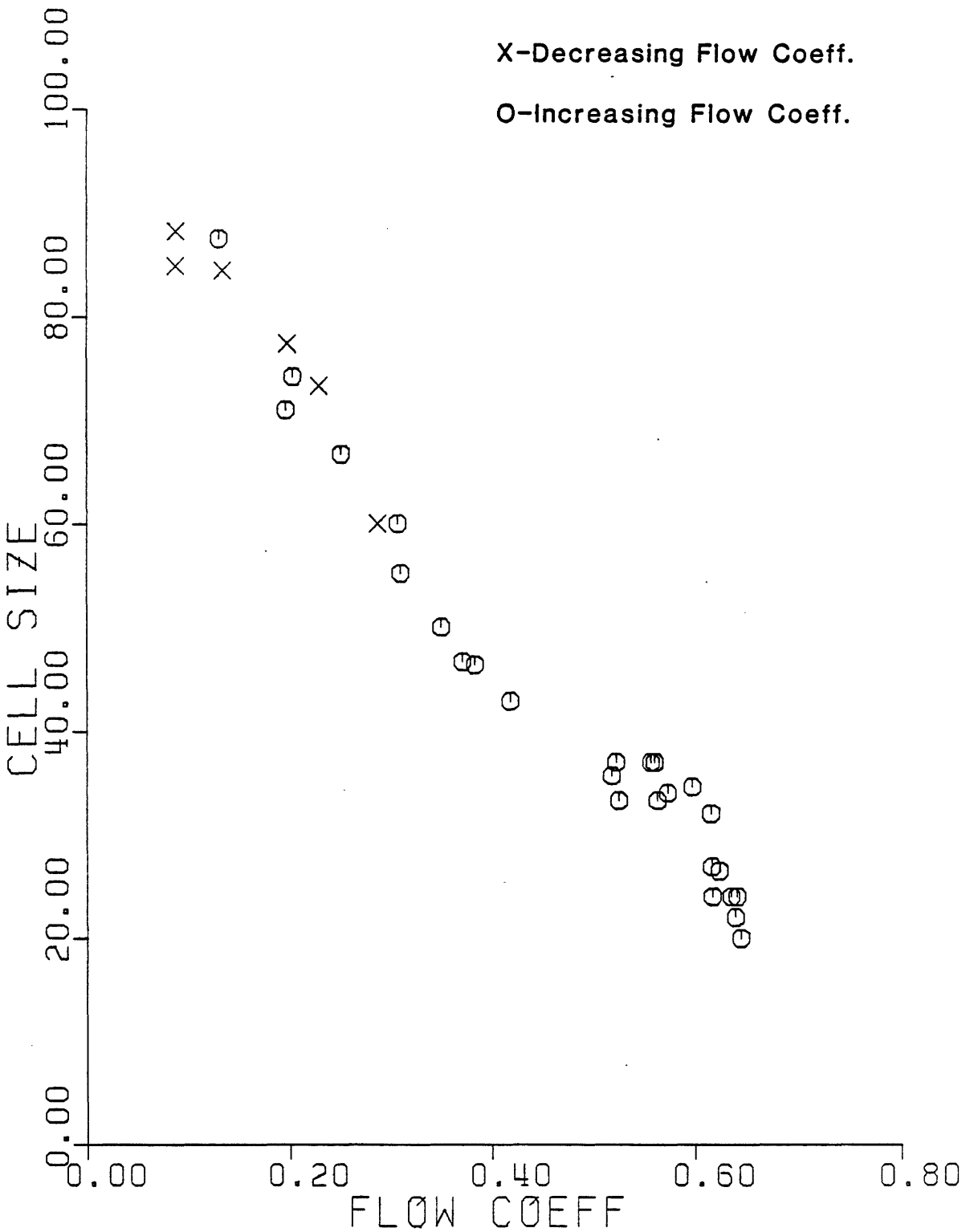

FIGURE 34: Stall Cell Size

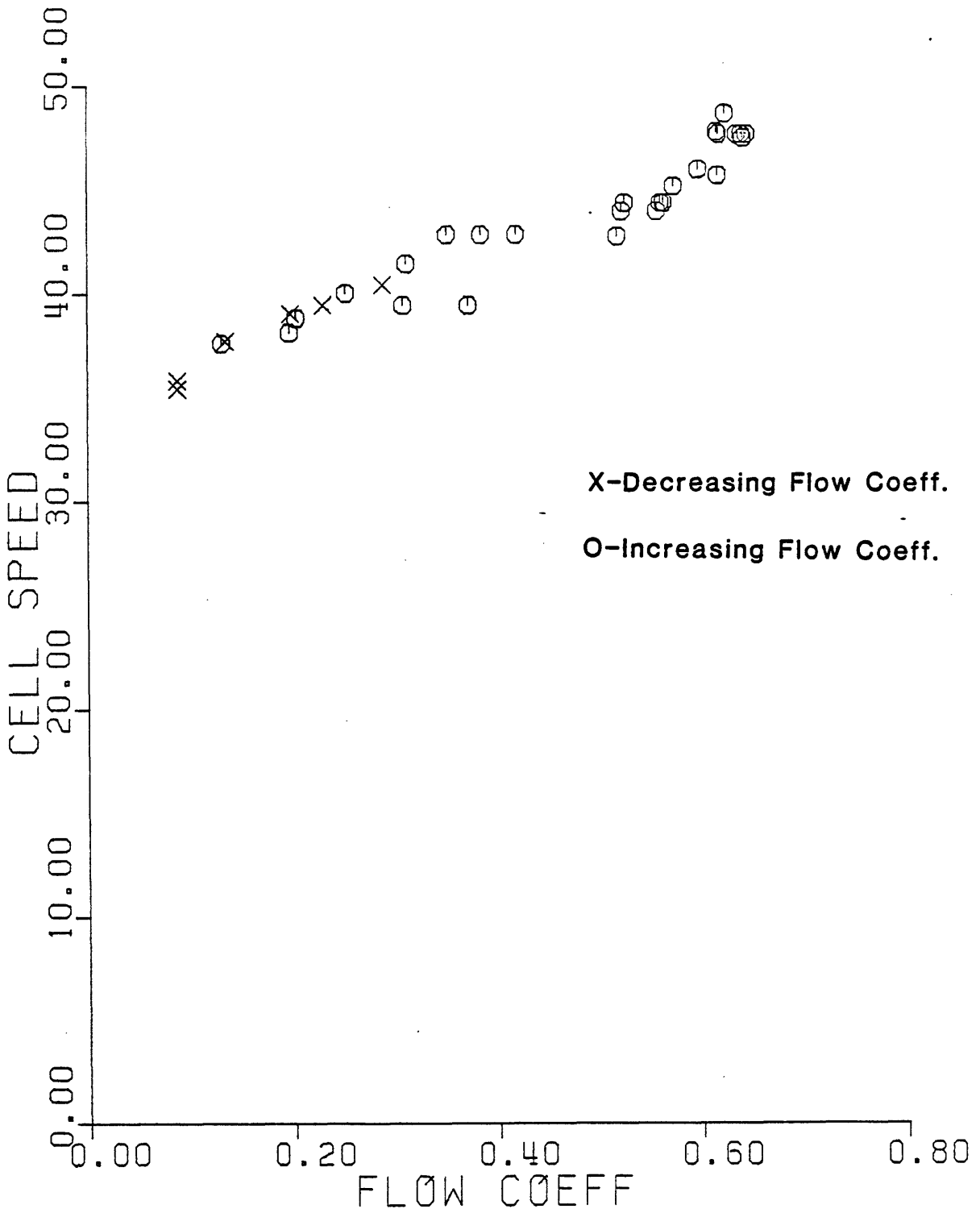

FIGURE 35: Stall Cell Speed

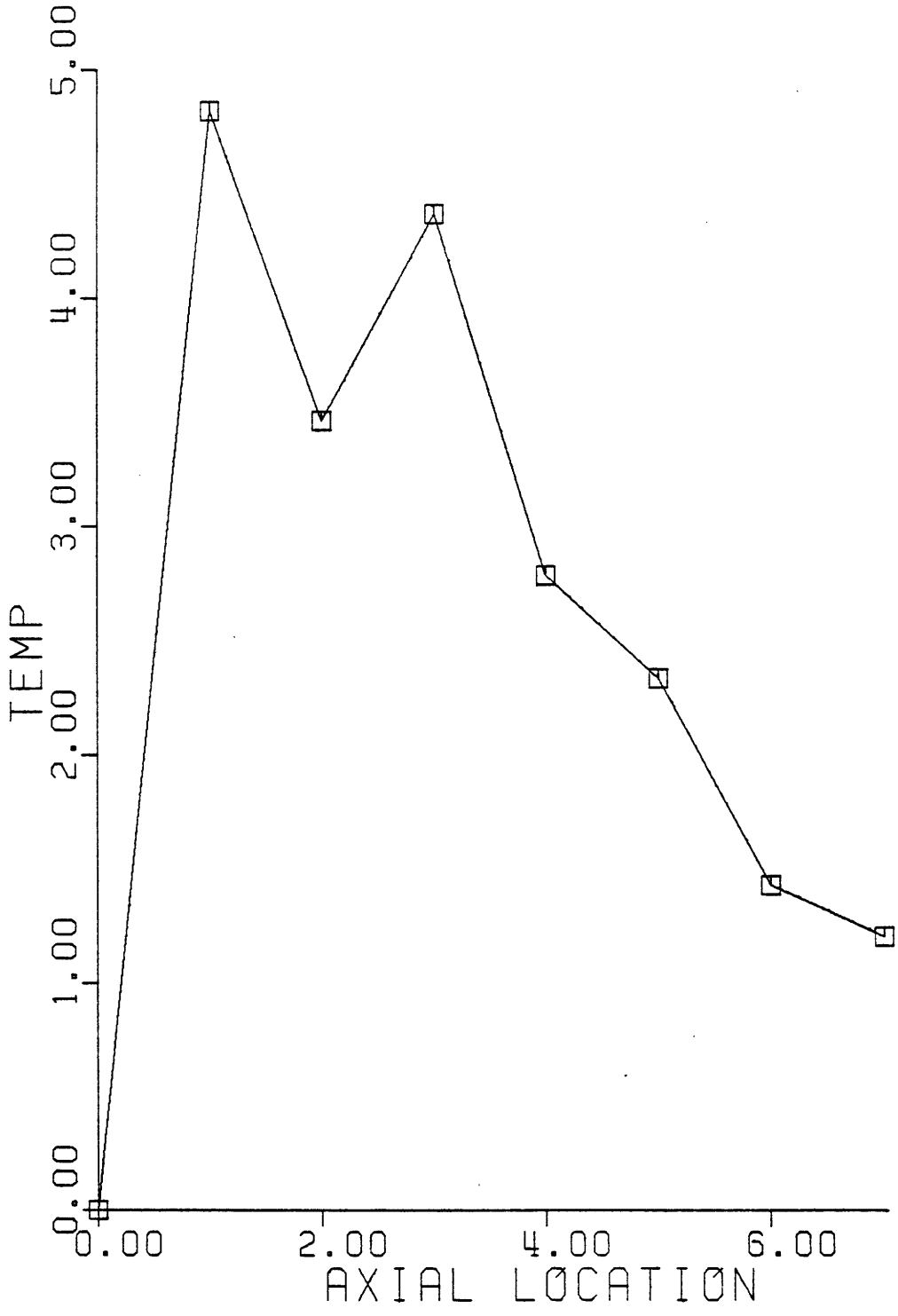

FIGURE 36: Temperature Distribution at Flow Coeff. 0.075

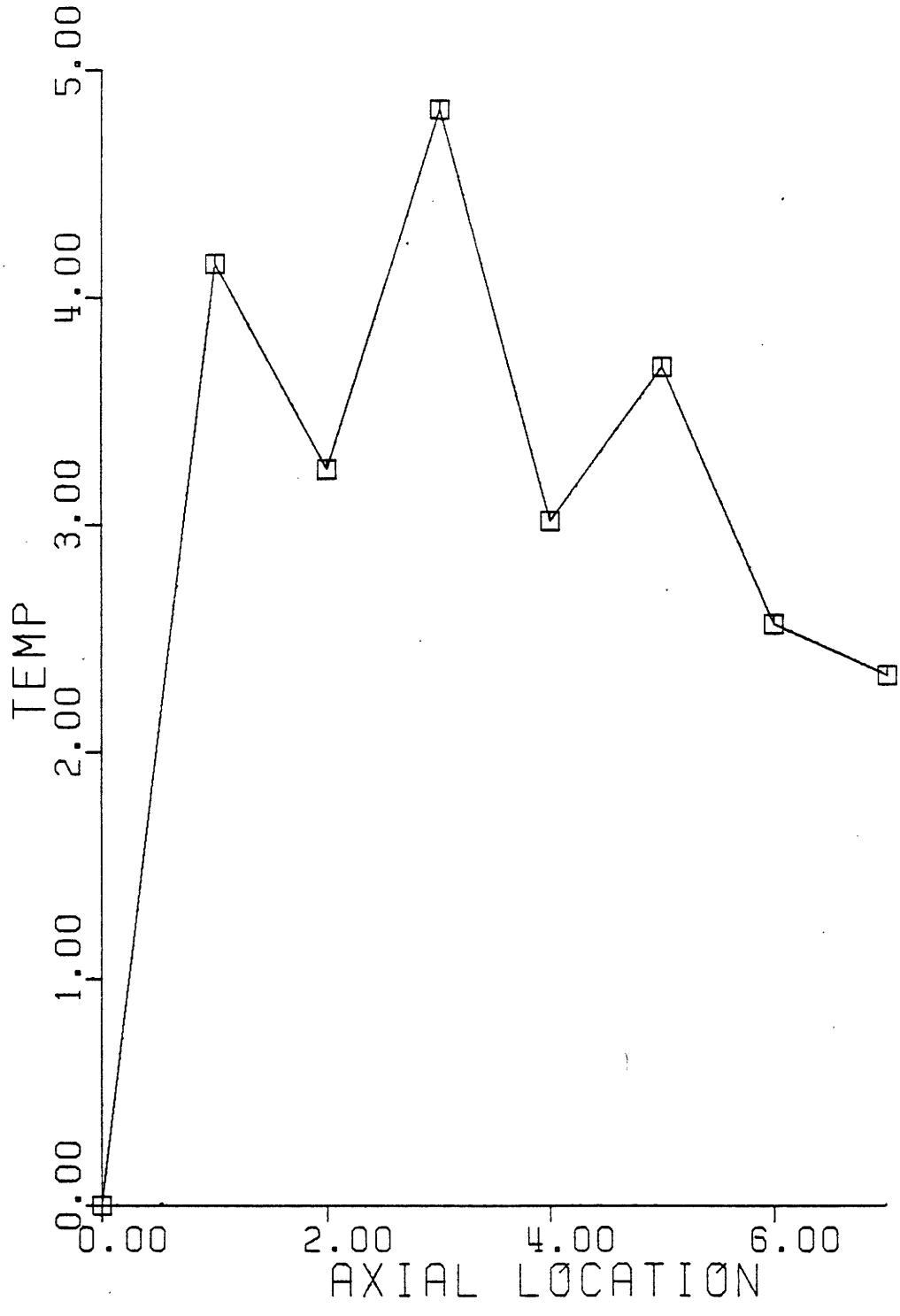

FIGURE 37: Temperature Distribution at Flow Coeff. 0.262

REFERENCES

1. Day, Greitzer, and Cumpsty, "Prediction of Compressor Performance in Rotating Stall," J. Eng. Power, Vol. 100, No. 1, January 1978.
2. Day, "Axial Compressor Stall," Ph.D. Thesis, Cambridge University.
3. Sterning, "Rotating Stall and Surge," Chap. 15 in "Fluid Mechanics of Turbomachinery," ASME Lecture Course, Iowa State, 1973.
4. Emmons, Pearson, and Grant, "Compressor Stall and Surfe Propagation," ASME Trans., Vol. 27, April 1955, pp. 455-469.
5. Takata, and Nagano, "Nonlinear Analysis of Rotating Stall," ASME Paper 72-GT-3, 1972.
6. Day, and Cumpsty, "The Measurement and Interpretation of Flow within Rotating Stall Cells in Axial Compressors," J. Mech. Eng. Sci., Vol. 20, 1978, pp. 101-114.
7. Greitzer, "Surge and Rotating Stall in Axial Flow Compressor Part I: Theoretical Compression System Model," ASME J. Eng. Power, Vol. 98, April 1978, pp. 190-198.
8. Greitzer, "Surge and Rotating Stall in Axial Flow Compressors Part II: Results and Comparison with Theory," ASME J. Eng. Power, Vol. 98, April 1978, pp. 199-217.
9. Cumpsty, and Greitzer, "A Simple Model for Compressor Stall Cell Propagation," GT and PDL Report #148, M.I.T., February 1980.
10. Greitzer, "Review-Axial Compressor Stall Phenomena," J. Fluids Eng., Vol. 102, June 1980, pp. 134-151.

REFERENCES Continued

11. Greitzer, "The Stability of Pumping Systems," The 1980 Freeman Scholar Lecture, J. Fluids Eng., Vol. 103, June 1981, pp. 193-242.

12. Christianson, "An Experimental Investigation of a Three Stage Axial Flow Compressor with Cantilevered Stators using Low Aspect Ratio-Redesigned Endwork Blading in All Stages," UARL Report R232752-1.

13. Prell, "An Experimental Investigation of Stator Hub Treatment in an Axial Flow Compressor," GT and PDL Report #161.

14. Greitzer, Mazzawy, and Fulkerson, "Flow Field Coupling Between Compression System Components in Asymmetric Flow," J. Eng. Power, Vol. 101, January 1978, pp. 66-72.

15. Ower, and Pankhurst, The Measurement of Airflow, Chap. 7, Pergammon Press.

16. Whitfield, Kelly, and Barry, "A Three-Dimensional Analysis of Rotor Wakes," Aero. Quarterly, November 1972, pp. 285-300.

17. Freeman, Private Communication.

18. Iura, and Rannie, "Experimental Investigations of Propagating Stall in Axial Flow Compressors," Trans. ASME, Vol. 78, No. 3, 1954.

APPENDIX A

OPERATION OF SCANIVALVE INTERFACE CIRCUIT AND SOFTWARE FOR DATA ACQUISITION AND HOT WIRE ANALYSIS

Operation of Scanivalve Interface Circuit

When the instruction: Mov @(R5)+, @#171772 is carried out, the DRV-11 sends a data ready pulse which triggers the 74123. This sends a pulse which causes the scanivalve motor to step to the next channel. When the transients associated with the stepping have attenuated the scanivalve sends out a ready-to-read pulse causing the 7474 to send a request pulse to the DRV-11. This request pulse sets bit 15 of the DRCSR and the digital address is read. The data transmitted pulse from the DRV-11 is used to put bit 15 to zero. The A/D converter can now be initiated to measure the transducer output.

```
C THIS PROGRAM CONTROLS THE AQUISITION, REDUCTION AND
C PRESENTATION OF STEADY STATE PRESSURE, TEMPERATURE
C AND TORQUE DATA .THE TOTAL TO STATIC PRESSURE RISE
C COEFFICIENTS UP TO THE LAST DATA POINT ARE PLOTTED
C ON THE TERMINAL SCREEN AFTER EACH DATA POINT, AND A
C COMPLETE SET OF REDUCED DATA IS PRINTED ON THE
C LINEPRINTER.
C
C A PLOT OF ANY CHARACTERISTIC MAY BE OBTAINED USING
C THE PROGRAM GRA3 AND A PRINTOUT OF THE RAW AND
C REDUCED DATA MAY BE OBTAINED USING THE PROGRAM
C PRINT3.
C
C THE PROGRAM USES SUBROUTINES FROM THREE LIBRARIES:
C      ADLIB-FOR DATA AQUISITION FROM THE uMAC 4000
C            TEMPERATURE MULTIPLEXER
C      IBLIB-TO READ THE FREQUENCY COUNTER USING THE
C            INSTRUMENT BUS
C      GRLIB-TO PLOT THE TOTAL TO STATIC PRESSURE RISE
C            CHARACTERISTIC ON THE TERMINAL SCREEN
C
C THERE IS A COMMAND FILE SSMEAS.COM TO CREATE SSMEAS.SAV,
C AND BEFORE RUNNING THE PROGRAM USER MUST ASSIGN DY1: 8,
C LP 7 AND LOAD THE INSTRUMENT BUS.
C
C USER INPUT IS:
C      A TWO DIGIT RUN NO.
C      THE AMBIENT PRESSURE IN MM HG
C      THE AMBIENT TEMPERATURE IN DEG. C
C
C TO ALL QUESTIONS ANSWER 1 FOR YES
C                         0 FOR NO
C
C TO END DATA AQUISITION ANSWER NO WHEN ASKED 'ANOTHER POINT ?'
C
C THE DATA IS STORED IN DIMENSIONAL FORM ON FLOPPY DISK
C WITH THE FILENAME SS__.DAT, THE TWO BLANKS BEING THE
C RUN NUMBER.
C
C NOTE THAT ONLY 60 POINTS MAY BE PLACED IN ANY ONE
C FILE.
C
C THE DATA REDUCTION IS SET UP FOR A MICROMANOMETER
C READING mm OF ALCOHOL WITH SPECIFIC GRAVITY OF 0.79
C
C THE SCANIVALVE SHOULD BE PLUMBED AS FOLLOWS:
C       1-8      INLET STATICS
C       9-15     BLADE ROW STATICS
C       16-23    EXIT STATICS
C       24-29    INLET TOTALS
C       30-33    BELLMOUTH TOTALS
C       34-39    EXIT TOTALS
C       40-45    DOWNSTREAM TOTALS
C       46       UPSTREAM O.P.
C       47       DOWNSTREAM O.P.
C       48       REFERENCE
C
C THE TEMPERATURE MULTIPLEXER SHOULD BE CONNECTED AS FOLLOWS:
C       1 AND 3  COMPRESSOR BEARINGS
C       2 AND 4  DUCT
C       5-12     COMPRESSOR STATIONS
```

```
C
C
      BYTE POINT(13)
      DIMENSION DPR(48),PR(48),DTEMP(12),TEMP(12)
      DIMENSION PROW(7),TROW(7),PSTA(3),TSTA(3)
      DIMENSION IBUF(30),X(50),Y(50)
      COMMON/DIG/DPR,DTEMP,DTORQ,IPT
      COMMON/VAL1/UMEAN,IST
      COMMON/VAL2/TORQ,RPM
      COMMON/VAL3/TEMP,PR,PAMB,TAMB,DELP
      COMMON/RES1/PHI,TT,TS,SS,SSIGV,TTD,TTBELL,TSBELL
      COMMON/RES2/PREF,PBELL,TDEL,TSTA,PSTA,TROW,PROW
      DATA POINT/'D','Y','1',':','S','S',' ',' ',
     1'.','D','A','T',0/
      IPT=0
      WRITE(5,*)'ENTER RUN NO.'
      ACCEPT 2,POINT(7),POINT(8)
2     FORMAT(2A1)
      WRITE(5,*)'ENTER PAMB IN MM HG'
      ACCEPT 3,PAMB
3     FORMAT(F6.2)
      WRITE(5,*)'ENTER TAMB IN DEG C'
      ACCEPT 6,TAMB
6     FORMAT(F5.2)
      OPEN(UNIT=8,NAME=POINT,ACCESS='DIRECT',TYPE='NEW',
     1RECORDSIZE=75,INITIALSIZE=60)
10    IPT=IPT+1
      DECODE(2,1,POINT(7))IP
1     FORMAT(I2)
      IPOINT=100*IP+IPT
      WRITE(7,*)'POINT NO.',IPOINT
C
C
C     TAKE DATA(DATA),
C     CONVERT TO ENGINEERING UNITS, NONDIMENSIONALISE
C     AND STORE(CALIB)
C     PERFORM DATA REDUCTION(REDUCE)
C     PRINT REDUCED DATA(WRITE)
C
C

      CALL DATA
      CALL CALIB
      CALL REDUCE
      CALL WRITE
C
C
C     TAKE HOT WIRE DATA ON STALL CELL SPEED AND SIZE
C     IF REQUIRED
C
C
      WRITE(5,*)'ARE YOU TAKING STALL CELL DATA ?'
      ACCEPT *,IHW
      IF(IHW.NE.1)GO TO 1000
      CALL CELL(PHI,RPM)
1000  WRITE(7,*)'*****************************************'
C
C
C     PLOT TOTAL-STATIC CHARACTERISTIC
C
C
```

```
C
      CALL GRINIT(IBUF)
      CALL GRSCAL(IBUF,0.,1.,0.,2.5,0)
      X(IPT)=PHI
      Y(IPT)=TS
      CALL GRAPHS(IBUF,65,X,Y,IPT,0.,0)
      PAUSE
      CALL VTCLR
      WRITE(5,*)'ANOTHER POINT ?'
      ACCEPT 7,J
7     FORMAT(I1)
      IF(J.NE.0)GO TO 10
      CLOSE(UNIT=8)
      END
```

```
C THIS PROGRAM CONTROLS DATA AQUISITION. NOTE THAT SV SHOULD BE ON
C A/D CONVERTER CHANNEL 15, TORQUE METER ON CHANNEL 14.
C
      SUBROUTINE DATA
      BYTE SPEED(17)
      DIMENSION ID(30),DPR(48),DTEMP(12),IT(50)
      COMMON/DIG/DPR,DTEMP,DTORQ,IPT
      COMMON/VAL2/TORQ,RPM
      KL=5
C
C
C     READ TORQUE AND RPM, TAKING 50
C     SAMPLES OF THE TORQUE METER VOLTAGE.
C
C
      CALL TORQUE(IT)
      CALL IBRECV(SPEED,17,'0')
      CALL IBIFC
      DECODE(10,111,SPEED(6))R1
C
C
C     AVERAGE TORQUE METER SAMPLES, AND CONVERT
C     TO A VOLTAGE (V1) AND A TORQUE (T1)
C
C
      DT1=0
      DO 50 M=1,50
50    DT1=DT1+FLOAT(IT(M))/50.
      V1=2.5*(DT1-2048.)/2048.
      T1=-380.062*V1/2.599
C
C
C     READ ALL 48 PORTS OF THE SCANIVALIVE, TAKING
C     30 SAMPLES AT EACH PORT-USING DLV-11 INTERFACE
C     TO STEP SCANIVALVE AND READ CHANNEL CODE AND
C     A/D CONVERTER TO READ TRANSDUCER OUTPUT.
C
C
      DO 20 K=1,48
      CALL SCAN(KL,IPOS,ID)
C
C
C     CONVERT DIGITAL CODE FROM OPTICAL
C     ENCODER INTO CHANNEL NO.
C
C
      CALL CHAN(IPOS,ICHN)
      ICH=ICHN+1
      IF(ICH.GT.48)ICH=ICH-48
C
C
C     AVERAGE SAMPLES (IGNORING FIRST 5
C     TO ALLOW FOR TRANSIENTS AFTER THE
C     SCANIVALVE STEPS)
C
C
      DPR(ICH)=0
      DO 10 L=6,30
10    DPR(ICH)=DPR(ICH)+FLOAT(ID(L))/25.
20    CONTINUE
C
```

```
C
C       READ 12 TEMPERATURES USING uMAC-4000
C       READ TORQUE AND RPM AGAIN
C
C
        CALL AD(0,11,DTEMP,IER)
        WRITE(5,*)'ERROR=',IER
        CALL IBRECV(SPEED,17,'0')
        CALL IBIFC
        CALL TORQUE(IT)
        DT2=0
        DO 40 N=1,50
40      DT2=DT2+FLOAT(IT(N))/50.
        V2=2.5*(DT2-2048.)/2048.
        T2=-380.062*V2/2.599
        DECODE(10,111,SPEED(6))R2
111     FORMAT(E10.0)
C
C
C       AVERAGE TWO READINGS OF BOTH TORQUE
C       AND RPM
C       TYPE ON SCREEN THE TWO INDIVIDUAL
C       READINGS OF BOTH TORQUE AND RPM AND THE
C       BEARING TEMPERATURES.
C
C
        RPM=(R1+R2)/2.
        DTORQ=(T1+T2)/2.
        WRITE(5,*)'SPEEDS',R1,R2
        WRITE(5,*)'TORQUES',T1,T2
        WRITE(5,*)'BEARING TEMPS.=',DTEMP(1),DTEMP(3)
        RETURN
        END
```

```
        .GLOBL TORQUE
TORQUE: MOV (R5)+,R0
        MOV (R5)+,R3            ;STARTING ADDRESS FOR DATA
        CLR R1
        MOV #61,R2              ;TAKE 50 SAMPLES
LOOP1:  MOV #4402,@#170400      ;SET A/D COMM. REG.
        MOV #216,@#170402       ;GAIN=4,CHANNEL=14
LOOP2:  TST @#170400            ;DATA READY ?
        BPL LOOP2
        MOV @#170402,(R3)+      ;YES,THEN STORE
        INC R1
        CMP R2,R1               ;FINISHED ?
        BPL LOOP1
        RTS PC
        .END TORQUE
```

```
        .GLOBL SCAN
SCAN:   MOV (R5)+,R0
        CLR @#171770
        MOV @(R5)+,@#171772      ;STEP SCANIVALVE
        CLR R1
        MOV #35,R2               ;TAKE 30 SAMPLES
ADDRES: TST @#171770             ;CHANNEL CODE READY ?
        BPL ADDRES
        MOV @#171774,@(R5)+      ;YES,MOVE TO MEMORY
        MOV (R5)+,R3             ;STARTING ADDRESS FOR DATA
        MOV #4402,@#170400       ;SET A/D COMM. REG.
LOOP1:  MOV #217,@#170402        ;GAIN=4,CHANNEL=15
LOOP2:  TST @#170400             ;DATA READY ?
        BPL LOOP2
        MOV @#170402,(R3)+       ;YES,MOVE TO MEMORY
        INC R1
        CMP R2,R1                ;FINISHED ?
        BPL LOOP1
        RTS PC
        .END SCAN
```

```
C THIS PROGRAM CALCULATES S/V CHANNEL NO. (ICHN) FROM THE CODE
C SENT BY THE OPTICAL ENCODER IN THE SCANIVALVE.
C
        SUBROUTINE CHAN(IPOS,ICHN)
        IF(IPOS.LT.10)GO TO 40
        IF(IPOS.GT.30)GO TO 10
        ICHN=IPOS-6
        GO TO 50
10      IF(IPOS.GT.42)GO TO 20
        ICHN=IPOS-12
        GO TO 50
20      IF(IPOS.GT.60)GO TO 30
        ICHN=IPOS-18
        GO TO 50
30      ICHN=IPOS-24
        GO TO 50
40      ICHN=IPOS
50      CONTINUE
        RETURN
        END
```

```
C THIS PROGRAM CONVERTS DATA  INTO SI UNITS,NONDIMENSIONALISES
C IT AND STORES THE RAW DATA ON FLOPPY DISK IN FILE SS__.DAT
C (THE TWO BLANKS BEING THE RUN NUMBER).
C
      SUBROUTINE CALIB
      BYTE SPEED(17)
      DIMENSION PR(48),DPR(48),DTEMP(12),TEMP(12),Z(48)
     1,DTEMC(12)
      COMMON/DIG/DPR,DTEMP,DTORQ,IPT
      COMMON/VAL1/UMEAN,IST
      COMMON/VAL2/TORQ,RPM
      COMMON/VAL3/TEMP,PR,PAMB,TAMB,DELP
C
C     VARIABLES IST AND IHYST INDICATE WHETHER THE
C     DATA POINT IS IN STALL AND/OR ON THE RETURN LEG
C     OF THE HYSTERESIS LOOP AND ARE STORED WITH THE
C     REST OF THE DATA.
C
C
      WRITE(5,*)'IS THIS POINT IN STALL ?'
      ACCEPT 111,IST
      WRITE(5,*)'IS THIS POINT ON THE RETURN LEG OF THE HYSTERESIS
     1LOOP ?'
      ACCEPT 111,IHYST
111   FORMAT(I1)
      RMEAN=0.286512
      AREA=0.0658444
C
C
C     CALCULATE AMBIENT DENSITY AND MEAN BLADE SPEED
C
C
      RHOA=0.4642*PAMB/(273.15+TAMB)
      UMEAN=RMEAN*RPM*0.1047
C
C
C     CORRECT TORQUE FOR WINDAGE LOSSES
C     AND NONDIMENSIONALISE IT
C
C
      CALL TQLOSS(RPM,CTORQ,DTORQ,TARE)
      TORQ=2*CTORQ/(RHOA*RMEAN*AREA*(UMEAN**2))
      WRITE(7,*)'TOTAL TORQUE=',DTORQ
      WRITE(7,*)'TARE TORQUE=',TARE
C
C
C     CONVERT DIGITISED PRESSURES TO PASCALS AND
C     NONDIMENSIONALISE THEM
C
C
      DPREF=DPR(48)
      DO 10 M=1,48
10    Z(M)=2.5*6.895E3*(DPR(M)-DPREF)/2048.
      DO 20 N=1,45
20    PR(N)=2*Z(N)/(RHOA*(UMEAN**2))
      PR(48)=DPR(48)
C
C
C     LEAVE THE ORIFICE PLATE PRESSURES IN PASCALS
C     AND IF THEIR DIFFERENCE IS OF THE SAME ORDER
C     AS THE SCANIVALVE TRANSDUCER ERROR TAKE READING
```

```
C       FROM THE MICROMANOMETER.
C
C
        PR(46)=Z(46)
        PR(47)=Z(47)
        DELP=PR(46)-PR(47)
        IF(DELP.GT.175)GO TO 500
        WRITE(5,*)'ENTER O.P. MICROMANOMETER READING'
        ACCEPT 555,D
555     FORMAT(F6.3)
        DELP=.79*9.81*D
C
C
C       CORRECT TEMPERATURES WITH INDIVIDUAL
C       THERMOCOUPLE CALIBRATIONS.
C
C
500     DTEMC(1)=DTEMP(1)
        DTEMC(2)=DTEMP(2)
        DTEMC(3)=DTEMP(3)
        DTEMC(4)=DTEMP(4)
        DTEMC(5)=DTEMP(5)
        DTEMC(6)=DTEMP(6)
        DTEMC(7)=DTEMP(7)
        DTEMC(8)=DTEMP(8)
        DTEMC(9)=DTEMP(9)
        DTEMC(10)=DTEMP(10)
        DTEMC(11)=DTEMP(11)
        DTEMC(12)=DTEMP(12)
C
C
C       NONDIMENSIONALISE THE TEMPERATURES IN THE
C       COMPRESSOR,LEAVE THE OTHERS IN DIMENSIONAL
C       FORM.
C
C
        DO 600 IA=5,12
600     TEMP(IA)=DTEMC(IA)*1.005E3*2/UMEAN**2
        DO 700 IB=1,4
700     TEMP(IB)=DTEMC(IB)
C
C
C       STORE RAW DATA
C
C
        WRITE(8'IPT)PAMB,TAMB,(DTEMP(JI),JI=1,12),(Z(JJ),JJ=1,48),
        1DELP,CTORQ,RPM,IST,IHYST
        RETURN
        END
```

```
C THIS PROGRAM CALCULATES THE TARE TORQUE USING
C DATA FROM THE P&W REPORT ON THE COMPRESSOR.
C
      SUBROUTINE TQLOSS(RPM,CTORQ,DTORQ,TARE)
      IF(RPM.GT.500.)GO TO 10
      T=RPM*3./500.
      GO TO 100
10    IF(RPM.GT.1000.)GO TO 20
      T=3.+(RPM-500.)*8./1000.
      GO TO 100
20    IF(RPM.GT.2000.)GO TO 30
      T=11.+(RPM-1500.)*4.5/500.
      GO TO 100
30    IF(RPM.GT.2500.)GO TO 40
      T=15.5+(RPM-2000.)*6./500.
      GO TO 100
40    IF(RPM.GT.3000.)GO TO 50
      T=21.5+(RPM-2500.)*7.5/500.
      GO TO 100
50    IF(RPM.GT.3500.)GO TO 60
      T=29.+(RPM-3000.)*8./500.
      GO TO 100
60    WRITE(5,*)'RPM TOO HIGH FOR TARE TORQUE CALIBRATION'
      WRITE(5,*)'TARE TAKEN AS 4.181 Nm (37 IN-LBF)'
      T=37.
100   TARE=T*0.113
      CTORQ=DTORQ-TARE
110   RETURN
      END
```

```
C THIS PROGRAM PERFORMS THE DATA REDUCTION.
C
      SUBROUTINE REDUCE
      DIMENSION PR(48),TEMP(12),TSTA(3),PSTA(3),TROW(7),PROW(7)
      COMMON/VAL1/UMEAN,IST
      COMMON/VAL3/TEMP,PR,PAMB,TAMB,DELP
      COMMON/RES1/PHI,TT,TS,SS,SSIGV,TTD,TTBELL,TSBELL
      COMMON/RES2/PREF,PBELL,TDEL,TSTA,PSTA,TROW,PROW
C
C
C     CALCULATE DENSITY IN EXIT DUCT.
C
C
      PPIPE=760.*PR(46)/1.01325E5
      TPIPE=0.5+(TEMP(2)+TEMP(4))/2.
      RHOP=0.4642*(PAMB+PPIPE)/(273.15+TPIPE)
      RHOA=0.4642*PAMB/(273.15+TAMB)
C
C
C     CALCULATE AVERAGE PRESSURES AT COMPRESSOR
C     INLET AND EXIT STATIONS.
C
C
      PSI=(PR(1)+PR(2)+PR(3)+PR(4)+PR(5)+PR(6)+
     1PR(7)+PR(8))/8.
      PSE=(PR(16)+PR(17)+PR(18)+PR(19)+PR(20)+
     1PR(21)+PR(22)+PR(23))/8.
      PTI=(PR(24)+PR(25)+PR(26)+PR(27)+PR(28)+PR(29))/6.
      PTE=(PR(34)+PR(35)+PR(36)+PR(37)+PR(38)+PR(39))/6.
      PTD=(PR(40)+PR(41)+PR(42)+PR(43)+PR(44)+PR(45))/6.
      PBELL=(PR(30)+PR(31)+PR(32)+PR(33))/4.
      PREF=PR(48)
C
C
C     IF COMPRESSOR IS STALLED TAKE INLET TOTAL
C     PRESSURE TO BE ATMOSPHERIC.
C
C
      IF (IST.EQ.1)PTI=0.
C
C
C     CALCULATE FLOW COEFFICIENT FROM INLET DYNAMIC
C     HEAD (FOR PURPOSES OF COMPARISON ONLY),
C     THEN CALCULATE FLOW COEFFICIENT FROM THE
C     PRESSURE DIFFERENCE ACROSS THE ORIFICE PLATE,
C     AND THE BLADE REYNOLDS NUMBER.
C
C
      CXIN=0.964335*SQRT(PTI-PSI)
      CALL OPCAL(RHOA,DELP,RHOP,CX)
      PHI=CX/UMEAN
      PDROP=PTI/PHI**2
      REBL=UMEAN*.0469/(1.568E-5)
      WRITE(7,*)'PHI=',PHI,'PHI IN=',CXIN
      WRITE(7,*)'DUCT TEMP.=',TPIPE
      WRITE(7,*)'DELP BELL SCREEN=',PDROP
      WRITE(7,*)'BLADE REYNOLDS NO.=',REBL
C
C
C     CALCULATE OVERALL,STAGE AND BLADE ROW
C     CHARACTERISTICS.
```

```
C
C
      TT=PTE-PTI
      TS=PSE-PTI
      SSIGV=PSE-PSI
      SS=PSE-PR(9)
      TTD=PTD-PTI
      TTBELL=PTE-PTBELL
      TSBELL=PSE-PTBELL
      PSTA(1)=PR(11)-PR(9)
      PSTA(2)=PR(13)-PR(11)
      PSTA(3)=PR(15)-PR(13)
      PROW(1)=PR(9)-PSI
      PROW(2)=PR(10)-PR(9)
      PROW(3)=PR(11)-PR(10)
      PROW(4)=PR(12)-PR(11)
      PROW(5)=PR(13)-PR(12)
      PROW(6)=PR(14)-PR(13)
      PROW(7)=PR(15)-PR(14)
      TDEL=TEMP(12)-TEMP(5)
      TSTA(1)=TEMP(8)-TEMP(6)
      TSTA(2)=TEMP(10)-TEMP(8)
      TSTA(3)=TEMP(12)-TEMP(10)
      TROW(1)=TEMP(6)-TEMP(5)
      TROW(2)=TEMP(7)-TEMP(6)
      TROW(3)=TEMP(8)-TEMP(7)
      TROW(4)=TEMP(9)-TEMP(8)
      TROW(5)=TEMP(10)-TEMP(9)
      TROW(6)=TEMP(11)-TEMP(10)
      TROW(7)=TEMP(12)-TEMP(11)
      RETURN
      END
```

```
C THIS PROGRAM CALCULATES THE AXIAL VELOCITY THROUGH THE
C COMPRESSOR FROM THE PRESSURE DROP ACROSS THE ORIFICE PLATE.
C
      SUBROUTINE OPCAL(RHOA,DELP,RHOP,CX)
C
C
C     CORRECT THE PRESSURE DIFFERENCE FOR DENSITY
C     AND PERFORM CALIBRATION
C
C
      DELCOR=SQRT(DELP*RHOP)/RHOA
      CX=2.76*DELCOR
110   RE=582.6051*CX
      IF(RE.GT.9350.)GO TO 100
      IF(RE.GT.4186.)GO TO 200
      CAL=4.1-(1.34*RE/5100.)
      GO TO 300
200   CAL=2.76+((9350.-RE)*0.24/5164.)
300   E=-0.01*CX
      F=0.01*CX
      CXA=CAL*DELCOR
      DIFF=CX-CXA
      CX=CXA
      IF(DIFF.GT.F)GO TO 110
      IF(DIFF.LT.E)GO TO 110
C
C
C     PRINT AXIAL VELOCITY AND THE REYNOLDS NO.
C     BASED ON THE VELOCITY THROUGH THE SMALL
C     ORIFICES AND THEIR DIAMETER.
C
C
100   WRITE(7,*)'CX=',CX,'RE=',RE
      RETURN
      END
```

```
C THIS PROGRAM PRINTS ALL THE REDUCED DATA.
C
      SUBROUTINE WRITE
      BYTE POINT(15)
      DIMENSION PR(48),TEMP(12),TSTA(3),PSTA(3),TROW(7),PROW(7)
      COMMON/VAL2/TORQ,RPM
      COMMON/VAL3/TEMP,PR,PAMB,TAMB,DELP
      COMMON/RES1/PHI,TT,TS,SS,SSIGV,TTD,TTBELL,TSBELL
      COMMON/RES2/PREF,PBELL,TDEL,TSTA,PSTA,TROW,PROW
      WRITE(7,*)'AMB. PRESS.=',PAMB,'AMB. TEMP.=',TAMB
      WRITE(7,*)'SPEED=',RPM
      WRITE(7,*)'FLOW COEFF.=',PHI
      WRITE(7,*)'COMPRESSOR CHARACTERISTICS:'
      WRITE(7,*)'TS=',TS
      WRITE(7,*)'TSBELL=',TSBELL
      WRITE(7,*)'SS=',SS
      WRITE(7,*)'SSIGV=',SSIGV
      WRITE(7,*)'TT=',TT
      WRITE(7,*)'TTD=',TTD
      WRITE(7,*)'TTBELL=',TTBELL
      WRITE(7,*)'TDEL=',TDEL
      WRITE(7,*)'TORQ=',TORQ
      WRITE(7,*)'STAGE AND BLADE ROW CHARACTERISTSCS:'
      WRITE(7,9)
9     FORMAT(4H0ROW,4X,3HIGV,7X,2HR1,8X,2HS1,8X,2HR2,8X,
      12HS2,8X,2HR3,8X,2HS3)
      WRITE(7,11)PSTA(1),PSTA(2),PSTA(3)
11    FORMAT(6H PRESS,14X,F7.5,2(13X,F7.5))
      WRITE(7,12)(PROW(I),I=1,7)
12    FORMAT(7X,7(F8.5,2X))
      WRITE(7,13)TSTA(1),TSTA(2),TSTA(3)
13    FORMAT(5H TEMP,15X,F7.4,2(13X,F7.4))
      WRITE(7,14)(TROW(J),J=1,7)
14    FORMAT(7X,7(F7.4,3X))
      PAUSE
      RETURN
      END
```

```
C THIS PROGRAM ALLOWS THE STALL CELL SIZE AND SPEED TO BE
C CALCULATED FROM MEASUREMENTS MADE ON THE OSCILLOSCOPE
C AND PRINTS THIS DATA.
C
C NOTE THAT THIS DATA IS NOT STORED ON FLOPPY DISK.
C
      SUBROUTINE CELL(PHI,RPM)
10    WRITE(7,*)'************'
      WRITE(5,*)'ENTER OSCILLOSCOPE TIME BASE (mS/CM)'
      ACCEPT *,OTB
      WRITE(5,*)'ENTER CELL SPEED(CM),CELL SIZE(CM)'
      ACCEPT *,VCELL,SIZE
      WCELL=60.E3/(RPM*VCELL*OTB)
      CELSIZ=SIZE/VCELL
      WRITE(7,*)'FLOW COEFF.=',PHI
      WRITE(7,*)'CELL SPEED=',WCELL
      WRITE(7,*)'CELL SIZE=',CELSIZ
      WRITE(5,*)'MORE HOT WIRE DATA ?'
      ACCEPT *,ICELL
      IF(ICELL.NE.0)GO TO 10
      RETURN
      END
```

APPENDIX B

DENSITY CORRECTION FOR ORIFICE PLATE CALIBRATION

The pressure drop across the orifice plate is proportional to the local dynamic head:

$$\Delta P_{OP} = K_1 \rho_p V_p^2 \tag{1}$$

Continuity:

$$A_c \rho_a C_{sc} = A_p \rho_p V_p \tag{2}$$

From Eq. (2)

$$V_p = K_2 C_{sc} \rho_a / \rho_p$$

Thus

$$\Delta P_{OP} = K_3 C_{sc}^2 \rho_a^2 / \rho_p$$

and

$$C_{sc} = C \sqrt{\Delta P_{OP} \rho_p} / \rho_a$$

APPENDIX C

GENERAL NOTES ON THE SYSTEM

When breaking the coupling on the three stage compressor shaft in preparation for running the single stage compressor:

1) remove the pipe fittings in the grease filler holes and replace them with the locking screws;
2) make sure both sides of the broken coupling are sealed; and
3) make sure the plate covering the upstream flange of the elbow is in place.

When breaking the coupling on the single stage compressor in preparation for running the three stage compressor:

1) bolt the locking plate onto the broken coupling;
2) replace the locking screws with the pipe fittings on the three stage compressor coupling that was broken; and
3) make sure that the plate has been removed from the upstream flange of the elbow, and that the hole through which the plenum of the single stage compressor exhausts to the duct system has been covered.

When running the three stage compressor in normal operation:

1) check that the fan rotor is locked, the fan inlet guide vanes are in the fully open position and the cover has been taken off the exit flange;
2) check that the oil mister for the bearings in the pillow blocks of the single stage compressor is on;

3) check that the throttle valve runs smoothly and that the microswitches are working (the potentiometer reads about +7 volts in the fully open position and about -3 volts in the fully closed position);
4) check that the slip rings in the torque meter are in the "down" position; and
5) check that the Instrument Bus is loaded, the Line Printer is assigned 7 and DY1: assigned 8.

Some general points:

1) At least once a month check the zero and gain on the scanivalve and torque meter.
2) Always connect the upstream orifice plate pressure top (the larger of the two) to the micromanometer first.
3) When running the fan make sure that the rotor is no longer locked and that there is sufficient oil in the bearings (the pillow blocks are not sealed and thus lose oil fairly quickly); also remove all pressure tubing from the manometer bank as the starting transient tends to suck the manometer fluid into the tubing.

APPENDIX D

PREDICTION OF THE FLOW COEFFICIENT OF THE FIRST POINT IN STALL USING AN EFFECTIVE THROTTLE AREA CALCULATED AT THE STALL POINT

The pressure drop across the throttle is proportional to the load dynamic head:

$$\Delta P_{TH} = K_1 \; 1/2 \, \rho_{TH} \, V_{TH}^2 \tag{1}$$

Continuity:

$$\rho_a \, A_c \, C_x = \rho_{TH} \, A_{TH} \, V_{TH} \tag{2}$$

Thus

$$\Delta P_{TH}/\tfrac{1}{2} \, \rho_a \, \bar{u}^{-2} = K_1 \, \phi^2 \left(\frac{A_c \rho_a}{A_{TH} \rho_{TH}} \right)^2 \frac{\rho_{TH}}{\rho_a}$$

or

$$\Delta P_{TH}/\tfrac{1}{2} \, \rho_a \, \bar{u}^{-2} = K_2 \, \frac{\rho_a}{\rho_{TH}} \, \phi^2 \tag{3}$$

where $1/K_2$ is defined as the effective throttle area.

Pressure and Temperature data are available at the compressor exit and just upstream of the orifice plate. Assuming:

1) the compressor exit conditions approximate the conditions just before the throttle, and
2) the conditions at the upstream orifice plate station approximate

conditions just after the throttle K_2 can be calculated at the stall point. K_2 is essentially constant for the stall point and the first point in stall and thus the flow coefficient for the first point in stall can be calculated.